ELECTRON BEAM IRRADIATION

OF POLYSTYRENE/POLY(VINYL METHYL ETHER) BLENDS

by

VALERIE PIETRI

Thesis submitted to the Faculty of the

Virginia Polytechnic Institute and State University

in partial fulfillment of the requirements for the degree of

MASTER OF SCIENCE

in

Chemical Engineering

APPROVED:

G.L. Wilkes, Chairman

E. Marand

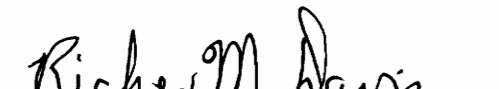

R.M. Davis

May, 1993

Blacksburg, Virginia

ELECTRON BEAM IRRADIATION OF

POLYSTYRENE/POLY(VINYL METHYL ETHER) BLENDS

by

Valérie Pietri

G. L. Wilkes, Chairman

ABSTRACT

The effects of electron beam radiation on the rheological behavior of a polystyrene/poly(vinyl methyl ether) blend as a function of absorbed dose, composition, and temperature, were investigated. The purpose of this research has been to modify the viscosity of polystyrene by studying the influences of the addition of a small amount of poly(vinyl methyl ether), combined with the exposure of the blends to low radiation doses. It is shown that the crosslinking behavior, in terms of the changes in the viscosity, is more pronounced and significant for the highest PVME content system composed of 10 wt % PVME. The other blends under consideration in this study do not display significant modifications in their rheological response after irradiation.

The effects of radiation and composition on the

temperature dependence of the viscosity is illustrated using the Arrhenius Law. The results obtained, in terms of flow activation energy, Ea, show that no real changes occurred due to radiation. On the other hand, it is found that the flow activation energy is strongly dependent on the blend composition.

The phase separation temperature as a function of radiation dose and composition is also examined. It is shown that the most noticeable change occurs at a radiation dose of 10 Mrads, the phase separation temperature increasing also as PVME content increases in the blend composition.

ACKNOWLEDGEMENTS

I would like to thank my advisor, Dr Wilkes, for his guidance, support, and advice. I appreciate his concern and help in the course of this study.

I would also like to express my appreciation and gratitude to David Rodriguez, Riley Chan, and Don Loveday for their help and advice in the laboratory.

Thanks also to all the group members for their advice.

Finally, I would like to say thanks to my friends outside the lab for their friendship and support, and a special acknowledgement to Dana Putnam for his moral support and advice throughout my study.

TABLE OF CONTENTS

LIST OF TABLES.....vii

LIST OF FIGURES.....viii

INTRODUCTION.....1

I-PHASE BEHAVIOR OF POLYMER MELTS.....5
1.1 Theory.....5
1.2 Phase Behavior of Polystyrene/Poly(vinyl methyl ether) Blends.....17

II-AN OVERVIEW OF THE RHEOLOGICAL PROPERTIES OF POLYMER MELTS.....26
2.1 Theory.....26
2.2 Temperature Dependence of Viscosity of Polymer Melts.....35
2.3 Blend Rheology of Polymer Melts.....40
2.4 Rheological Behavior of PS/PVME Blends.....48

III-EFFECTS OF RADIATION ON POLYMER BLENDS.....52
3.1 Brief History.....54
3.2 Types of radiation - Electron Beam Radiation.....55
3.3 Ionization and Excitation.....61
3.4 Chemical and Physical Changes Produced under Radiation.....67
3.4.1 Chemical Changes.....67
3.4.2 Effects of Radiation on The Physical Properties.....72
3.5 Factors Influencing the Radiation Behavior of Polymers.....79

IV-EXPERIMENTAL.....101
4.1 Materials.....101
4.2 Sample Preparation.....101
4.3 Radiation Exposure.....102
4.4 Cloud Point Temperature.....102

4.5 Gel Content Determination.....104
4.6 Rheological Measurements.....105

V-RESULTS AND DISCUSSION.....106
5.1 Characterization of the Unirradiated PS/PVME Blends.....106
5.2 Characterization of the Irradiated PS/PVME Blends.....119
Polystyrene.....121
98/2 Blend System.....122
95/5 Blend System.....128
90/10 Blend System.....134

CONCLUSION.....164

RECOMMENDATIONS FOR FUTURE STUDIES.....166

REFERENCES.....169

VITA.....173

LIST OF TABLES

Table 3.1 Classification of predominately crosslinking and chain scissioning polymers in the absence of oxygen. (ref.27).....69

Table 5.1 Values of the flow activation energy obtained with the unirradiated PS/PVME blend systems - Associated shear stress range (in N/m^2) of the rheological measurements for each system.....118

Table 5.2 Values of the flow activation energy in Kcal/mol obtained with the PS/PVME blend systems irradiated to the indicated dose. (error associate ± 2 Kcal/mol) - Associated shear stress range (in N/m^2) of the rheological measurements for each system.....163

LIST OF FIGURES

Figure 1-1a-c. Free energy diagrams of the partial molar change in free energy (ΔG_m) as a function of blend composition, Φ, for (a) completely immiscible, (b) completely miscible, and (c) partly miscible polymer blends. (ref.3).....9
Figure 1-2. Theoretical phase diagram for a symmetric ($N_A = N_B = N$) binary mixture of linear homopolymers. N, Φ_A, and χ are the polymer degree of polymerization, volume fraction of component A, and segment-segment interaction parameter, respectively. (ref.2).....10
Figure 1-3. Example of a phase diagram for polymer blends which illustrates both LCST and UCST behavior.(-) binodal line and (--) spinodal line. (ref.3).....12
Figure 1-4. Illustration of the LCST behavior. Phase diagram for a PS/PVME blend with PS and PVME M_w's of 210,000 and 51,500, respectively. (●) phase separation by nucleation and growth, (O) by spinodal decomposition. Φ = PS vol.fraction. (ref.4).....13
Figure 1-5. Time evolution of structure in phase-separating binary homopolymer mixtures by (1) nucleation and growth, and (2) by spinodal decomposition mechanisms. (ref.2).....15
Figure 1-6. Plot of the critical temperature (T_{min}) versus composition (w_{min}) of a PS/PVME blend series. PVME M_w = 99,000, and PS M_w given by (S M_w*10^{-3}). (ref.5).....18
Figure 1-7. plot of the critical temperature (T_{min}) versus $(M_w(PS))^{-1/2}$ of a PS/PVME blend series. PVME M_w = 99,000, and PS M_w given by (S M_w*10^{-3}). (ref.5).....19
Figure 1-8. Plot of $(w_{min})^{-1}$ versus $(M_w(PS))^{1/2}$ of a PS/PVME blend series. PVME M_w = 99,000, and PS M_w given by (S M_w*10^{-3}). (ref.5).....20
Figure 1-9. Chemical structures of (1) PVME and (2) PS....21
Figure 1-10. Effect of molecular weight of PS on the

phase diagram of a PS/PVME blend. Sketch of experimental binodal (-) and estimated spinodal (--). PVME M_w = 99,000 and PS M_w given by S M_w*10^{-3}. (ref.5).....23
Figure 1-11. Effect of Molecular weight of PVME on the phase diagram of a PS/PVME blend. Sketch of experimental binodal (-) and estimated spinodal (--). PS M_w = 106,000 and PVME M_w given by V M_w*10^{-3}. (ref.5).....24
Figure 2-1. Illustration of a simple shear deformation. Shear stress, shear strain, and shear rate for liquids. Newton's Law for perfectly viscous liquid. (ref.6).....28
Figure 2-2. General plot of six different types of shear stress-shear rate behavior: A, Newtonian; B, Bingham Newtonian; C, shear thinning; D, shear thickening; E, Bingham shear thinning; F, Bingham shear thickening. (ref.7).....29
Figure 2-3. Illustration of the oscillatory strain response technique.(ref.6).....31
Figure 2-4. General plot of the dynamic storage modulus (G') and loss modulus (G'') versus frequency (w) for a homogeneous high molecular weight linear polymer melt. (ref.6).....33
Figure 2-5. General sketches of four different types of instrumental geometries used for measuring rheological properties: A, parallel plates; B, Couette or coaxial cylinders; C, capillary flow; D, cone and plate. (ref.7).....34
Figure 2-6. General temperature dependence of the zero shear viscosity for different polymers: A, polyethylene; B, cellulose acetate; C, polystyrene; D, ethyl cellulose; E, poly(methyl methacrylate). (ref.7).....38
Figure 2-7. Illustration of the graphical method used to determine the viscosity at a constant shear stress and use the temperature dependence of these values to obtain the flow activation energy.....39
Figure 2-8. Zero-shear viscosity at 186°C for melts of polystyrenes. Component with narrow distribution (+), and binary blends (●). (ref.18).....44
Figure 2-9. Loss (G'') and storage (G') moduli for binary PS-blends at 160°C and their components (M_1 = 160,000 and M_2 = 670,000). experimental values (dots) and calculated values (lines) for the blends. (ref.19).....46
Figure 2-10. Loss (G'') and storage (G') moduli for binary PS-blends (M_1 = 12,900 and M_2 = 289,000). w_2 = weight fraction of component 2. (ref.17).....47

Figure 2-11. Storage modulus (G′) versus loss modulus (G′′) of a 80/20 wt % PS/PVME blend at temperatures below and above phase separation. (ref.20).....50
Figure 3-1. Schematic view of crosslinking a dispersed phase B (in phase A) by using electron beam irradiation between the blending and final processing step to achieve morphology fixation in the polymer blend. (ref.24).....53
Figure 3-2. Electromagnetic spectrum and assignments of various types of radiation. (ref.26).....56
Figure 3-3a-c. Sketches of (a) a typical photoelectric absorption process, (b) compton scattering process, and (c) pair production process. (ref.27).....59
Figure 3-4. Stopping power of various materials for fast electrons (energy loss per mg/cm^2). (ref.29).....63
Figure 3-5. Ionization density versus penetration for single irradiation from one side. (ref.29).....64
Figure 3-6. Illustration of the normalized depth-dose function. (ref.30).....66
Figure 3-7. Tensile strength and elongation at break of irradiated polyethylene versus irradiation dose. low density polyethylene, M_w = 21,000, irradiated to 800 kV electrons, tested at room temperature. (ref.29).....74
Figure 3-8. Dependence of $s + s^{0.5}$ on reciprocal of radiation dose in the irradiation of various samples of polyethylene: 1, linear polyethylene with M_n = 10,000; 2, linear polyethylene with M_n = 17,000; 3, branched polyethylene with M_n = 45,000; 4, branched polyethylene with M_n = 58,000. (ref.27).....78
Figure 3-9. Plot of the radiation-chemical yields for crosslinking (G(c.l.) = G(X)) as a function of 1/T of polyethylene (in the plot above, the results are normalized with other data on the basis of G(X) = 1 at -80°C and at -196°C). (ref.40)..... 83
Figure 3-10. Gel fraction versus irradiation temperature for polyethylene post-treated by (○) storage at 140°C for two hours, and (●) stored in air for three days. (ref.41).....85
Figure 3-11. Decrease in sol fraction with electron dose for 18 μ specimen irradiated in air or in vacuum. (ref.45).....88
Figure 3-12. schematic phase diagram showing the effect of crosslinking on the PS/PVME blend investigated. (ref.46).....90
Figure 3-13. plot of gel fraction versus composition of miscible PS/PVME blends that have been irradiated to the indicated dose. (ref.3).....91

Figure 3-14. Plots of gel fraction versus composition of PS/PVME blends that have irradiated to 50 Mrads after phase separation at 160°C for the indicated times. (ref.3).....93
Figure 3-15. Plot of the glass transition temperatures Tg versus composition for PS/PVME blends. (ref.3).....95
Figure 3-16. DSC scans of miscible PS/PVME blends. (ref.3).....96
Figure 3-17. DSC scans of PS/PVME blends that have been phase separated at 160°C for two minutes followed by irradiation to 100 Mrads. (ref.3).....97
Figure 3-18. Plot of the cloud point temperature versus composition (wt % PVME) for a series of PS/PVME blends. (ref.3).....98
Figure 4-1. Schematic drawing of the ESI CB150 electrocurtain: electron beam chamber and conveyor system.....103
Figure 5-1. Plot of the cloud point temperature, Ts, versus composition (wt % PVME) for the unirradiated PS/PVME blends investigated in this study.....107
Figure 5-2. Plot of the dynamic viscosity, eta', versus frequency, w, at different temperatures for pure unirradiated PS.....110
Figure 5-3. Plot of the dynamic viscosity, eta', versus frequency, w, at different temperatures for the unirradiated 98/2 PS/PVME blend.....111
Figure 5-4. Plot of the dynamic viscosity, eta', versus frequency, w, at different temperatures for the unirradiated 95/5 PS/PVME blend.....112
Figure 5-5. Plot of the dynamic viscosity, eta', versus frequency, w, at different temperatures for the unirradiated 90/10 PS/PVME blend.....113
Figure 5-6. Plot of the dynamic viscosity, eta', versus frequency, w, at different temperatures for pure unirradiated PVME.....114
Figure 5-7. Arrhenius plots of the log of the dynamic viscosity obtained at a constant shear stress for (1) pure unirradiated PS, and (2) unirradiated 2/98 PVME/PS blend.....116
Figure 5-8. Arrhenius plots of the log of the dynamic viscosity obtained at a constant shear stress for (1) unirradiated 5/95 PVME/PS blend, (2) unirradiated 10/90 PVME/PS blend, and (3) pure unirradiated PVME.....117
Figure 5-9. Plot of the cloud point temperature, Ts, versus composition (wt % PVME) for PS/PVME blends irradiated to the indicated dose.....120
Figure 5-10. Plot of the dynamic viscosity, eta', versus frequency, w, at different temperatures for pure PS

irradiated to 2 Mrads.....123
Figure 5-11. Plot of the dynamic viscosity, eta', versus frequency, w, at different temperatures for pure PS irradiated to 5 Mrads.....124
Figure 5-12. Plot of the dynamic viscosity, eta', versus frequency, w, at different temperatures for pure PS irradiated to 10 Mrads.....125
Figure 5-13. Superposition of the dynamic viscosity-frequency responses of pure PS (1) unirradiated (0 Mrad), and (2) irradiated to 2 Mrads, at 2 different temperatures.....126
Figure 5-14. Superposition of the dynamic viscosity-frequency responses of pure PS (1) unirradiated (0 Mrad), and (2) irradiated to 10 Mrads, at 2 different temperatures.....127
Figure 5-15. Plot of the dynamic viscosity, eta', versus frequency, w, at different temperatures for the 98/2 PS/PVME blend irradiated to 2 Mrads.....129
Figure 5-16. Plot of the dynamic viscosity, eta', versus frequency, w, at different temperatures for the 98/2 PS/PVME blend irradiated to 5 Mrads.....130
Figure 5-17. Plot of the dynamic viscosity, eta', versus frequency, w, at different temperatures for the 98/2 PS/PVME blend irradiated to 10 Mrads.....131
Figure 5-18. Superposition of the dynamic viscosity-frequency responses of the 98/2 PS/PVME blend (1) unirradiated (0 Mrad), and (2) irradiated to 2 Mrads, at 2 different temperatures.....132
Figure 5-19. Superposition of the dynamic viscosity frequency responses of the 98/2 PS/PVME blend (1) unirradiated (0 Mrad), and (2) irradiated to 10 Mrads, at 2 different temperatures.....133
Figure 5-20. Plot of the dynamic viscosity, eta', versus frequency, w, at different temperatures for the 95/5 PS/PVME blend irradiated to 2 Mrads.....135
Figure 5-21. Plot of the dynamic viscosity, eta', versus frequency, w, at different temperatures for the 95/5 PS/PVME blend irradiated to 5 Mrads.....136
Figure 5-22. Plot of the dynamic viscosity, eta', versus frequency, w, at different temperatures for the 95/5 PS/PVME blend irradiated to 10 Mrads.....137
Figure 5-23. Superposition of the dynamic viscosity-frequency responses of the 95/5 PS/PVME blend (1) unirradiated (0 Mrad), and (2) irradiated to 10 Mrads, at 230°C.....138
Figure 5-24. Superposition of the dynamic viscosity-fre quency responses of the 95/5 PS/PVME blend (1) unirradiated (0 Mrad), and (2) irradiated to 2 Mrads, at 2 different temperatures.....139

Figure 5-25. Plot of the dynamic viscosity, eta′, versus frequency, w, at different temperatures for the 90/10 PS/PVME blend irradiated to 2 Mrads.....141
Figure 5-26. Plot of the dynamic viscosity, eta′, versus frequency, w, at different temperatures for the 90/10 PS/PVME blend irradiated to 5 Mrads.....142
Figure 5-27. Plot of the dynamic viscosity, eta′, versus frequency, w, at different temperatures for the 90/10 PS/PVME blend irradiated to 10 Mrads.....143
Figure 5-28. superposition of the dynamic viscosity-frequency responses of the 90/10 PS/PVME blend (1) unirradiated (0 Mrad), and irradiated to 2 Mrads, at 2 different temperatures.....145
Figure 5-29. Superposition of the dynamic viscosity-frequency responses of the 90/10 PS/PVME blend (1) unirradiated (0 Mrad), and (2) irradiated to 10 Mrads, at 2 different temperatures.....146
Figure 5-30. Plot of the gel composition (PVME wt %) versus blend composition (PVME wt %) of miscible PS/PVME blends. (data taken from (3)).....147
Figure 5-31. Plots, at the indicated temperatures, of the storage modulus (G′) versus loss modulus (G′′) of the 98/2 PS/PVME blend (1) unirradiated (0 Mrad), and (2)irradiated to 10 Mrads.....149
Figure 5-32. Plots, at the indicated temperatures, of the storage modulus (G′) versus loss modulus (G′′) of the 95/5 PS/PVME blend (1) unirradiated (0 Mrad), and (2) irradiated to 10 Mrads.....150
Figures 5-33. Plots, at the indicated temperatures, of the storage modulus (G′) versus loss modulus (G′′) of the 90/10 PS/PVME blend (1) unirradiated (0 Mrad), and (2) irradiated to 10 Mrads.....151
Figure 5-34. Plot of the dynamic viscosity, eta′, versus dose and composition (wt % PVME) obtained at 170°C and 0.2 rad/s.....153
Figure 5-35. Arrhenius plot of the log of the dynamic viscosity obtained at a constant shear stress for pure PS (1) unirradiated (0 Mrad), and (2) irradiated to 2 Mrads.....155
Figure 5-36. Arrhenius plot of the log of the dynamic viscosity obtained at a constant shear stress for pure PS (1) irradiated to 5 Mrads, and (2) irradiated to 10 Mrads.....156
Figure 5-37. Arrhenius plot of the log of the dynamic viscosity obtained at a constant shear stress for the 2/98 PVME/PS blend (1) unirradiated (0 Mrad), and (2) irradiated to 2 Mrads.....157
Figure 5-38. Arrhenius plot of the log of the dynamic viscosity obtained at a constant shear stress for

the 2/98 PVME/PS blend (1) irradiated to 5 Mrads, and (2) irradiated to 10 Mrads.....158
Figure 5-39. Arrhenius plot of the log of the dynamic viscosity obtained at a constant shear stress for the 5/95 PVME/PS blend (1) unirradiated (0 Mrad), and (2) irradiated to 2 Mrads.....159
Figure 5-40. Arrhenius plot of the log of the dynamic viscosity obtained at a constant shear stress for the 5/95 PVME/PS blend (1) irradiated to 5 Mrads, and (2) irradiated to 10 Mrads.....160
Figure 5-41. Arrhenius plot of the log of the dynamic viscosity obtained at a constant shear stress for the 10/90 PVME/PS blend (1) unirradiated, and (2) irradiated to 2 Mrads.....161
Figure 5-42. Arrhenius plot of the log of the dynamic viscosity obtained at a constant shear stress for the 10/90 PVME/PS blend (1) irradiated to 5 Mrads, and (2) irradiated to 10 Mrads.....162

INTRODUCTION:

The effects of radiation on polymeric materials have gained interest in recent years. Research in the subject has been greatly stimulated by a numbers of factors both technical and scientific. In reactor technology, there has been a constant search for radiation-resistant materials, capable of long-term use in the presence of intense radiation. In the chemical industry, the possibility appeared of inducing beneficial changes in structure by use of radiation. Here the interest is directed towards materials which are chemically sensitive to radiation.

For example, small chemical changes, such as are produced by low doses of radiation, cause large changes in the physical properties of some polymers. This fact has attracted attention to the radiation chemistry of polymers. Exposure to high energy radiation may therefore be useful to improve their process abilities and applications. In this study, the author is particularly interested in investigating the irradiation and melt rheological behavior of a blend composed of two homopolymers, polystyrene, (PS), and poly(vinyl methyl ether) (PVME). Indeed, during the past two decades, there has been

scientific and commercial progress in the area of polymer blends, driven by the observations that novel materials, and therefore novel properties, can be realized more rapidly and economically by blending two or more homopolymers together than by developing a new homopolymer. Blend systems, composed of existing materials, can be produced more rapidly as new polymers, giving more time to manufacturers to respond to new market requirements at a potentially lower cost. Since the properties of a blend system are functions of both components and composition, an existing blend can often be easily modified to meet performance and cost objectives.

The purpose of this thesis is to study the effects of electron-beam radiation on the rheological properties of a series of polystyrene/poly(vinyl methyl ether) PS/PVME blends. This system is composed by two different components in terms of their radiation resistance, the principal goal is to modify the rheological response of the blend by varying the composition and the radiation dose applied. Most thermoplastics pass through the melt state during their process into useful forms by extrusion or molding. Behavior during melt processing can be very complicated due to the viscoelastic nature of polymeric systems. Rapid and efficient processing requires careful control of flow properties, which depend on molecular characteristics, especially molecular weight and molecular weight distribution. The blend composed

of PS/PVME has been chosen for several reasons: (1)- since PS and PVME have significantly different sensitivities to radiation induced crosslinking, the analysis of the system crosslinking behavior may be particularly interesting. (2)- although the two components are chemically different at equilibrium, they display miscibility over the entire composition range at room temperature. The work presented in this thesis considers the effects of dose and blend composition on the rheological response using electron-beam irradiation. The purpose is to modify the viscosity of PS by investigating the effects of adding a small amount of PVME, and by inducing some grafting between the two components under irradiation. As a result, the viscosity shear rate response may possibly be significantly altered. Such modifications, if noted, could be used to improve melt processes like blow molding where a higher viscosity, at low shear rates, would prevent the collapse or sagging of the tube of molten polymer prior to expansion.

The first section of this study will provide a review of the recent literature related to the effects of irradiation on polymers, especially on the blend of interest in this study composed of PS/PVME. Prior to discussion of the research carried out by the author, a review of the recent literature related to the effects of irradiation on polymers will be presented. In the first part some background on the phase

behavior of polymer blends will be provided, followed by some discussion of their rheological properties and response, with an emphasis on the blend of interest in this work. Finally, this review will present the effects of radiation on polymer blends, a limited subject in literature. The next section of the thesis will address the experimental work carried out. The final section will provide the results and discussion, as well as present the conclusions and suggested future studies.

I-PHASE BEHAVIOR OF POLYMER MELTS

1.1 Theory

Chemically different polymers can be mixed together into one material in many ways thereby providing a wide range of phase behavior that directly influences the associated physical properties and final applications.

The phase behavior is governed by a balance between enthalpy H, (H = U + PV where U, P, and V represent the system internal energy, pressure and volume respectively), absolute temperature T, and entropy S, that constitute the Gibbs free energy G

$$G = H - TS \qquad (1)$$

$$\Delta G_m = \Delta H_m - T\Delta S_m \qquad (2)$$

The way the free energy of mixing ΔG_m, given by Equation (2), is affected by composition and temperature controls the phase behavior of mixtures. Fifty years ago, Flory (1) and Huggins, independently, estimated the change in free energy per segment, ΔG_m, associated with mixing random walk (Gaussian) polymer chains in an incompressible lattice,

$$\Delta G_m = \Delta H_m - T\Delta S_m = RT(N\Phi_1\Phi_2\chi_{12} + (x_1 Ln\Phi_1 + x_2 Ln\Phi_2)) \qquad (3)$$

where R is the gas constant

T is the temperature

N is the total number of lattice sites in the system

Φ_i is the volume fraction of species i (i=1,2)

x_i is the mole fraction of species i

χ_{12} is the interaction parameter between species 1 and 2.

Mixing increases the system randomness, and therefore, ΔS_m naturally increases, thereby promoting the free energy of mixing to decrease. The enthalpy of mixing, ΔH_m, can either increase or decrease ΔG_m, depending on the sign of χ_{12}, its value being temperature dependent and often concentration dependent. From the second law of thermodynamics, equilibrium occurs in a closed system when the Gibbs Free Energy is at a minimum. Furthermore, for the process to be spontaneous, the change in Gibbs Free Energy must be negative and the second partial derivative must be positive.

$$\Delta G_m < 0 \tag{4}$$

$$\frac{(\partial^2 \Delta G_m)}{(\partial \Phi_i^2)_{T,P}} > 0 \tag{5}$$

The phase behavior can be predicted using Equation (3), based on the standard criteria for equilibrium, the limits of

stability, and critical point at constant temperature and pressure

equilibrium :

$$\frac{\partial \Delta G_m(\Phi_1')}{\partial \Phi_1} = \frac{\partial \Delta G_m(\Phi_1'')}{\partial \Phi_1} \tag{6}$$

stability:

$$\frac{\partial^2 \Delta G_m}{\partial_1^2 \Phi} = 0 \tag{7}$$

critical point:

$$\frac{\partial^3 \Delta G_m}{\partial \Phi_1^3} = 0 \tag{8}$$

where the subscripts refer to the separate phases.

Figures 1-1a-c represent the free energy diagrams as a function of blend composition, Φ, for (a) completely immiscible, (b) completely miscible and (c) partly miscible polymer blends. In the first case, the system is in

equilibrium only when the two components are completely separated from each other. Any mixing will provide an increase in the free energy of the blend, and therefore will not spontaneously occur. For a completely miscible blend, on the contrary, any demixing will promote a rise in the free energy of at least one of the two phases, and therefore, will not occur.

Figure 1-1c shows a free energy of mixing diagram for a blend that can undergo phase separation. Between the points A and B, two phases can appear by phase separation, resulting in the formation of two phases with compositions given by points A and B at equilibrium. Outside the range between A and B, phase separation cannot occur spontaneously because it would result in an increase in the free energy.

The case where NA = NB = N is illustrated in Fig.1-2. The solid curve represents the equilibrium solution of Equation (4). Inside this curve, the mixture separates into two phases with composition Φ' and Φ''. Between the solid and dashed curves, a homogeneous mixture is thermodynamically metastable (the system must overcome a free energy or activation barrier to undergo phase separation), while inside the dashed curve, it is thermodynamically unstable. The critical point is given at the intersection between the equilibrium and stability curves.

Phase separation can either occur by increasing the

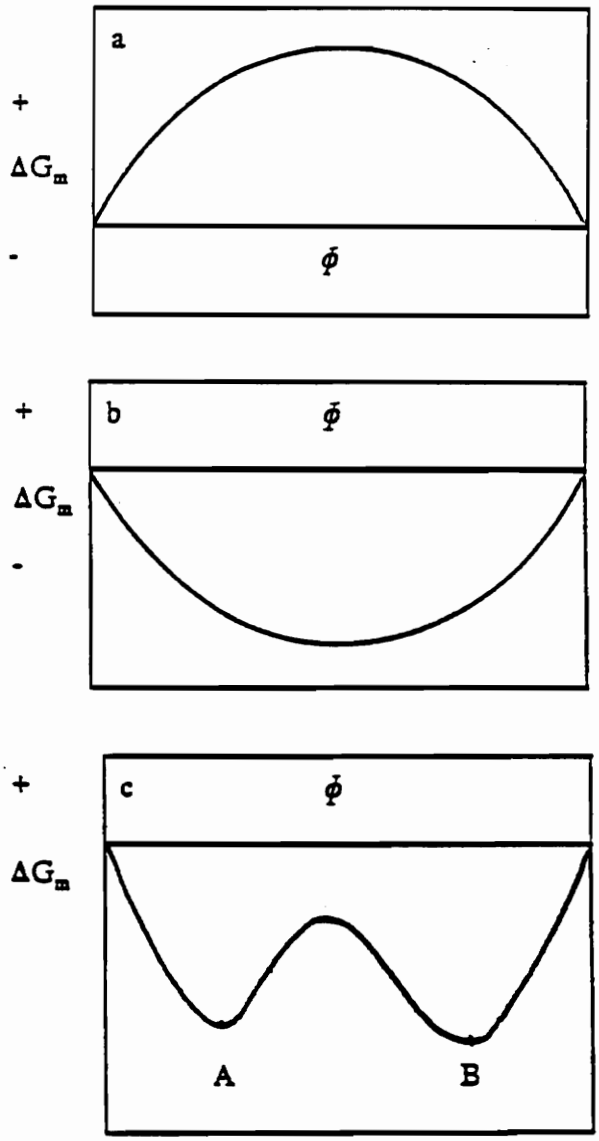

Figure 1-1a-c. Free energy diagrams of the partial molar change in free energy (ΔG_m) as a function of blend composition, Φ, for (a) completely immiscible, (b) completely miscible, and (c) partly miscible polymer blends. (ref.3)

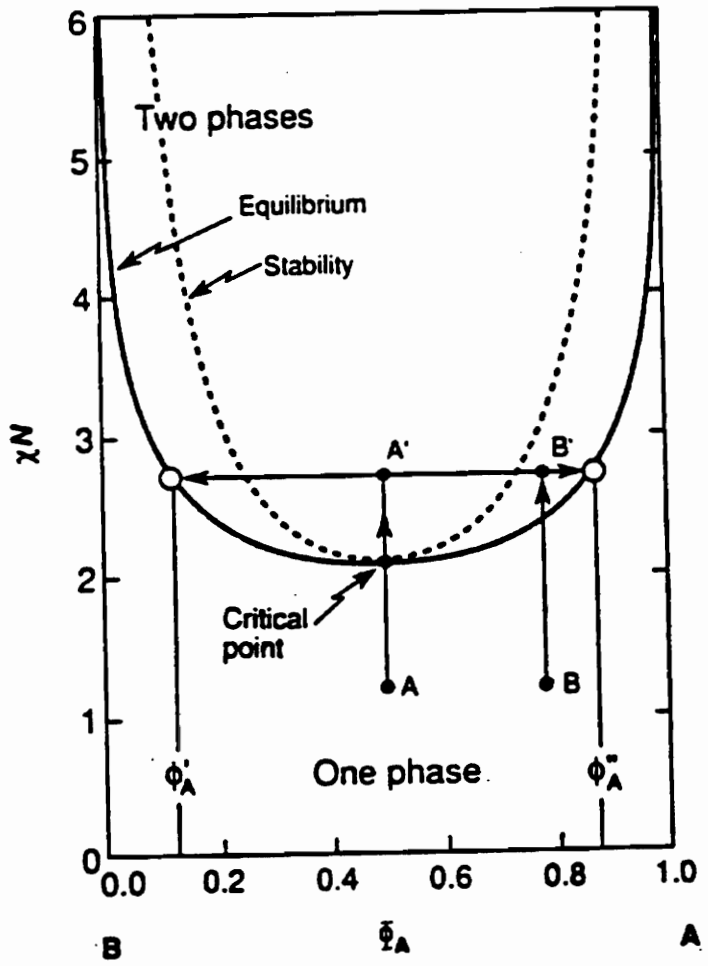

Figure 1-2. Theoretical phase diagram for a symmetric ($N_A = N_B = N$) binary mixture of linear homopolymers. N, Φ_A, and χ are the polymer degree of polymerization, volume fraction of component A, and segment-segment interaction parameter, respectively. (ref.2)

system temperature or by decreasing it. The first response has been called the lower critical solution temperature (LCST), and the second one, the upper critical solution temperature (UCST). Figure 1-3 illustrates these two types of behavior. The dashed lines represent the compositions corresponding to the inflection points between the two minima in Fig.1-1c versus temperature. They are called the spinodal lines and represent boundaries between the metastable and unstable states. They are significant of the mechanisms and kinetics of the phase separation processes taking place in thermodynamically unstable multicomponent systems. The solid line is the binodal curve illustrating the boundaries between the stable and metastable states, and define the equilibrium-phase behavior.

The Flory-Huggins theory predicts only the existence of UCST behavior. Figure 1-4 depicts a lower critical solution temperature (LCST). As shown, as the temperature is raised from the miscible region, phase separation occurs and the method of the phase separation is generally by a nucleation and growth process, that will be described later. In the Flory-Huggins theory, the interaction parameter is only a function of temperature, but in practice, it is often a function of concentration as well. On the other hand, the new theories, called equation-of-state theories, can predict LCST-type behavior without requiring the interaction parameter to

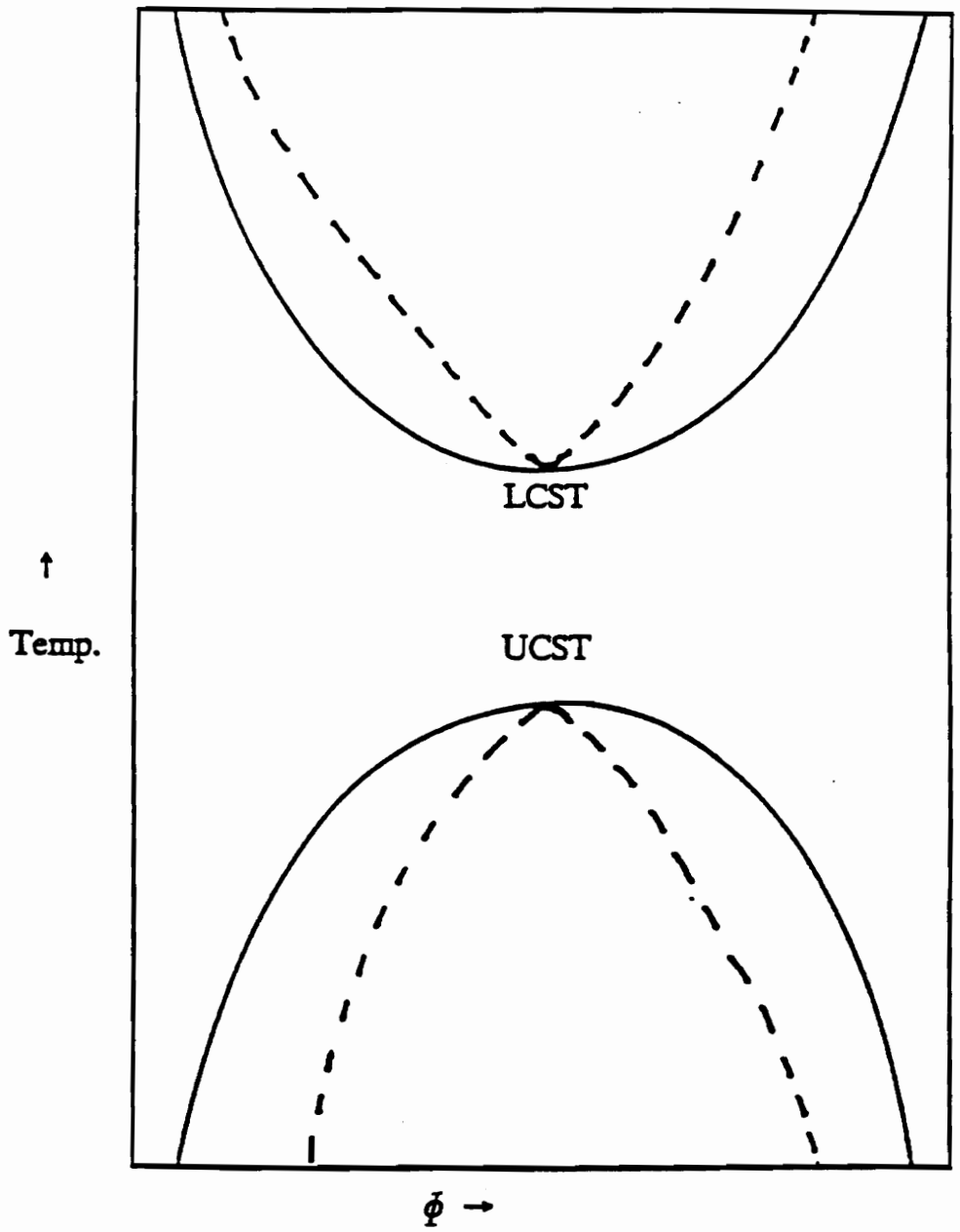

Figure 1-3. Example of a phase diagram for polymer blends which illustrates both LCST and UCST behavior. (-) binodal line and (--) spinodal line. (ref.3)

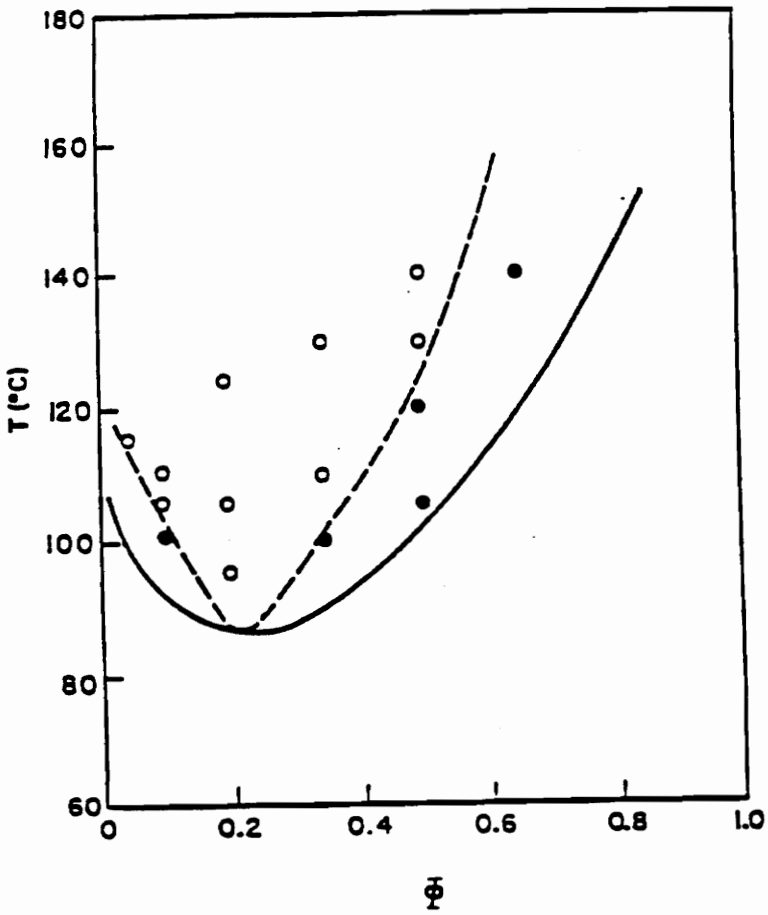

Figure 1-4. Illustration of the LCST behavior. Phase diagram for a PS/PVME blend with PS and PVME M_w's of 210,000 and 51,500, respectively. (●) phase separation by nucleation and growth, (O) by spinodal decomposition. Φ = PS vol. fraction. (ref.4)

be a function of temperature. According to these new theories, the preferential existence of LCST behavior is a manifestation of differences in the thermal expansion coefficients of the blend components.

Phase separation can occur by two different mechanisms, depending on the state of the blend system, nucleation and growth, or spinodal decomposition. These two processes are shown in Fig.1-5. If the system is within the metastable region, the phase separation will proceed by the nucleation and growth mechanism, whereas if the system is in the unstable region (within the spinodal lines), then spinodal decomposition will occur.

Nucleation and growth is characterized by the formation and growth of small droplets of a minority phase over time in a homogeneous mixture. This results in a finely dispersed two-phase structure. The final droplet size and the inter-particle size are both controlled by the time scale of the experiment and by the rate of diffusion.

Spinodal decomposition, on the other hand, is a spontaneous process resulting in a disordered bicontineous two-phase structure. The reaction starts by the appearance, at the beginning, of a fine, uniformly dispersed precipitate which slowly and gradually coarsens and develops into distinct regions of coexisting stable phases. Two essential features characterize spinodal mechanism: (1)- a true instability, i.e.

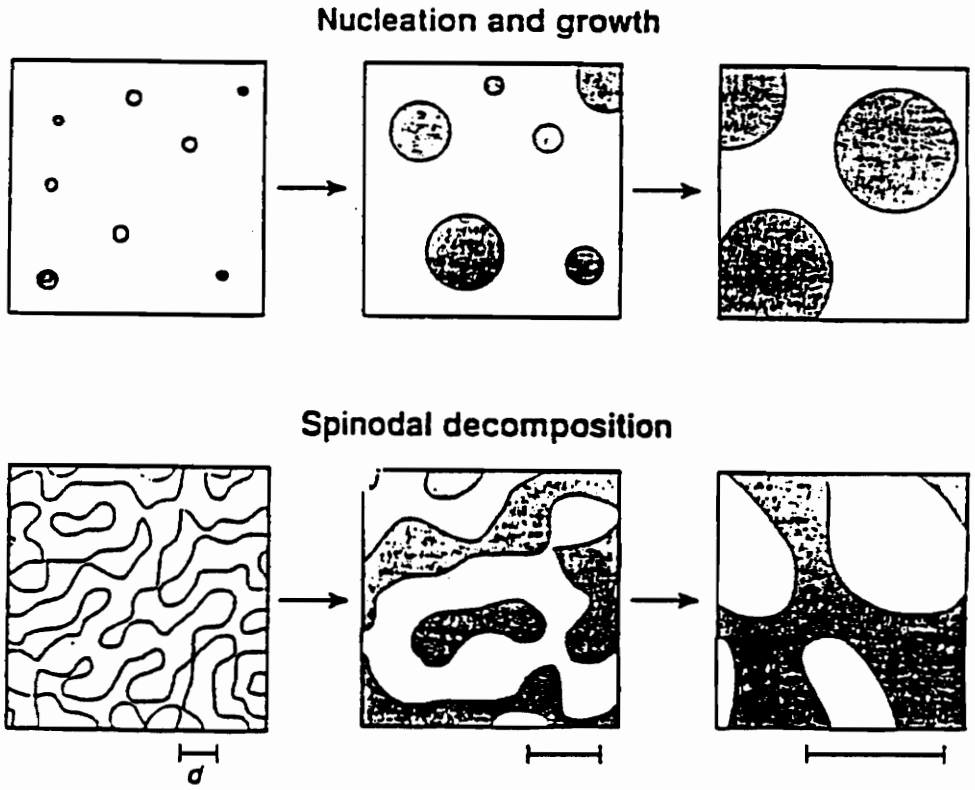

Figure 1-5. Time evolution of structure in phase-separating binary homopolymer mixtures by (1) nucleation and growth, and (2) by spinodal decomposition mechanisms. (ref.2)

in contrast to nucleation, spinodal decomposition is not an activated process. (2)- the process is limited by diffusion, i.e. the stages of precipitation and coarsening occur increasingly slowly because of the diffusion of material occurs across larger and larger distances. In both mechanisms, coarsening in the late stage of phase separation can be explained because the process minimizes the interfacial tension by decreasing the interfacial area.

Ubrich et al. (5) have investigated the influence of polymer chain length (molecular weight) on the phase diagram of PS/PVME by systematically varying the component molecular weights. Measurements were carried out using fluorescence microscopy. Some experiments were performed under continuous heating at a rate range from 0.2 to 16 $°C.min^{-1}$, while others were carried out under isothermal conditions, waiting at least 30 min for the phase separation to occur. The temperature at which the phase separation is detected depends on both the blend composition and the heating rate. The molecular weight dependence of $\Delta T = T_{16} - T_{min}$, defined to be the difference between the temperatures at which the phase separation is detected in experiments at $16°C.min^{-1}$ and under isothermal conditions, is shown in Fig.1-6. Below a value of 70,000 g/mol for the PS weight-average molecular weight $M_w(PS)$, ΔT is zero, and then it increases linearly with $M_w(PS)$. As shown in Fig.1-6, T_{min} varies linearly with w_{min}, the PS weight

fraction corresponding to the minima of the boundaries curves. The same trend has been observed with T_{min} versus $M_w(i)^{-1/2}$, illustrated in Fig.1-7. Therefore, a linear relation exists between $(w_{min}(i))^{-1}$ and $(M_w(i))^{1/2}$, as shown in Fig.1-8. The general equation can be written in the form

$$(w_{min}(i))^{-1} = 1 + k(M_w(i))^{1/2} \qquad (9)$$

The specific phase behavior of the polystyrene/poly(vinyl methyl ether) PS/PVME blend will now be presented.

1.2 Phase behavior of Polystyrene/Poly(vinyl methyl ether) Blends

The particular blend composed of polystyrene and poly(vinyl methyl ether), PS/PVME, is of interest in this study, since the author will investigate the rheological properties of this miscible blends. The chemical structure of each polymer is displayed in Fig.1-9. The two components form a unique pair since they display compatibility over the entire composition range at room temperature (5).

Nishi et al. (4) have studied the thermally induced phase separation behavior of PS/PVME blends using light transmission, optical transmission, and pulsed NMR methods. The process of phase separation can occur either by spinodal decomposition or by the nucleation and growth mechanism for this particular pair, depending on composition and temperature. The blend displays LCST behavior with a critical point at a polystyrene composition of about 0.2 and a

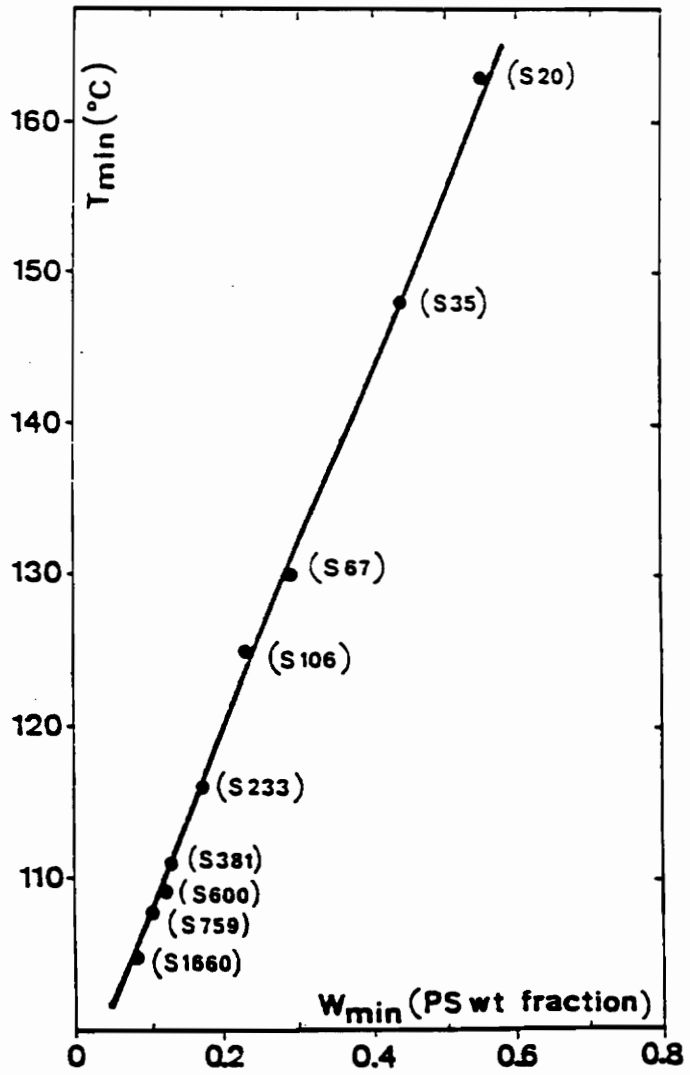

Figure 1-6. Plot of the critical temperature (T_{min}) versus composition (w_{min}) of a PS/PVME blend series. PVME M_w = 99,000, and PS M_w given by (S M_w*10^{-3}). (ref.5)

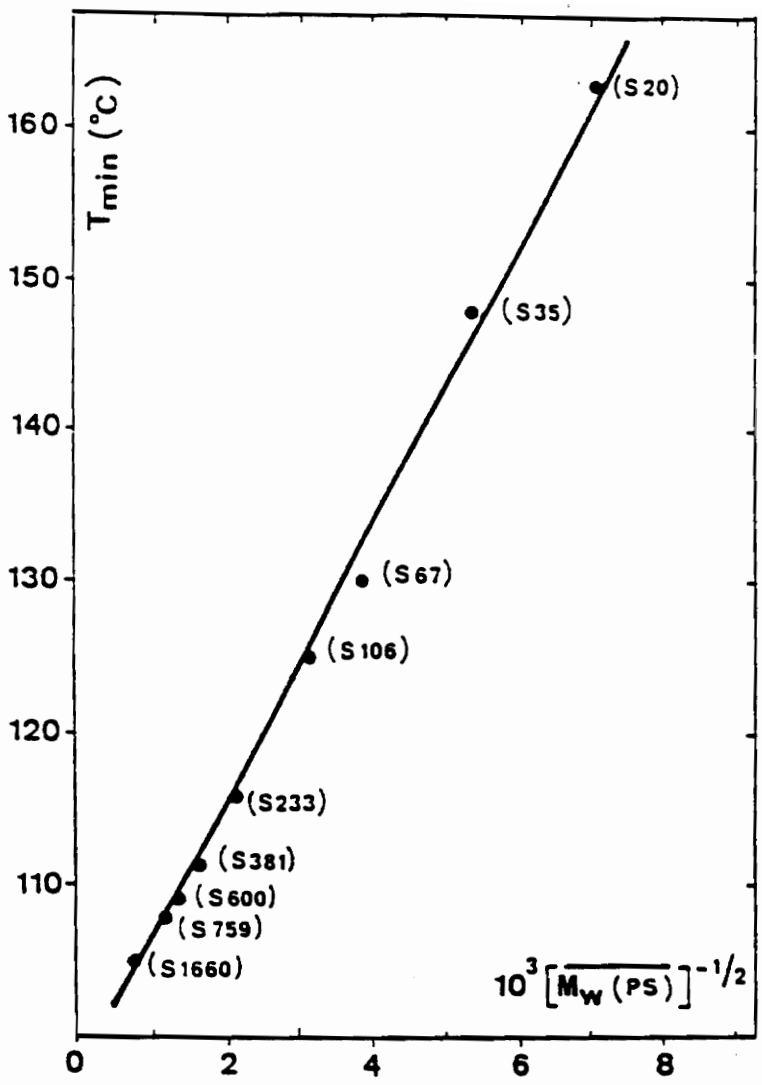

Figure 1-7. Plot of the critical temperature (T_{min}) versus $(M_w(PS))^{-1/2}$ of a PS/PVME blend series. PVME M_w = 99,000, and PS M_w given by (S M_w*10^{-3}). (ref.5)

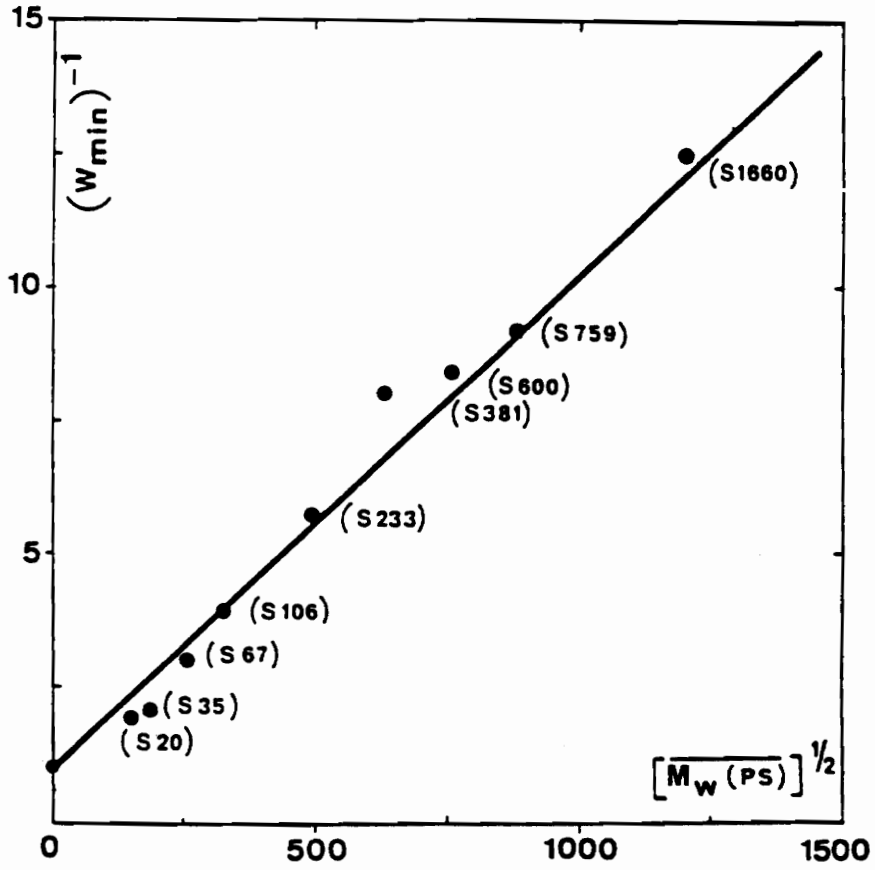

Figure 1-8. Plot of $(w_{min})^{-1}$ versus $(M_w(PS))^{1/2}$ of a PS/PVME blend series. PVME M_w = 99,000, and PS M_w given by (S M_w* 10^{-3}). (ref.5)

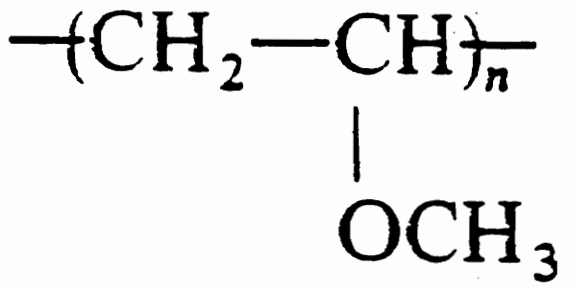

PVME

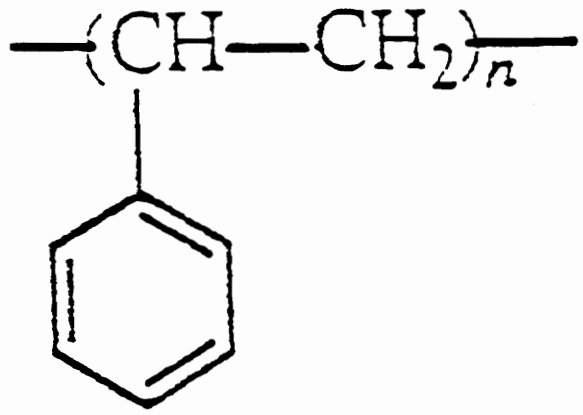

PS

Figure 1-9. Chemical structures of (1) PVME and (2) PS.

temperature of 85°C with PS and PVME weight average molecular weights of 21,000 and 51,500 respectively.

Figure 1-4 shows a phase diagram of this specific system. It must be stressed that this phase behavior is *only valid for this specific blend*, the phase diagram being strongly influenced by the characteristics of the components. The molecular weight of each homopolymer is one of the most influential factors. To illustrate the effect of this parameter, Ubrich et al (5) have studied the phase diagram of different PS/PVME blends, varying the molecular weight of one component while keeping the other constant. As shown in Fig.1-10, the critical point temperature and the polystyrene weight fraction decrease as the molecular weight of polystyrene increases. This is indicative of a reduction of the blend compatibility by a lowering of the critical point temperature T_c. The same decrease of the critical point temperature is observed when the molecular weight of poly(vinyl methyl ether) is increased. In this case, illustrated in Fig.1-11, the shift of the critical polystyrene weight fraction, as the PVME molecular weight increases, is more pronounced. It goes from 25 wt% polystyrene to 80 wt% polystyrene when the molecular weight of poly(vinyl methyl ether) goes from 45,000 g/mol to 1330,000.

This behavior can be explained using the Gibbs Free Energy from the Flory-Huggins theory. As the molecular weight

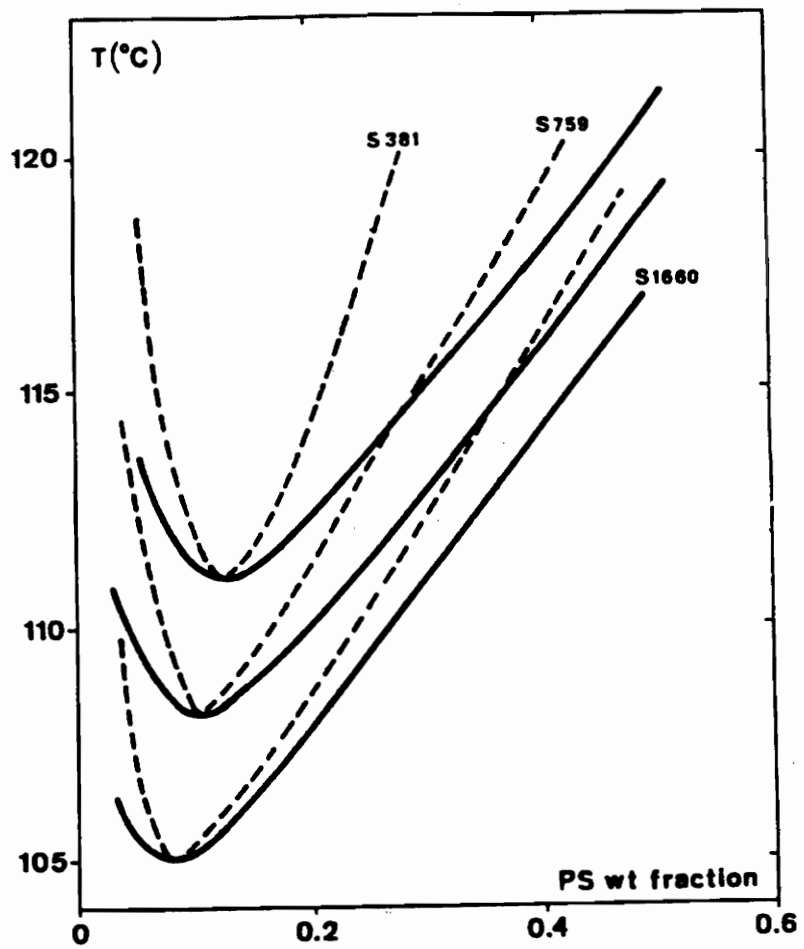

Figure 1-10. Effect of molecular weight of PS on the phase diagram of a PS/PVME blend. Sketch of experimental binodal (-) and estimated spinodal (--). PVME M_w = 99,000 and PS M_w given by S M_w*10^{-3}. (ref.5)

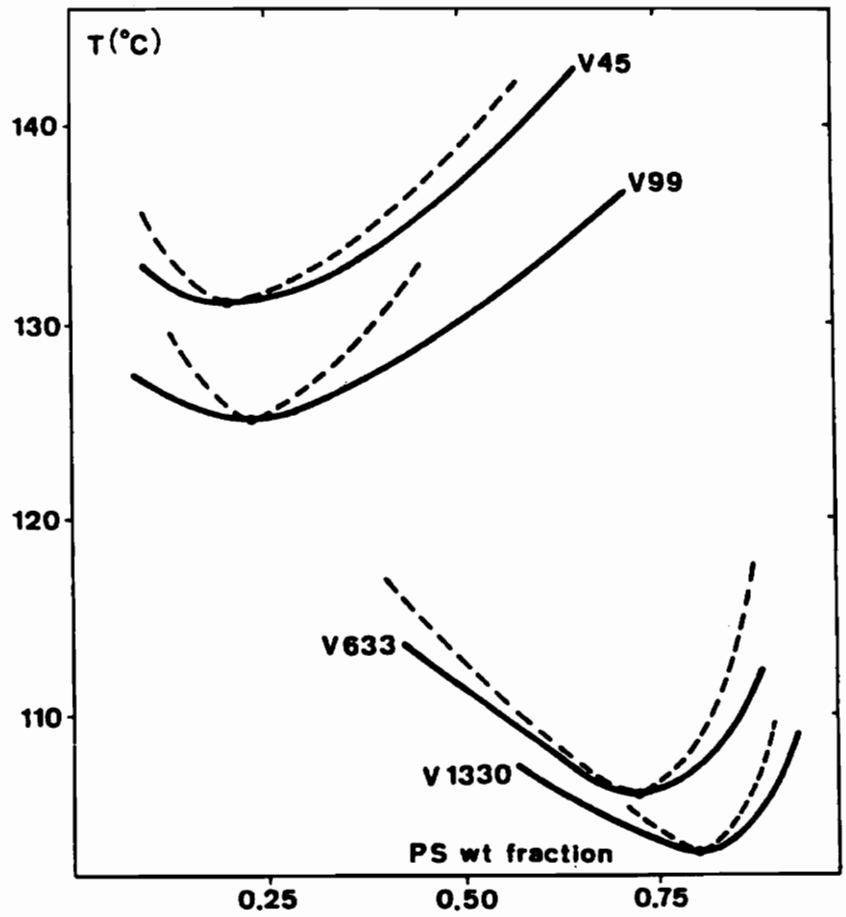

Figure 1-11. Effect of molecular weight of PVME on the phase diagram of a PS/PVME blend. Sketch of experimental binodal (-) and estimated spinodal (--). PS M_w = 106,000 and PVME M_w given by V M_w*10^{-3}. (ref.5)

of one component is increased, the mole fraction for a given volume fraction is reduced. Therefore, as shown in Eq.(3), the terms ($Ln\Phi_i$) reach a lower value. This term being the contribution from the entropy of mixing, it is always negative. Hence, the entropy contribution is reduced, and the Gibbs Free energy is increased, resulting in a reduction of the compatibility of the system. These observations illustrate the molecular weight influence on the phase diagram.

The next section will focus on the rheological properties of polymer melts with an emphasis on the blend of interest, since the purpose of this study is to investigate the effects of radiation on the rheology of the PS/PVME blend.

II-AN OVERVIEW OF THE RHEOLOGICAL PROPERTIES OF POLYMER MELTS

2.1 Theory

The rheological properties of polymer melts affect both processing behavior and final properties. Many of the current methods of characterization utilize linear viscoelastic response under dynamic conditions. The objectives of such measurements are to correlate the observed rheological response with molecular structure, and to utilize this information to develop simple methods for relating such fundamental rheological parameters to more complex flows encountered in real processing environnements.

Rheology, by definition, is the study of the deformation and flow of materials. A polymer solution or melt can be deformed by shear, tensile (elongation), or hydrostatic bulk deformation. If the deformation is small or applied slowly, the molecular arrangements stay close to equilibrium and the mechanical response reflects the dynamic processes that go on. This is the domain of linear viscoelasticity. A fluid is said to be viscoelastic if it displays both energy dissipation and energy storage in its mechanical properties.

Figure 2-1 shows an element undergoing deformation by shear, due to a force F applied on the top surface of area A.

Shear stress, τ, is the shear force per unit area of the surface it acts upon. Shear strain, γ, is the displacement per unit distance normal to the shear plane. shear rate $\dot{\gamma}$ is defined as the rate of change of shear strain with time. This is an important parameter related to the speed of the shearing process. When a shear stress is imposed on a material, the viscosity expresses its resistance to flow, and relates the shear stress to the applied shear rate. The shear stress-strain behavior for Newtonian fluids is given at the bottom of Fig.2-1. The Newtonian fluids exhibit a shear stress that is a linear function of shear rate. The viscosity, η, is independent of $\dot{\gamma}$ in this case. Polymer melts often deviate from this linear response, particularly as $\dot{\gamma}$ increases. Indeed, Fig.2-2 illustrates the shear stress - shear rate behavior of several types of fluids, the examples being: shear-thinning (C), the shear-thickening (D), and the Bingham Newtonian or plastic Newtonian fluid behavior (B) that flows after a certain stress level is imposed, and called the critical shear stress or yield stress; above this value, the fluid can flow as any of the above types, shear thinning, shear thickening, or Newtonian.

A useful expression often used to describe the flow behavior is the power law equation given in a very generalized form (neglecting dimensions) as

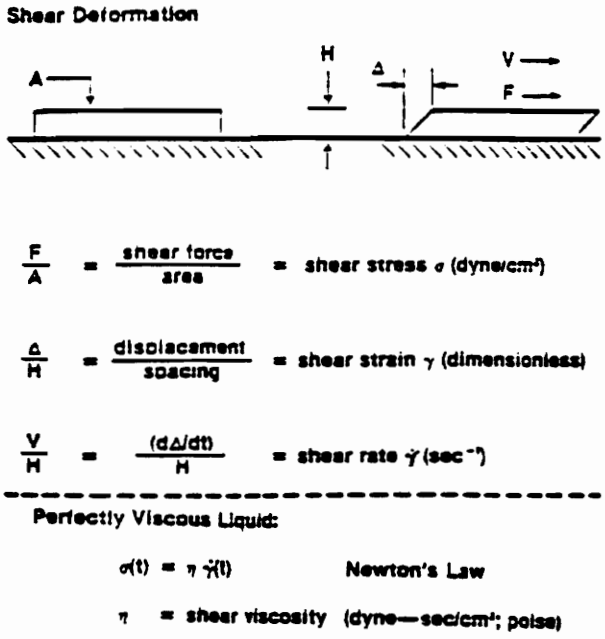

Figure 2-1. Illustration of a simple shear deformation. Shear stress, shear strain, and shear rate for liquids. Newton's Law for perfectly viscous liquid. (ref.6)

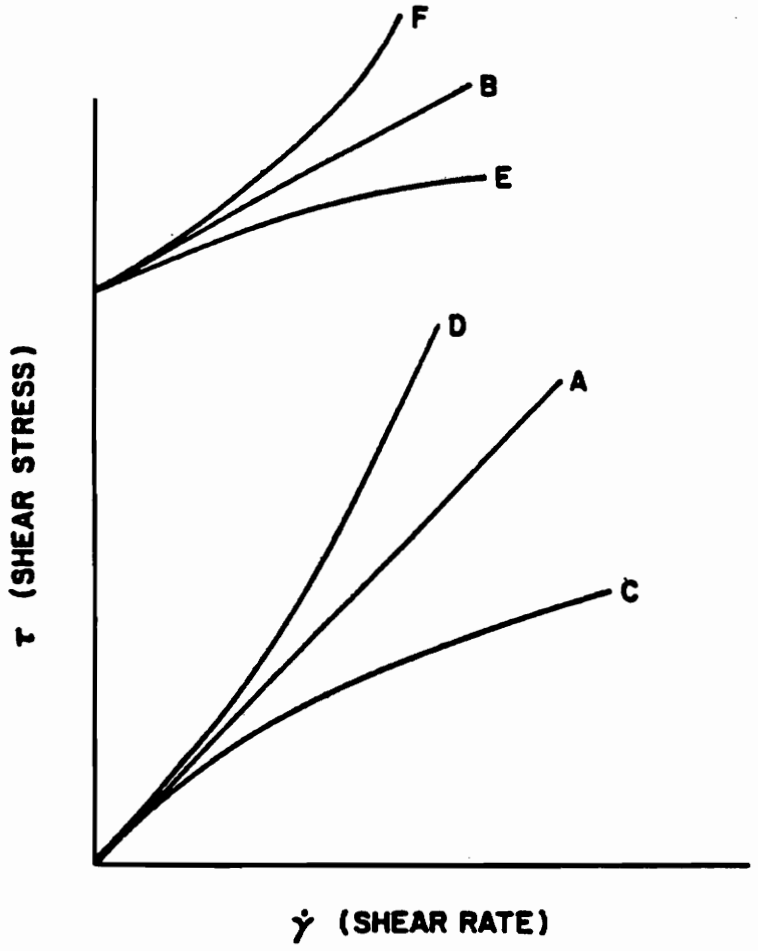

Figure 2-2. General plot of six different types of shear stress - shear rate behavior: A, Newtonian; B, Bingham Newtonian; C, Shear thinning; D, Shear thickening; E, Bingham shear thinning; F, Bingham shear thickening. (ref.7)

$$\tau = A\dot{\gamma}^B \tag{10}$$

Note that if B is unity, then A is the viscosity η and this equation appears as Newton's law.

The logarithm form of this expression leads to

$$\text{Log}\tau = \text{LogA} + B\text{Log}\dot{\gamma} \tag{11}$$

Plotting Log τ versus Log$\dot{\gamma}$ will result in a linear response of slope B. The slope would be unity, less than one, greater than one for a Newtonian, shear-thinning, and shear-thickening fluid respectively.

Oscillatory strain response is one of the most common methods used to determine linear viscoelastic properties. Figure 2-3 illustrates this technique. $G'(\omega)$ is the in-phase component of stress and is called the dynamic storage modulus. It is associated with the energy stored in elastic deformation. It is high when a polymer is in its glassy state, and drops with increasing temperature as the polymer goes through the glass transition and becomes soft and rubbery. $G''(\omega)$ is the 90° out-of-phase component of stress, and is called the dynamic loss modulus. It is associated with viscous energy dissipation. Figure 2-4 shows the general behavior of $G'(\omega)$ and $G''(\omega)$ for a homogeneous high molecular weight linear polymer melt. At low frequencies, also called the terminal region, the viscous behavior is dominant, illustrated by a value of $G''(\omega)$ higher than that of $G'(\omega)$. At intermediate frequencies, $G'(\omega)$ becomes larger than $G''(\omega)$

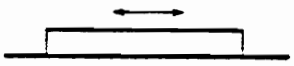

Strain: $\gamma(t) = \gamma_o \sin \omega t$; $\dot{\gamma}(t) = \frac{d\gamma}{dt} = \gamma_o \omega \cos \omega t$

γ_o = strain amplitude

ω = frequency (radian/sec, sec^{-1})

Viscous liquid: $\sigma(t) = \gamma_o \omega \eta \cos \omega t$ (in-phase with strain rate)

Viscoelastic liquid: $\sigma(t) = \gamma_o A(\omega) \sin (\omega t + \phi(\omega))$

or $\sigma(t) = \gamma_o [G''(\omega) \sin \omega t + G'(\omega) \cos \omega t]$

$G'(\omega)$ = dynamic storage modulus (in phase with strain)

$G''(\omega)$ = dynamic loss modulus (out of phase with strain)

$A(\omega)$ = amplitude factor

$\phi(\omega)$ = phase angle (loss angle)

$\eta'(\omega) = G''(\omega)/\omega$ dynamic viscosity

Figure 2-3. Illustration of the oscillatory strain response technique. (ref.6)

and remains relatively constant. At high frequencies, called the transition region, the response reverses again. Finally, $G'(\omega)$ eventually levels off, and $G''(\omega)$ falls again, the material becoming glass like at high frequencies, where the relaxation time is very long.

The equations given before describing the rheological behavior of polymer melts can be investigated through different types of instruments. Various kinds of instrumental geometries used commonly today are illustrated in Fig.2-5. In the parallel plate geometry, the fluid is sheared between two parallel plates (by rotational or torsional motion). The upper plate moves at a constant velocity V shown earlier in Fig.2-1, while the lower one remains immobile, and is connected to a torque transducer to determine the shear-stress. Layers of fluid appear to "slide" over one another in this case. Measuring the force required to promote the flow and the distance separating the two plates provides the rheological behavior of the fluid. In the coaxial cylinder viscometer, the fluid is placed in the gap in between two concentric cylinders. The outer or the inner cylinder is rotated at a given speed, which promotes "sliding" of the fluid layers over one another as well as torsional motion. In capillary flow, the shear stress is calculated from the pressure (stress) that produces a volumetric throughput in a capillary of given dimensions. Finally, the cone and plate

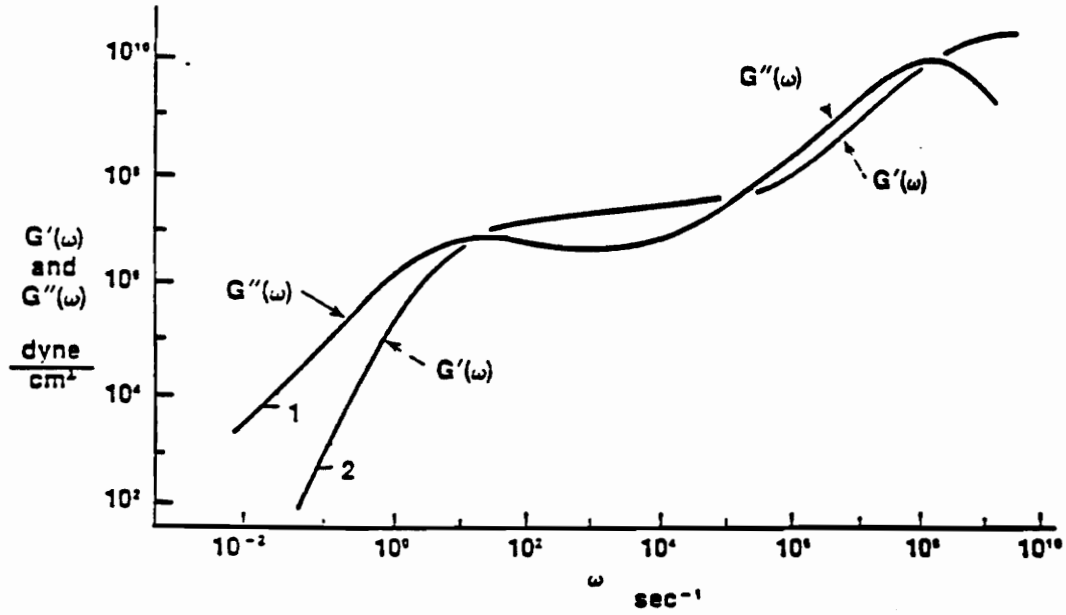

Figure 2-4. General plot of the dynamic storage modulus (G′) and loss modulus (G′′) versus frequency (w) for a homogeneous high molecular weight linear polymer melt. (ref.6)

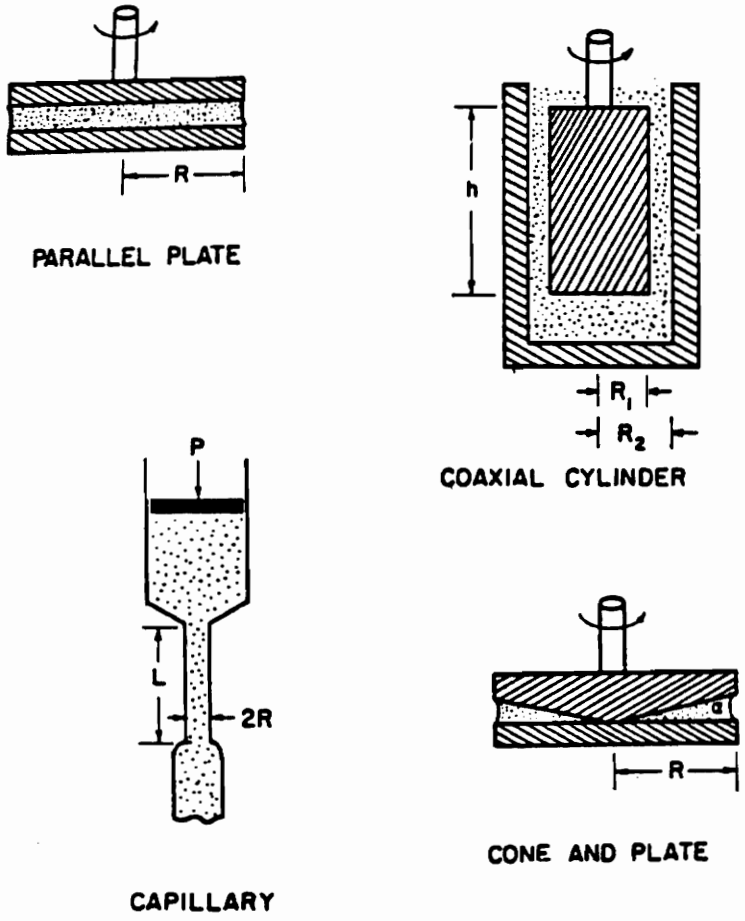

Figure 2-5. General sketches of four different types of instrumental geometries used for measuring rheological properties: A, parallel plates; B, Couette or coaxial cylinders; C, capillary flow; D, cone and plate. (ref.7)

viscometer is similar to the parallel-plate system, but the upper plate is conical with a small angle α. Its use is limited to relatively low shear rates by the onset of flow-instabilities as well as viscous heating. Indeed, at high shear or low viscosities, the fluid may be "ejected" from between the cone and plate gap due to centrifugal forces. In this case, a capillary viscometer is preferable to use.

Before closing the review on the rheological behavior of polymer melts, the following section will describe the effect of the external variable of temperature on the viscous behavior. Indeed, the temperature dependence of viscosity is quite significant in macromolecular systems. This study will present the effects of irradiation dose and blend composition on the temperature dependence of viscosity investigated for a series of PS/PVME systems.

2.2 Temperature Dependence of Viscosity of Polymer Melts

In order for a polymer melt to flow, two conditions are required. First, the chain segments must have space to move. Second, the chain segments must have sufficient thermal energy to overcome energy barriers that impede their changing conformational motion, such as the barrier to rotation about a valence bond. The glass transition temperature, Tg, defined as the temperature beyond which a glassy polymer softens and becomes rubberlike, determines the first condition. Near Tg, the temperature dependence of viscosity is described by the

Williams-Landel-Ferry (WLF) equation

$$\text{Log}\,\eta(T)/\text{Log}\,\eta(Tg) = -17.44(T - Tg)/[51.6+(T - Tg)] \quad (12)$$

The WLF equation is used to describe the temperature dependence of viscosity from Tg to about Tg+100. Above this upper temperature regime, the viscosity can often be expressed using an Arrhenius form

$$\eta_0(T) = A\exp(Ea/RT) \quad (13)$$

where $\eta_0(T)$ is the zero-shear viscosity, i.e. the shear viscosity at a low enough shear rate such that the behavior is Newtonian or shear rate independent

A is a constant

Ea is a flow activation energy (energy for segmental movement)

R is the gas constant.

Taking the logarithm of Eq.(13) yields

$$\text{Log}\,\eta_0(T) = A + Ea/RT \quad (14)$$

Plotting $\text{Log}\,\eta_0(T)$ versus 1/T should result in a straight line with a slope equal to Ea/R if this Arrhenius law applies. Figure 2-6 presents the general temperature dependence of the zero shear viscosity for several polymers. As shown, the slope varies with the different materials, being sensitive to the different chain chemistry. However, it should be noted that the slope is independent of molecular weight, meaning that Ea depends only on the local character of the chain. In general, any change in chemistry or structure that makes the

chain stiffer or more resistant to altering conformation (i.e. effect of branching) will often result in an increase of Ea. For example, linear polyethylene has a value of Ea of about 7 Kcal/mol, while for branched polyethylene, the value may reach the order of 11 Kcal/mol, depending on the level of branching. In some cases like the high molecular weight polymers, and due to instrumental limitations, it is not possible to carry out the rheological experiments at a low enough shear rate to accurately measure the zero-shear viscosity. In this case, another approach must be used to obtain the value of Ea. One such method is to determine the viscosity at a constant shear stress and use the temperature dependence of these values to obtain Ea. This graphical method is illustrated in Fig.2-7. A line of slope (-1) is drawn to obtain the values of the viscosity at a constant shear stress *as long as it is a log-log plot*. These values, obtained for all the temperatures investigated, are used to make the temperature dependent plots.

This concludes the brief review on the temperature dependence of viscosity of polymer melts. Since the work presented in this thesis focuses on a polymeric blend composed of PS/PVME, the rheological response of two-phase systems will now be briefly described.

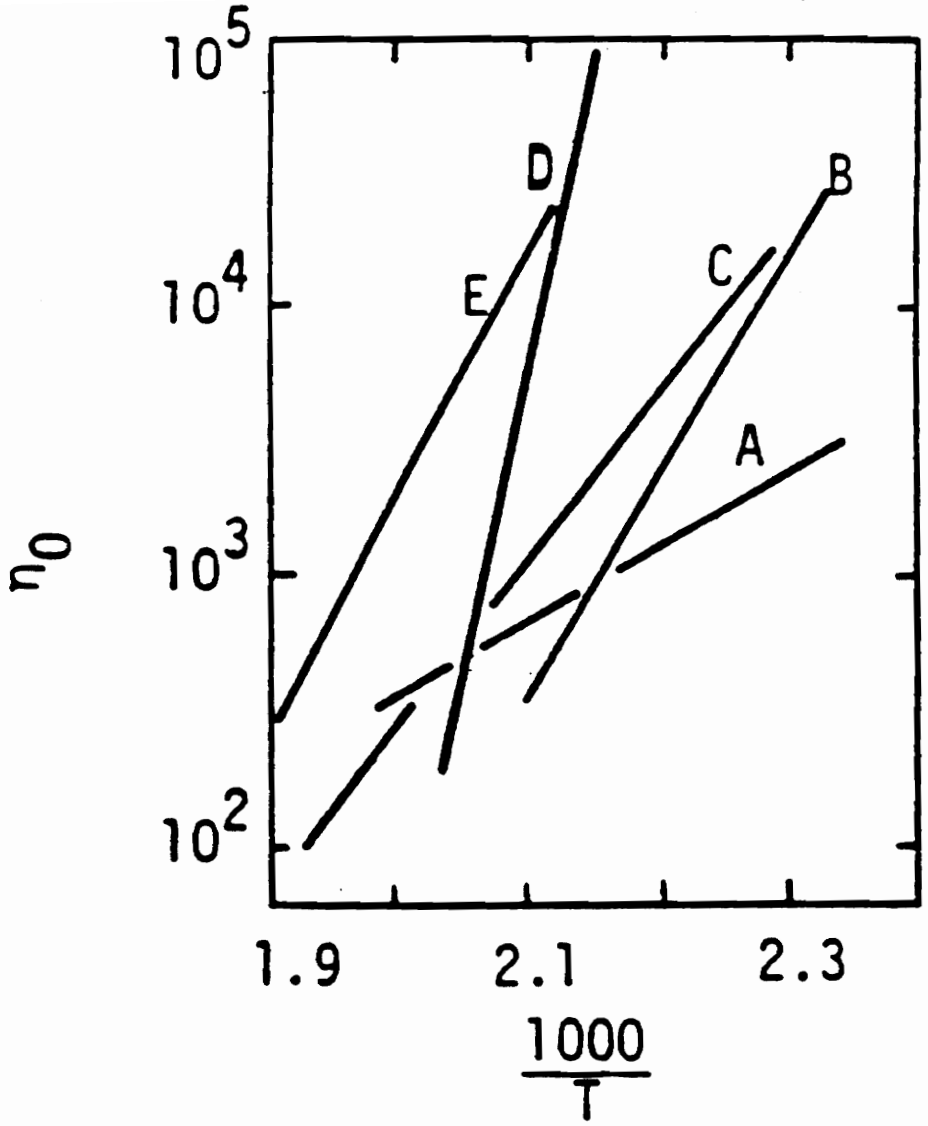

Figure 2-6. General temperature dependence of the zero shear viscosity for different polymers: A, polyethylene; B, cellulose acetate; C, polystyrene; D, ethyl cellulose; E, poly(methyl methacrylate). (ref.7)

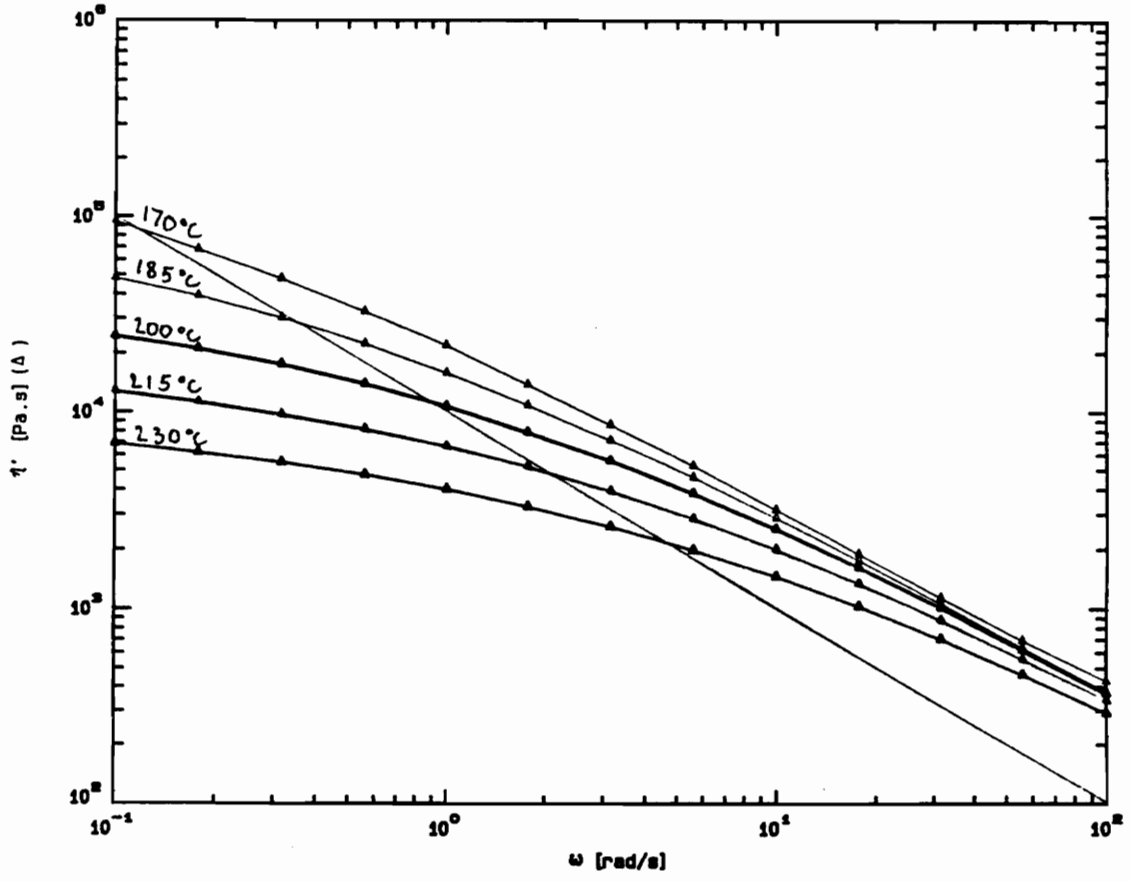

Figure 2-7. Illustration of the graphical method used to determine the viscosity at a constant shear stress and use the temperature dependence of these values to obtain the flow activation energy: line of slope (-1) on a log-log scale.

2.3 Blend Rheology of Polymer Melts

Extensive studies have been carried out on the rheological behavior of blends of molten plastics. Many experimental studies have shown that the viscosity varies monotonically with composition (8), whereas other studies have described blend systems which show either minima (9) or maxima (10). Some systems were found to exhibit either minima or maxima, depending on the shear rate (11), but others may exhibit both maxima and minima at the same shear rate or shear stress. Such results were found by Han and Kim (12) who investigated the rheological behavior of an incompatible polymer blend system composed of high-density polyethylene and polystyrene, using a capillary rheometer. To explain this behavior, they assumed that the experimental conditions were such that very few droplets broke up while flowing through the tube. Hence, the suspended droplets would not impede the flow as strongly as the continuous phase, which wets the tube wall. Their argument centered on the deformability of viscoelastic droplets, which have the capacity to store recoverable elastic energy. They observed that the blend that gave the lowest viscosity also gave the highest elasticity, and vice-versa. They assumed that the droplets dissipate less of the elastic energy while flowing through the tube than the continuous phase, which wets the tube wall. Hence, the dispersed phase (droplets) would store more recoverable elastic energy than

the continuous phase. Therefore, the total recoverable elastic energy at the die exit would be greater in the two-phase system containing deformable droplets than in a single-phase system or a two-phase system containing few deformable droplets. They concluded that a two-phase fluid containing deformable droplets will give less resistance to flow (lower apparent viscosity) and more recoverable elastic energy (higher apparent elasticity) than a single-phase system or a two-phase system which contains nondeformable particles. In other words, they concluded that the viscoelastic properties of a two-phase fluid depend on the type of morphology, i.e. the type of dispersion, created by the components.

Although extensive experimental investigations of two-phase flow of polymer melts have been done, there is less literature on the quantitative representation of the dependence of viscosity on composition. One widely quoted relation is that proposed by Hayashida et al. (13)

$$1/\eta = \Phi/\eta_A + (1 - \Phi)/\eta_B \qquad (15)$$

where Φ is the volume fraction of phase A

η_A and η_B are the shear viscosities of phases A and B at the same shear stress.

It is assumed that the flow takes place between parallel plates. This equation predicts a monotonic variation of the shear viscosity with composition.

Investigations of blends using cone-plate (14) and

capillary viscometers (15) have also been carried out. Shear viscosity-composition plots were found to exhibit the same behavior in that in some blends, these showed minima or maxima in their shear-viscosity versus composition response.

The classical theory by Taylor (16) predicts the viscosity μ of an emulsion by

$$\eta = \eta_0[1 + (5k + 2)\Phi/(2k+2)] \qquad (16)$$

where η_0 is the viscosity of the suspending medium

k is the ratio of the dispersed phase viscosity to the continuous medium viscosity

Φ is the volume fraction of the dispersed phase.

Equation (16) assumes that no chemical interaction occurs between the dispersed and continuous phases, that the dispersed phase forms spherical droplets of uniform size, and that the droplets retain their spherical shape in the shear flow field. This model predicts that the viscosity is higher than that of the suspending medium. Suspensions of one liquid in another are more complex than dispersions of rigid particles, due to the deformability of the dispersed phase. During the flow, the suspended particles are deformed, and thus affect the flow. Furthermore, the size and the morphology (geometric type of the suspension) of the suspended phase depend on the flow conditions. The nature of the fluid phase behavior is often determined by the balance of the viscous forces, with those of the interfacial tension. The

processes occurring are the deformation of the dispersed phase, which may lead to break-up, and coalescence of colliding droplets or fibers, depending on the morphology.

Schuch (17) investigated a semi-empirical blending rule for the components of the complex shear viscosity of homopolymer melts. This rule is shown to be valid over a broad range of unbranched polymers, and describes the experimental results for binary blends of linear polymers. The basis is the empirical relationship

$$\eta_0 = \text{const} * M^{3.4} \tag{17}$$

where M is the weight average molecular weight of the material. The constant factor depends on the material and the temperature of the melt, but not on the molecular weight distribution. This equation leads to a blending rule for the zero-shear viscosity η_0 by using the definition of the average molecular weight M_b for a blend of components with weight molecular weights $M_1<M_2$ and weight fractions w_1, w_2 ($w_1 + w_2 = 1$)

$$M_b = w_1 M_1 + w_2 M_2 \tag{18}$$

Replacing the molecular weights by the corresponding zero-shear viscosities η_{0b}, η_{01}, and η_{02} yields

$$\eta_{0b}^{1/3.4} = w_1 \eta_{01}^{1/3.4} + w_2 \eta_{02}^{1/3.4} \tag{19}$$

An example for a test on binary mixtures of polystyrenes is shown in Fig.2-8. The mixtures obey the same relationship, Eq.(17), as the components. Equation (19) has been shown to

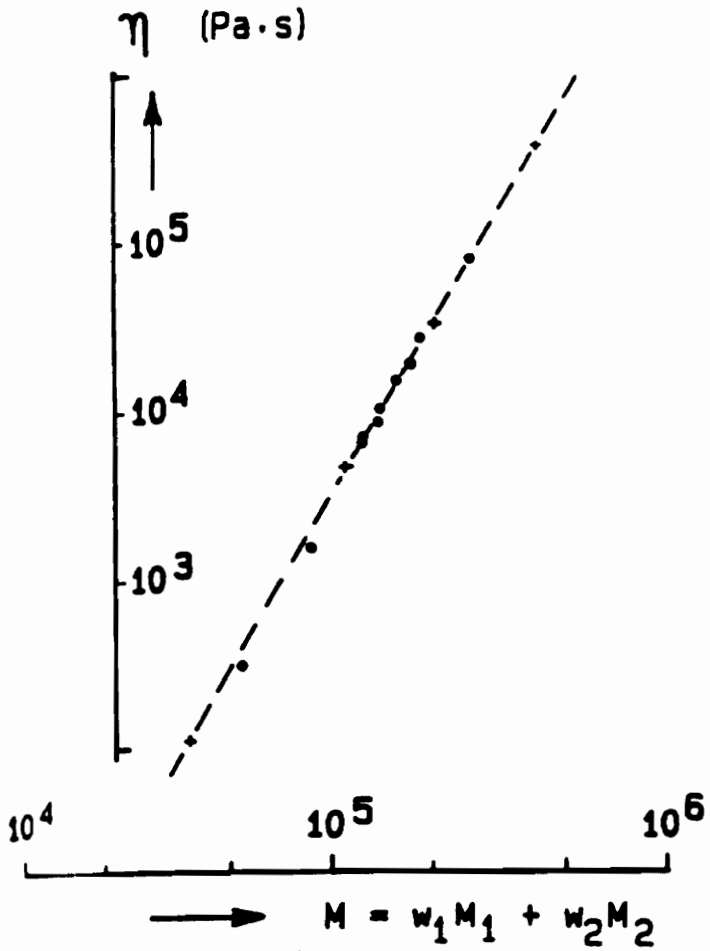

Figure 2-8. Zero-shear viscosity at 186°C for melts of polystyrenes. Component with narrow distribution (+), and binary blends (●). (ref.18)

be valid with the use of the complex viscosity. An oscillatory shearing of the melt with a frequency w and a small amplitude $\dot{\gamma}$ leads to a complex shear stress $\tau^*(w)$. An analogy can be made between the complex notation of the resistance of electrical alternating current with the complex viscosity

$$\eta^*(w) = \tau^*(w)\,(\dot{\gamma}e^{iwt}) \tag{20}$$

Thus, according to the investigation of Montfort et al. (18), Eq.(19) can be generalized as follow

$$\eta_b^*(w)^{1/3.4} = w_1(\eta_1^*(w))^{1/3.4} + w_2(\eta_2^*(w))^{1/3.4} \tag{21}$$

An experimental test on binary blends is shown in Fig.2-9. This example is taken from the literature (19). The blending rule (lines) corresponds well to the experimental data (single points). Figure 2-10 shows another example, taken from the literature (17), where the molecular weight of the high molecular weight component is common to commercial products. Again, the mixing rule is appropriate in describing the experimental data, excepts for the points at small frequencies due to the experimental limitations. So far, the blending rule turned out to describe the experimental results for melts of linear polymers, but the relationship was not found to be fulfilled by branched polymers. Indeed, the experimental results with a 3-arm star molecule show a deviation from the prediction of the blending rule at low frequencies.

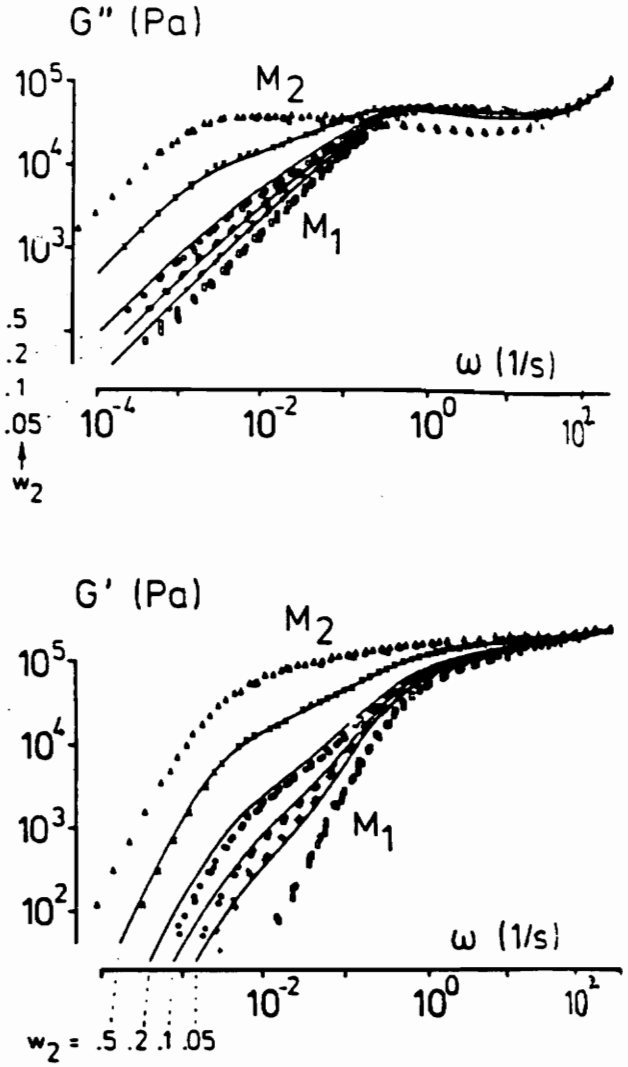

Figure 2-9. Loss (G'') and storage (G') moduli for binary PS-blends at 160°C and their cmponents (M_1 = 160,000 and M_2 = 670,000). Experimental values (dots) and calculated values (lines) for the blends. (ref.19)

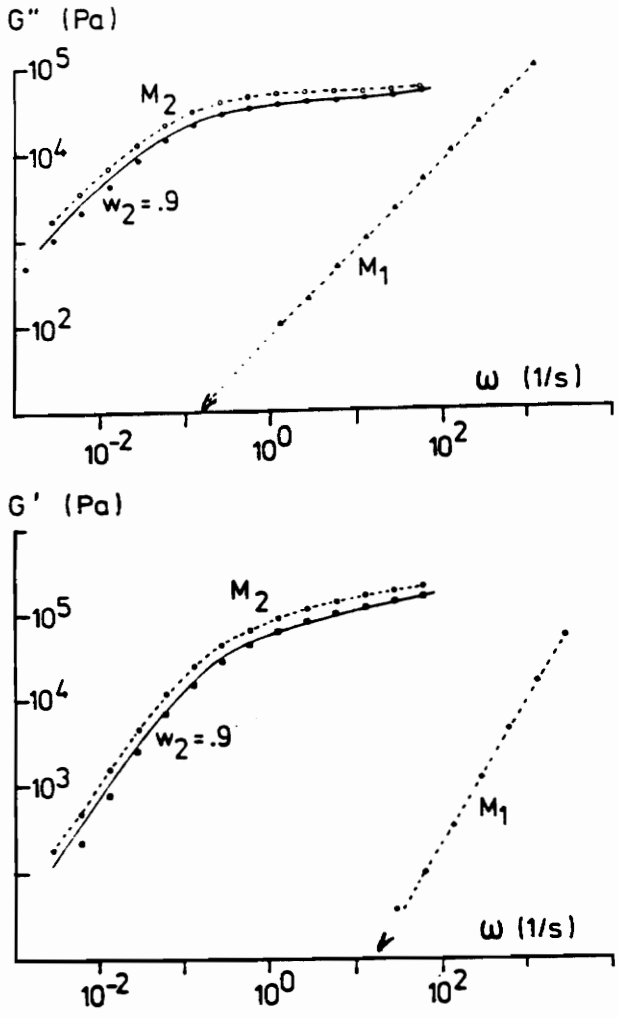

Figure 2-10. Loss (G'') and storage (G') moduli for binary PS-blends (M_1 = 12,900 and M_2 = 289,000). w_2 = weight fraction of component 2. (ref.17)

This above section has focused on the rheological behavior and rules of polymer blends. The following section will now describe the rheological behavior of the blend system investigated in this thesis.

2.4 Rheological Behavior of PS/PVME Blends

Ajji et al (20) investigated the rheological behavior of monodisperse PS/PVME blends using a rheometer with parallel plate geometry. The dynamic properties were studied at different temperatures, below, near, and above the phase separation temperature T_s (LCST), and in a frequency range from 0.05 to 100 rad/s. The goal was to observe the changes in the rheological properties in the vicinity of T_s, i.e. the influence that the two phase morphology would have on the rheological behavior of the blends. They found that for any composition, below T_s, the blend is miscible and homogeneous as expected; as the temperature is increased to above T_s, a dispersed phase appears composed of droplets dispersed in a matrix (metastable region) ; then, the size of the droplets increase by nucleation and growth, until they interpenetrate. They concluded that below and far from T_s, the storage and loss moduli G' and G'' show good superposition at all temperatures and frequencies. On the other hand, close to T_s, lack of superposition of G' and G'' occurs at low frequencies. They explained this anomalous behavior by the presence of significant concentration fluctuations.

Han (21) studied the linear viscoelastic properties of several homopolymer blends, including the PS/PVME blend system, and observed that a modified Cole-Cole plot (i.e. a logG'(w) versus logG''(w) plot) is not dependent on temperature in the miscible region, but becomes temperature dependent in the immiscible region. The temperature at which the change occurs was assigned to be the phase separation temperature T_s for the blend. Figure 2-11 illustrates this behavior for a (PS/PVME) blend composed of 80% of polystyrene. In the miscible region, the results obtained at different temperatures lie on the same curve. In the immiscible region, the experimental points obtained at different temperatures are on the same curve only in a frequency range of 5-100 rad/s. Outside this range,i.e. at lower frequencies, they do not superpose.

Schneider and Wirbser (22) analyzed the dynamic mechanical behavior of PS/PVME blends, and considered that flow of the blends is related to the Tg of the system. Molecular weight influences were observed, related mainly to the stiffer PS component. They also found that the influence of the molecular weight of PVME is less critical. In an earlier paper, Schneider et al.(23) concluded that the dynamic mechanical properties depended greatly on the molecular weight of polystyrene. It can result either in a diluting effect with a low molecular PS, or in an increased polydispersity

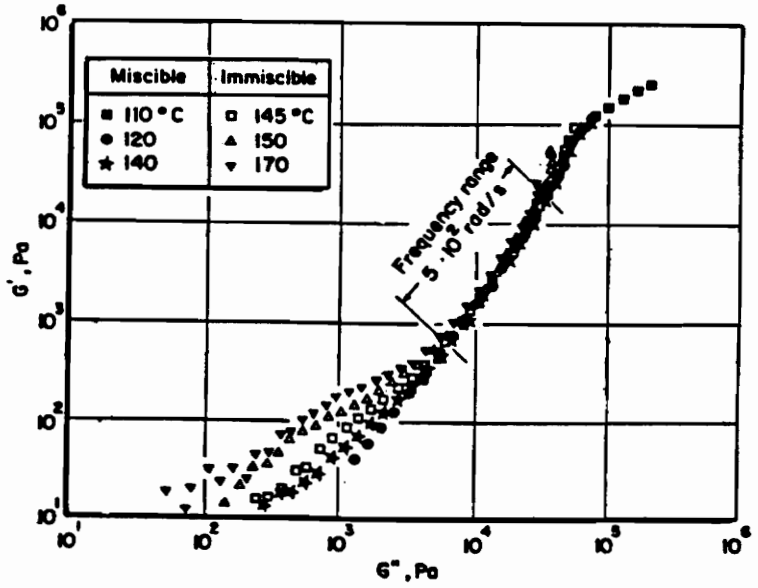

Figure 2-11. Storage modulus (G′) versus loss modulus (G′′) of a 80/20 wt % PS/PVME blend at temperatures below and above phase separation. (ref.20)

with high molecular PS. They observed that the viscoelastic behavior of the PS/PVME blends is influenced by both the nature of the matrix (i.e. the component in excess) and the component dispersed in the matrix. Moreover, they found that the rheological response reflects the composition dependence of Tg i.e. the addition of the stiffer component into the matrix of the mobile phase makes the flow more viscous as might be expected.

The above section has focused on the rheological properties of polymer melts, and especially on the particular response and behavior of the PS/PVME blend. The following section will now briefly outline the history of polymer radiation chemistry, the various types of radiation, and some general aspects of the effects of radiation with matter, more specifically, with polymeric materials.

III-EFFECTS OF RADIATION ON POLYMER BLENDS

There have been very great developments in the last decades in the radiation chemistry of polymers for practical reasons. While polymers are processed by extrusion or molding, most pass through the melt state. During this stage, the viscoelastic nature of the system is very important because of its affects on the process. Therefore, by altering the chemical and physical structure of the materials with radiation, their physical properties may be modified. An example is illustrated in Fig.3-1. Van Gisbergen et al. (24) used electron-beam radiation to improve the processability of polypropylene/ethylene-propylene-diene monomer PP/EPDM blends (controlled rheology). Here, electron-beam radiation was used to fixate the morphology in the blends by inducing crosslinking in the dispersed PP/EPDM phase.

A brief history of radiation chemistry, and more specifically of polymer radiation chemistry, now will be outlined. In subsequent sections, a review of various types of radiation, their interaction with organic systems and their effects on polymers will be presented.

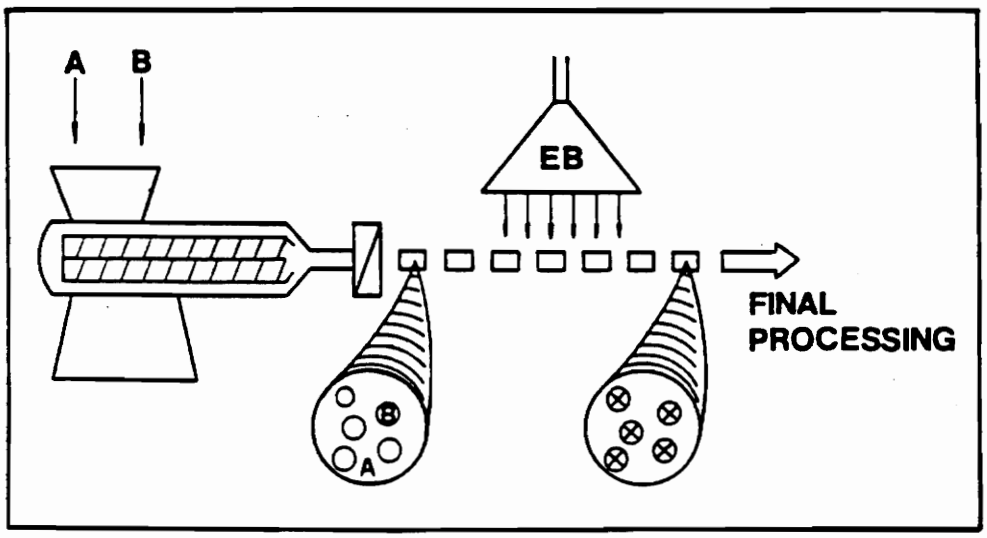

Figure 3-1. Schematic view of crosslinking a dispersed phase B (in phase A) by using electron beam irradiation between the blending and final processing step to achieve morphology fixation in the polymer blend. (ref.24)

3.1 Brief History

The first radiation chemistry effect observed was the blackening of photographic emulsions with X-rays by Roentgen in 1895, and with natural radioactivity by Becquerel in 1896. Following the studies of Madame Curie, who discovered and isolated radium, the chemical effects of radiation were investigated with increasing interest. High energy radiation (α, β, and γ) emitted by radioactive elements were studied in terms of their effects on a variety of materials, like water, organic compounds, or gases. In 1901, Becquerel compared the effects of α and β-radiation with those produced by light. Coolidge (25), in 1925, studied the chemical effects produced on acetylene and several liquids and solids, using cathode rays from a high voltage source of up to 250 kV. At the end of the 1930's, the radiation chemistry of some simple monomers began with the development of X-rays, γ-rays, and neutron radiation to induce polymerization. At this time, the restricted penetration of the radiation sources available limited the extension of this work. During the Second World War, the first nuclear reactor was developed, as part of the Manhattan Project, and a new era in radiation chemistry started. Powerful radiation sources were developed.

In the last decade, adequate radiation sources have become available, and there has been a growing interest in the effects of radiation on different materials, especially

polymers. The chemical changes produced when polymers are exposed to radiation are not chemically different from those occurring in low molecular weight compounds. On the other hand, owing to their high molecular weight, polymers often exhibit profound changes in their properties for only minor chemical modifications.

3.2 Types of Radiation - Electron Beam Radiation

Figure 3-2 shows the electromagnetic spectrum with the corresponding types of radiation based on their specific energy and frequency. The various types of energy associated with molecules are very useful in that they indicate how the different kinds of radiation can interact with molecules. For example, X-rays will preferentially interact with the electrons in the inner orbital of a molecule. Due to these differences in energy and frequency, the various types of radiation are used in different applications in chemical science. Functional groups and atomic structures can be detected by infrared radiation since its frequency is in the same region as the vibrational modes of molecules. Changes in chemical structures can be induced using ultra-violet, gamma, or electron-beam radiation.

The different types of high-energy ionizing radiation also may be classified according to the distance they penetrate through materials. High energy electromagnetic radiation, such as 1 Mev γ-rays, and the neutral particles,

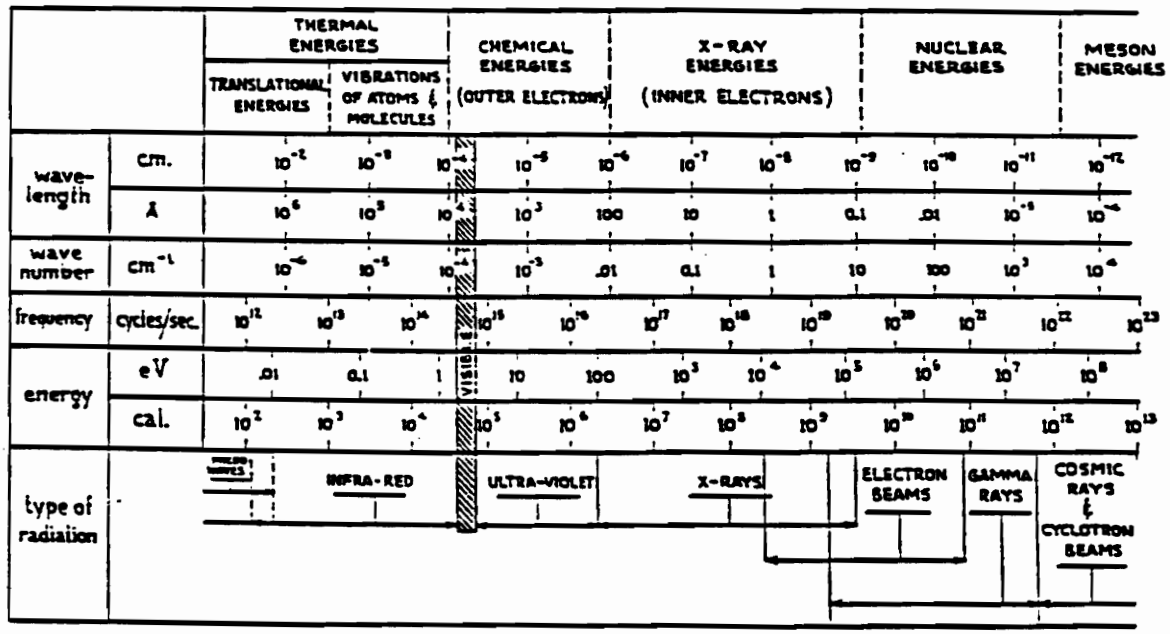

Figure 3-2. Electromagnetic spectrum and assignments of various types of radiation. (ref.26)

like neutrons, may penetrate through about one meter of solid or liquid. On the other hand, charged particles like electrons, β-particles, protons, and α-particles can penetrate no more than a few millimeters in solids or liquids, and only many centimeters in gases. The important features are the amount of energy deposited by the radiation and its microscopic spatial distribution in the irradiated material. X-rays and γ-rays are electromagnetic radiation like visible or ultra-violet light, but of much shorter wavelength, and hence greater photon quantum energy. X-rays are produced by a target hit by a stream of fast-moving electrons, accelerated by an electric field in a vacuum. They usually present a very broad spectrum of energies, the maximum energy being very close to the energy of the incident electrons.
Gamma-rays can be emitted from several radioactive nuclei. They are often emitted during nuclear transmutations of unstable atomic nuclei as excess energy. They have discrete energies. There are three important processes by which X- or γ-rays transfer energy to matter : photoelectric absorption, Compton scattering, and pair production.

In the photoelectric process, an X- or γ-ray gives up all its energy to an electron ejected from the valence shell. The ejected electron is called a photon-electron. The loss of an electron provides a vacancy in the inner shell which is filled by an electron from an outer shell. This mechanism is

illustrated in Fig.3-3a. This process gives off energy, which in the case of elements of high atomic number appears as a soft X-ray photon which may in turn undergo photoelectric absorption. In the case of elements of low atomic number, the energy usually is used up in ejecting another electron from the same atom. This process is called the Auger effect, and the ejected electron is known as the Auger electron.

In Compton scattering, illustrated in Fig.3-3b, an X- or γ-ray photon loses part of its energy by ejecting an electron from an atom. This electron is deflected and continues its path with a reduced energy. The ejected electrons, called Compton electrons, will usually give energy to the medium. The scattered photons will in general escape.

In the pair-production process, displayed in Fig.3-3c, the X- or γ-ray photon, in passing close to the nucleus, becomes converted into a positron-electron pair. The positrons and electrons lose energy in the medium, leading to chemical or physical change, and the positron is ultimately destroyed by combining with an electron.

Alpha-particles are proton beams that consist of the positively charged nuclei of atoms shorn of their orbital electrons. They lose most of their energy in matter by causing excitation and ionization that will be discussed in the next section. Neutrons arise from fission events in

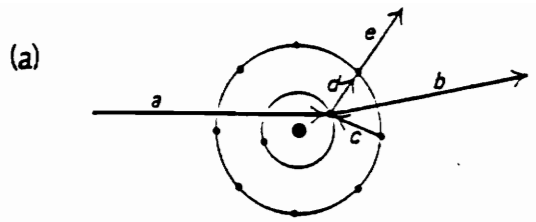

Typical photoelectric absorption process. (*a*) photon enters atom (*b*) electron ejected from inner shell: kinetic energy equals energy of photon minus binding energy (*c*) vacancy in inner shell filled by electron dropping from outer shell (*d*) virtual X-ray collides with electron in outer shell (e) electron ejected from outer shell (Auger electron): kinetic energy equals energy of virtual X-ray minus second ionization potential of atom.

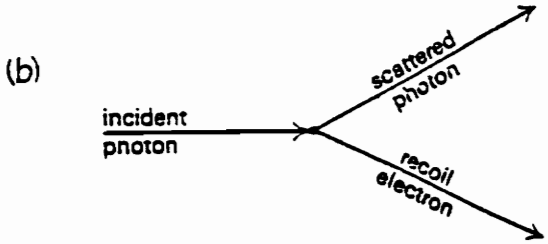

Compton scattering process. In this process the electrons in the medium behave to a close approximation as if they are free. If inner electrons are ejected, further processes take place within the atom, as after photoelectric absorption

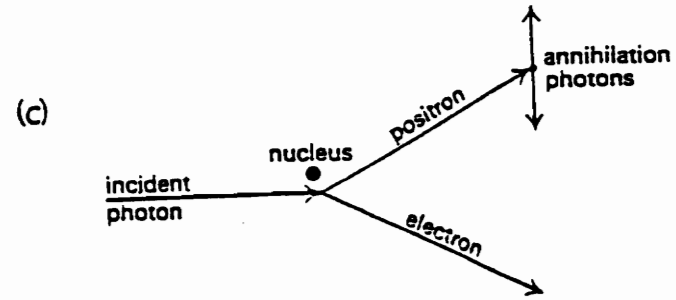

Figure 3-3a-c. Sketches of (a) a typical photoelectric absorption process, (b) compton scattering process, and (c) pair production process. (ref.27)

atomic reactors or when α-particles, accelerated charged particles, high-energy X-rays or γ-rays impinge on certain targets. Beta-particles are produced during the decay of radioactive nuclei. Most of the radiation is of lower energy.

High-energy electron beams used in radiation work may either be substantially mono-energetic, or they may cover a wide spectrum of energies, as in radioactive β-emitters. They are produced by various accelerating machines. Electrons from a hot filament acquire energy by passing through a high-voltage field in a vacuum. The energy of the beam is controlled by the voltage of the system (from 0.5 to 20 Mev). This voltage also determines the penetration of the electrons, which is much smaller than that of electromagnetic radiation having the same quantum energy. For 1-Mev electrons, the maximum penetration in water is 5-6 mm. This explains why electron-beams are very suitable for radiating thin films. In passing through the material, the incident electrons eject orbital electrons producing ionization. Thus, the primary electrons are slowed down, and several secondary, tertiary ... electrons are produced. Sometimes, the high-energy electrons can interact with nuclei, leading to the emission of X-rays called Bremstrahlung, which may be later absorbed by the material.

In order to understand the mechanism of electron-energy deposition, the processes of ionization and excitation of

matter will now be reviewed.

3.3 Ionization and Excitation

The interaction of the electron beams with the orbital electrons of the material results in the loss of most of their energy. The primary electron is deflected, and the bound electron may either gain enough energy to be ejected from the atom (process of ionization), or move to an orbit of higher energy (process of excitation). The first process results in a positive atom or molecule (ion) and a free electron. Being in an unstable state, the ion may either decompose, or react with molecules or ions. The free electron, on the other hand, may either go back to its original molecule, giving a highly excited molecule, or may be captured, giving a negative ion. The probability of one mechanism to the other depends on the velocity of the electron and the environment. This is due to the longer time for the electron to interact with another electron as its velocity decreases. On the other hand, the electron losses more energy early on its path when it has its maximum energy. Therefore, an electron liberated by ionization is capable of causing further ionization and excitation events. These secondary electrons are called δ-electrons. After losing most of its energy, the electron is no longer able to cause further ionization or excitation. The average amount of energy lost due to inelastic collisions (known as the stopping power of the medium) by a fast charged

particle per unit path length traversed in a medium can be expressed as

$$dE/dS = -7.84*10^{10}(\rho/E)\Sigma_i C_i(Z_i/A_i)\ln(\gamma E/J_i) \qquad (22)$$

where E is the electron energy (ev)

S is the the electron path length (cm)

ρ is the density of the medium (g/cm)

C_i is the weight fraction of species i

Z_i is the atomic number of species i

A_i is the atomic weight of species i

J_i is the mean ionization energy given by

$J_i = (9.76 + 58.8Z_i^{1.19})Z_i$

$\gamma = 1.166$

This relationship was originally developed from quantum mechanical considerations by Bethe in 1933 (28). Figure 3-4 illustrates this concept for various materials. This stopping number varies with the excitation potentials of the atoms of the medium traversed.

The ionization density also varies with depth of the specimen traversed. Figure 3-5 shows the change in the ionization density with penetration. It is often preferable to obtain a uniform ionization density. This can be nearly achieved by using thin samples, so that the ionization produced occupies a portion near the maximum of the curve.

The Grun range gives the penetration depth of an

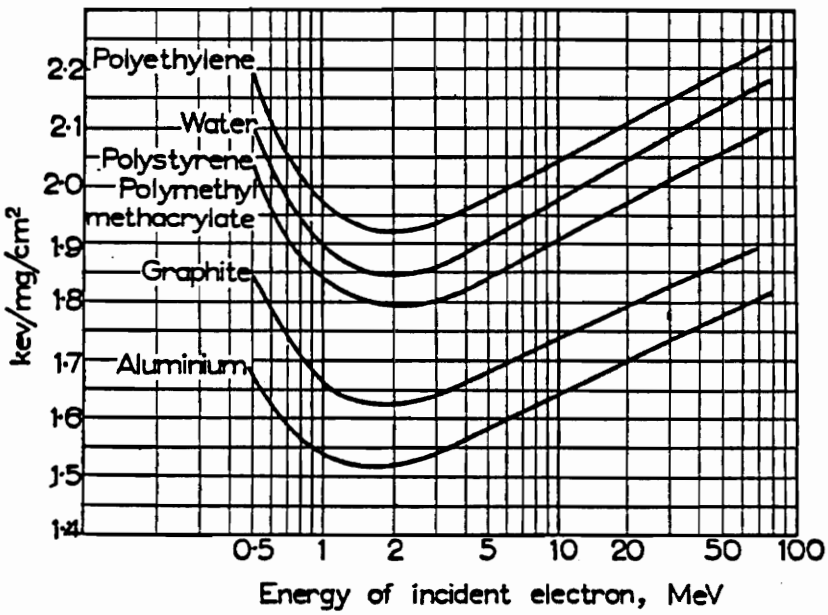

Figure 3-4. Stopping power of various materials for fast electrons (energy loss per mg/cm^2). (ref.29)

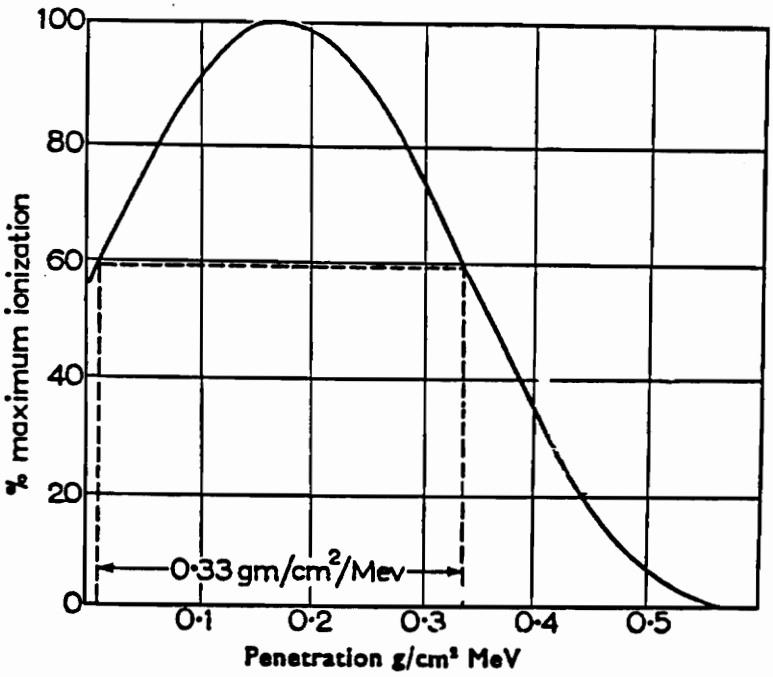

Figure 3-5. Ionization density versus penetration for single irradiation from one side. (ref.29)

electron, and can be determined from the following equation

$$R_g = (0.047/\rho) E_0^{1.75} \quad (23)$$

where R_g is the Grun Range (microns)

ρ is the sample density (g./cm^3)

E_0 is the incident electron energy (Kev).

This expression results from the studies of Grun on the energy dissipation of electrons in air. The normalized depth-dose function $\Lambda(f)$ can be expressed as

for $5<Z<15$, $\Lambda(f) = 0.74 + 4.7f - 8.9f^2 + 3.5f^3$ (24)

for $10<Z<15$, $\Lambda(f) = 0.6 + 6.21f - 12.4f^2 + 5.69f^3$ (25)

with $\Lambda(f) = (dE/dE_0)/d(Z/R_g)$ (26)

$f = Z/R_g$ (27)

This is an empirical function, as opposed to the stopping power (Eq.(22)). Figure 3-6 illustrates this depth-dose function. When the penetration depth is small, the stopping power increases as the electron loses velocity. Therefore, the rate of energy dissipation increases and the energy of the electron decreases, limiting the energy dissipation. The depth-dose function decreases, approaching zero as the Grun range is reached.

This section has covered the types of radiation that can be used today, and the interactions of fast electrons with matter. The effects of such radiation, i.e. the permanent chemical changes that occur in irradiated polymers will now be briefly reviewed.

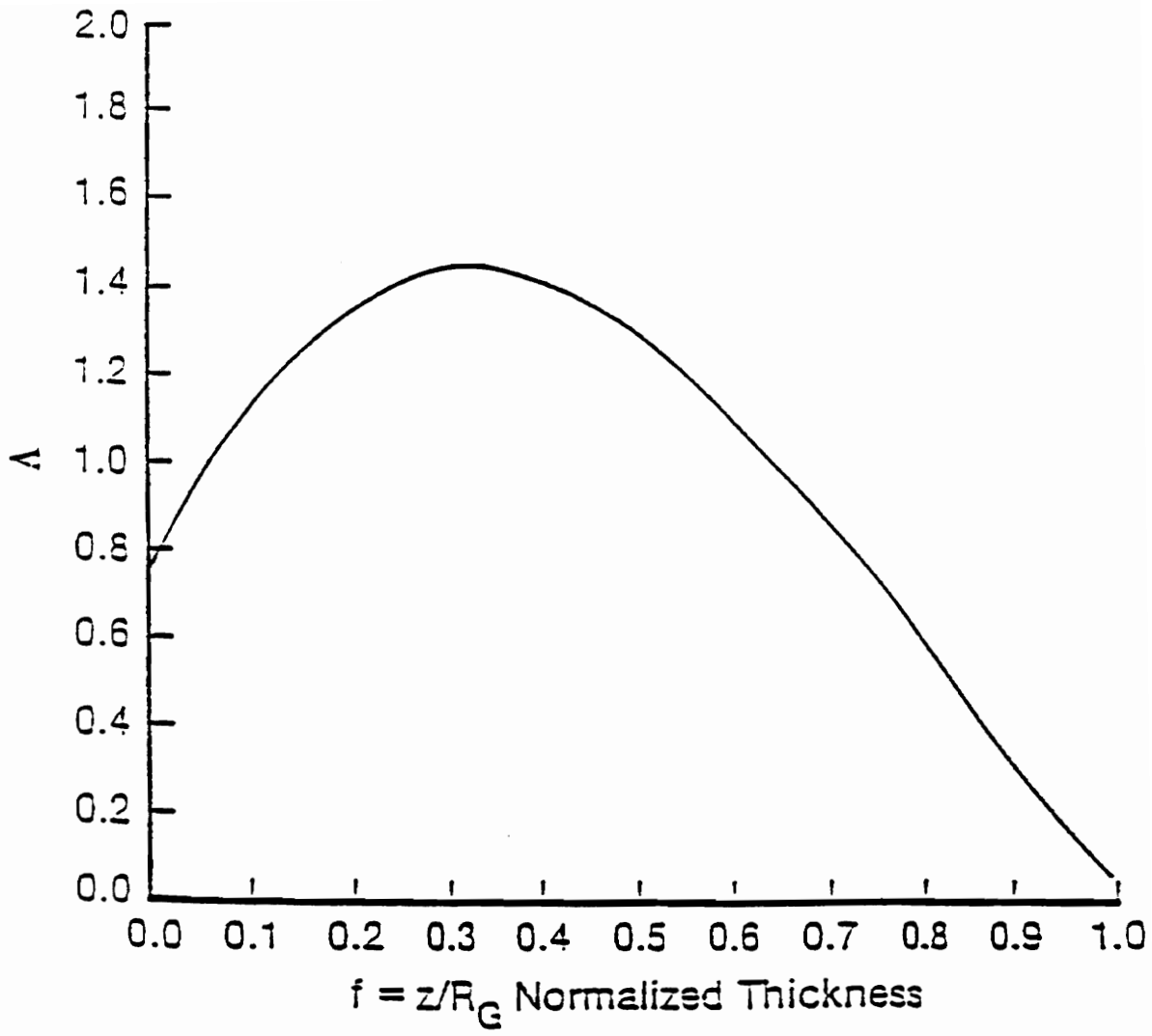

Figure 3-6. Illustration of the normalized depth-dose function. (ref.30)

3.4 Chemical and Physical Changes Produced under Radiation

One of the most important parameters that describes a polymer is its molecular weight. Radiation, by inducing chemical reactions and changes in the structure of the polymeric system, can profoundly affect its molecular weight, and therefore its physical properties. Small chemical transformations, such as are produced by low doses of radiation, cause large alterations in the physical properties, making polymers particularly interesting for radiation processing. These changes in the structure of the system are central to an understanding of the effects of radiation on polymers. They are the basis for the explanation of the physical changes. This section will focus on a qualitative description of the transformations in the structure and in the physical properties of polymeric materials that may occur due to irradiation.

3.4.1 Chemical Changes

Under radiation, polymers either crosslink, undergo chain scission, or do both, depending on their chemical structure. This observation was initially reported many years ago by Charlesby (29) and has since been confirmed. Chain crosslinking causes an increase in molecular weight by formation of covalent bonds between the polymeric chains. A macroscopic network appears as crosslinking develops, resulting in an insoluble fraction (gel) that increases with

radiation dose. Chain scission or degradation produces a decrease in molecular weight by the breaking of covalent bonds within a molecule.

Both crosslinking and degradation may occur simultaneously in the same polymer. Polymers have been classified with respect to which process dominates over the other. Table 3-1 shows the classification of polymeric materials into two groups, obtained after irradiation in the absence of oxygen. The ratio of crosslinking over chain scission depends on parameters such as chemical structure, physical state, radical stability, radiation rate, and environment.

By looking at the structure of polymers belonging to each group, a general conclusion can be derived as a general rule, valid under an inert atmosphere : if one or two hydrogen atoms are attached to the main chain carbon of a vinyl polymer, it will have the tendency to crosslink, whereas if a tetrasubstituted carbon atom is present in the monomer unit, the polymer will undergo chain scission. This rule is not universally valid . For some methacrylates containing long side chains, some crosslinking can occur.

Several mechanisms can explain these two different chemical transformations. First, two side chains may induce a steric strain on the carbon backbone, weakening the carbon-carbon link, and hence, promoting chain scission. Or, they

Table 3-1. Classification of predominately crosslinking and chain scissioning polymers in the absence of oxygen. (ref.27)

Predominant crosslinking	*Predominant degradation*
Polyethylene	Polyisobutylene
Polypropylene	
Poly(vinyl chloride)	Poly(vinylidine chloride)
Chlorinated polyethylene	Polychlorotrifluoroethylene
Chlorosulphonated polyethylene	Polytetrafluoroethylene
Polyacrylonitrile	Polymethacrylonitrile
Poly(acrylic acid)	Poly(methacrylic acid)
Polyacrylates	Polymethacrylates
Polyacrylamide	
Polyvinylpyrrolidone	
Poly(vinyl alkyl ethers)	
Poly(vinyl methyl ketone)	
Polystyrene	Polyα-methylstyrene
Sulphonated polystyrene	
Natural rubber	Cellulose plastics
Synthetic rubber (except polyisobutylene)	
Polysiloxanes	
Polyamides	
Poly(ethylene oxide)	
Polyesters	

may provide some resonance stabilization to a backbone carbon free radical, reducing its reactivity, and therefore, the probability of its recombination with another free radical at a scission site. Another explanation is that a hydrogen atom is easily removed from a carbon chain, leaving a site for crosslinking to occur.

Charlesby (31) and Lawton et al.(32) observed that both the degree of crosslinking and degree of degradation are directly proportional to the radiation dose but are independent of its intensity.

Most of the existing theories on crosslinking or degradation assume some form of radical reactions. Sun (33) proposed a list of reactions that can be expected to occur in irradiated long chain paraffin molecules, and that also modelize the mechanism for polyethylene and other polymers. These comprise :

-ionization and excitation

-decomposition of ionized or excited molecules to give radicals and possibly ions

-recapture of an electron by an ion, giving a highly excited molecule

-molecular rearrangement within a molecule

-migration of a radical along a molecular chain, and transfer between chains

-combination of two radicals to give a crosslink

$$R_1\bullet + R_2\bullet \rightarrow R_1R_2\bullet \quad (28)$$

-abstraction of hydrogen..., from a radical species by means of hydrogen, giving unsaturation

$$R_1C\bullet H\text{-}CH_2R_2 + H \rightarrow R_1CH{=}CHR_2 + H_2 \quad (29)$$

-elimination of a double bond, leaving a radical

$$R_1CH{=}CHR_2 + H \rightarrow R_1CH_2\text{-}C\bullet HR_2 \quad (30)$$

-direct formation of unsaturation by removal of molecular hydrogen

$$R_1CH_2\text{-}CH_2R_2 \rightarrow R_1CH{=}CHR_2 + H_2\bullet \quad (31)$$

All these processes involve radical reactions.

Another important chemical change is the formation of gases, hydrogen being the main gaseous product from the irradiation of poly(olefins), and also from many other polymers. With polyethylene, the evolved gas is mainly composed of hydrogen, which accounts for 90-98 % of the total gas, the balance being chiefly methane, ethane, propane, and butane (31). In polymethylene, a polymer without side-chains, the evolved gas contains more than 99 % hydrogen (34). The yield of gas is much higher if the irradiation is carried out at higher temperatures, and particularly above its glass transition temperature (35). Thus, the amount of gas produced depends on the nature of the polymer, on the dose, temperature, and type of radiation.

Hence, the primary effect of ionizing radiation results in an alteration of the molecular weight and distribution of

polymeric materials. As a consequence, the physical properties undergo modification. The following section will describe some of the possible changes observed in the physical properties of polymers.

3.4.2 Effects of Radiation on the Physical Properties

The influence of radiation on the mechanical properties of polymers differs, depending on the polymer, whether it crosslinks or undergoes chain scission. In general, scission produces a steady decrease in most of the properties of polymeric materials, while controlled crosslinking can provide some beneficial changes. El-Naggar et al.(36) studied the changes in the mechanical properties of electron-beam-irradiated poly (4-methyl pentene-1). Their results showed that the elongation at break decreases drastically as dose increases. At very high degrees of crosslinking, the polymer can become very hard and brittle, which leads to a deterioration of its physical properties. Moreover, whether the material is amorphous or crystalline, the effects of radiation will differ. Crosslinking will have a greater influence in initially uncrosslinked polymers than in materials already crosslinked. In crystallizable polymers, the decrease in strength as crosslinking increases (in the melt) is typically due to the interference of these crosslinks with crystallization.

The general effect of increasing crosslink density on the

physical properties is an increase in the tensile strength and in the elastic modulus, and a decrease in the elongation at break and in the solubility. But, the extent of these modifications depends on the polymeric system. For example, the effects of radiation on polyethylene, as shown in Fig.3-7, is to increase the tensile strength at room temperature, for radiation doses up to 10 Mrads. Above this value, it decreases slowly. The elongation at break increases also slightly, and then falls rapidly. At room temperature, the elastic properties of polyethylene are largely affected by the presence of crystallinity. At low radiation doses, the value of the elastic modulus is very little affected by radiation. The changes produced are due to a combination of a small degree of crosslinking and a small reduction in crystallinity. As the dose is increased, crystallinity is reduced, which has more impact than the simultaneous increase in crosslinking density. Further increase in the radiation dose provides a rapid rise in the modulus, explained by the formation of a very dense crosslinked network. Other changes can also occur in the properties after irradiation of polymeric materials, like changes in the melting behavior or in the electrical or optical properties. For example, low density polyethylene melts at about 115°C, but after sufficient crosslinking has occurred, it no longer converts into a liquid on heating above the normal melting point, but it is converted instead into a

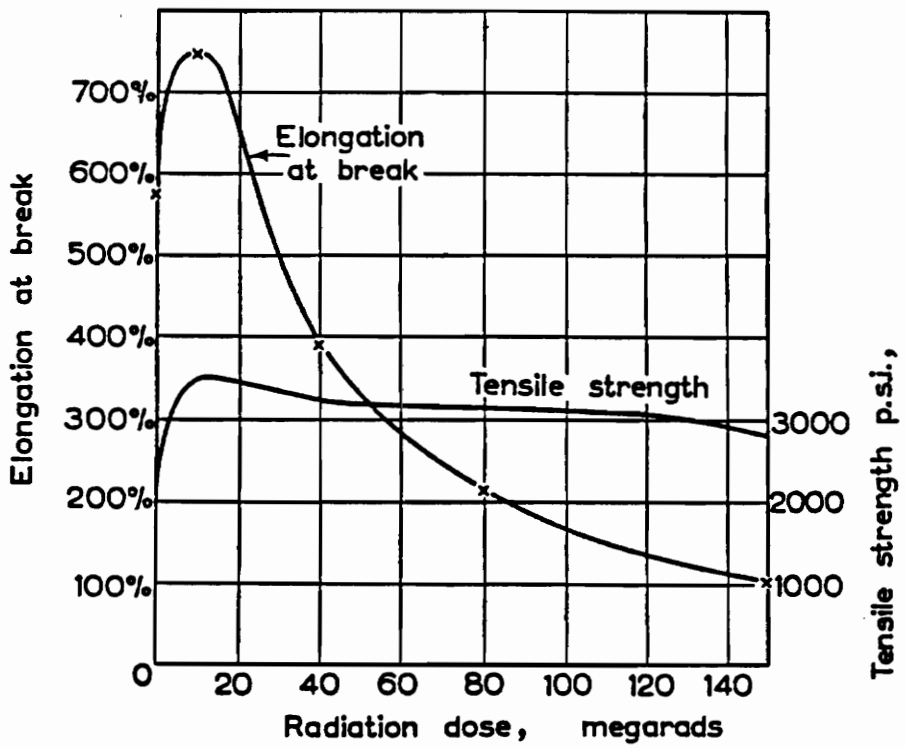

Figure 3-7. Tensile strength and elongation at break of irradiated polyethylene versus irradiation dose. Low density polyethylene, M_w = 21,000, irradiated to 800 kV electrons, tested at room temperature. (ref.29)

rubber-like material. This change in behavior occurs when a three-dimensional gel first extends through the system. On the other hand, at room temperature, the permittivity rises very slightly, less than 1% at frequencies between 10^3 c/s and 10^8 c/s for a radiation of 100 Mrads. These changes in electrical properties may be caused by the formation of unsaturation by radiation, and probably comes mainly from small amounts of oxidation.

The ratio of crosslinking over degradation can be determined by measuring the changes in molecular weight. The G-values estimate the number of crosslinking (G(X)) or chain scission (G(S)) that occurs per 100 eV of absorbed energy, and they are related to the changes in molecular weights averages M_n, M_w, and M_z. They are estimated by measuring changes in the solubility of the irradiated polymer. If crosslinking is predominant over scission (i.e., $G(X) > 4\ G(S)$), then measurement of the decrease in the soluble fraction above the gel dose may, in certain cases, be used to derive the G-values. This ratio is useful to determine whether a polymer undergoes crosslinking, degradation, or both under irradiation, since its value indicates which phenomenon is dominant over the other.

If crosslinking has reached the gel point, the polymer will become partially insoluble (formation of a gel), and a three dimensional network appears. The presence of

crystallinity, or whether the material is a glass or elastomer, does not affect its ultimate solubility, and hence these variables have no effect on the determination of the G-values. The part of the sample which forms an infinite network is insoluble in solvents that would have dissolved the original polymer. This part is called the gel fraction. The other molecules in the sample are still soluble, even though some of them have become branched through crosslinking. This part is called the sol fraction.

For molecules which have an initially random distribution of molecular weight and have been irradiated in the amorphous state, the following relationship developed by Charleby and Pinner holds

$$s + s^{0.5} = G(S)/2G(X) + 100N_A/M_0G(X)mD \qquad (32)$$

where s is the soluble fraction

G(S) is the G-value for chain scission

G(X) is the G-value for crosslinking

N_A is Avogadro's Number

M_0 is the initial weight average molecular weight

m is the molecular weight of the repeat unit

D is the absorbed dose (Mrads).

This equation describes the relationship between the soluble fraction of polymer and the G-values, as well as the absorbed dose.

A plot of $s + s_{0.5}$ against 1/D (known as a Charlesby-Pinner

plot) should give a linear response and estimate the G(S)/G(X) ratio, as illustrated in Fig.3-8. The individual G-values can be calculated once the ratio G(S)/G(X) has been estimated. Knowing the initial weight average molecular weight and the molecular weight m of the repeat unit, G(X) can be determined directly from the slope of the gelation region. To obtain the G(S) value, the following relationship, valid for any initial molecular weight distribution, can be used

$$1/M_n = 1/M_0 + GD/100N_A \qquad (33)$$

where M_n is the number average molecular weight after exposure to dose D

M_0 is the initial number average molecular weight

D is the absorbed dose (Mrads)

$G = G(S) - G(X)$.

By plotting $1/M_n$ versus D, the overall G-value (G(S)-G(X)) can be calculated from the slope of the resulting line.

This section has described the changes of the chemical and physical properties of polymers after irradiation. The way properties are transformed can determine the relative extent of crosslinking versus scission. The next section will review the factors that can influence the chemistry and the structural changes occurring in irradiated polymers.

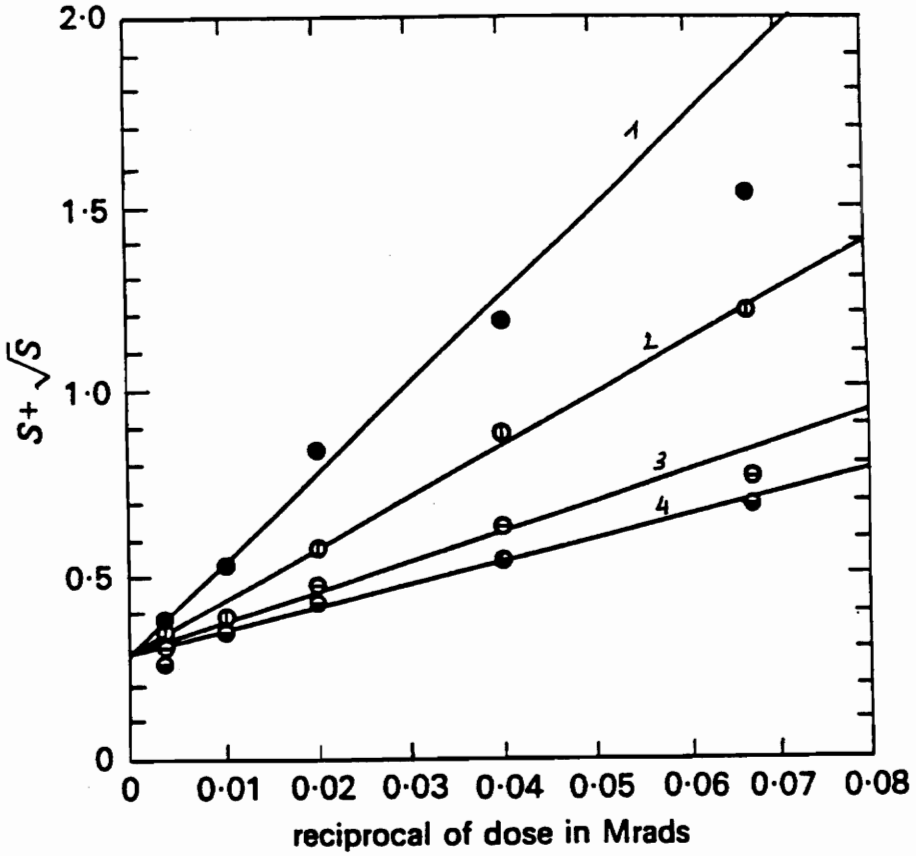

Figure 3-8. Dependence of $s^{0.5} + s$ on reciprocal of radiation dose in the irradiation of various samples of polyethylene: (1), linear polyethylene with M_n = 10,000; (2), linear polyethylene with M_n = 17,000; (3), branched polyethylene with M_n = 45,000; (4), branched polyethylene with M_n = 58,000. (ref.27)

3.5 Factors Influencing the Radiation Behavior of Polymers

The presence of species like oxygen, as well as parameters characteristic of the polymer are important in that they can greatly influence their response to radiation. Some have only little affect on the radiation behavior, while others can cause drastic modifications. This depends also on the material being irradiated. The following section will address parameters listed below and provide some explanation on how they can modify the response of irradiated polymers: crystallinity, molecular weight, temperature, presence of oxygen, and morphology.

(a)-Crystallinity

The influence of the extent of crystallinity can be investigated at constant temperature by studying the behavior of a material with various initial degrees of crystallinity. This has been examined by different authors with polyethylene. Charlesby et al.(37) irradiated low and high density polyethylene with 2 Mev electrons. Their results showed that the crosslinking density for a given dose was the same in both polymers, which indicate that crosslinking occurs as readily in crystalline as in amorphous regions. In contrast, Lawton et al.(38) concluded that crosslinking occurred mainly in the amorphous areas of the polymer. They irradiated low and high density polyethylene with 800 Kev at different temperatures, and determined the extent of crosslinking by measuring the gel

content in the polymer. All gel measurements were performed after storing the irradiated material for seven days in air at room temperature. The purpose of this procedure was to eliminate the trapped radicals which were found to be abundant in the crystalline regions. The fact that the radicals are more strongly trapped in the highly crystalline regions of the material is explained by the more organized and rigid molecular structure of the crystallites in these areas. In the crystalline regions of polyethylene, molecular chains are more tightly packed and less mobile than in the amorphous regions. This effect has been particularly studied with polyethylene. It was found that the free radicals which are formed in the amorphous regions can undergo several chemical processes, like crosslinking or grafting, whereas those in the crystalline areas tend to react at higher temperature when melting begins. Another effect of the crystallinity results in the reduction of the permeability of gases, due to the dense structure.

(b)-Molecular Weight

The effect of molecular weight on the response of irradiated polymers is directly related to the gelation behavior, i.e. the critical dose required for incipient gelation to occur.

The critical condition for incipient gel formation were first established by Flory (1) in the case of an initially

monodisperse polymer, assuming that crosslinking occurs at random, and only takes place between different molecules. The critical condition for incipient gel formation then becomes

$$P_c = 1/(P-1) \qquad (34)$$

where P_c is the probability that any one monomer unit is crosslinked.

A similar relation was given by Stockmayer (39) who examined the condition for incipient gelation in a polymer having an initially random molecular weight distribution. In this case, the critical condition is

$$P_c = 1/(P_w-1) \approx 1/P_w \qquad (35)$$

where P_w is the weight average degree of polymerization of the original polymer. Therefore, it can be concluded from this relation that as the molecular weight of a polymer increases, fewer crosslinks are required to form a gel, i.e. the value of the critical dose decreases. However, deviations from this theory can occur, with low molecular weight materials. This can be explained by the presence, at lower molecular weight, of more end groups on the chain ends per unit volume of polymer. Therefore, if these end groups are more reactive (eg, unsaturation) under radiation, the value of the critical dose will be less than that predicted by theory. On the other hand, if these end groups are saturated (hydrogenated), then the value will be close to the theoretical one.

(c)-Temperature

The temperature during the irradiation of the material is an important factor that can alter the chemistry of the response for different reasons.

First of all, since the morphology of the polymer depends on temperature, this factor will affect the mechanism of irradiation because the response will depend on the physical state of the system. Another consideration is the value of the irradiation temperature compared to the glass transition temperature of the material. The radicals will be more trapped in the glassy state and less able to react because of the reduced mobility of the polymer chains. As the temperature increases, the chains gain more mobility, and the radicals display a larger reactivity.

The influence of temperature on the crosslinking yield of polyethylene has been studied over a very broad range of temperatures. The experimental results are summarized in Fig.3-9 which is a plot of the radiation-chemical yields for crosslinking G(X) (denoted G(c.l.) in the figure) as a function of (1/T). It shows that below ca.-50°C, G(C.1) is always independent of temperature, but above this value, the yield of crosslinking steadily rises. No significant difference appears between the results obtained for these specific low and high density polyethylenes.

Finally, the temperature affects the kinetics of the free radical reactions i.e. as the temperature increases, the

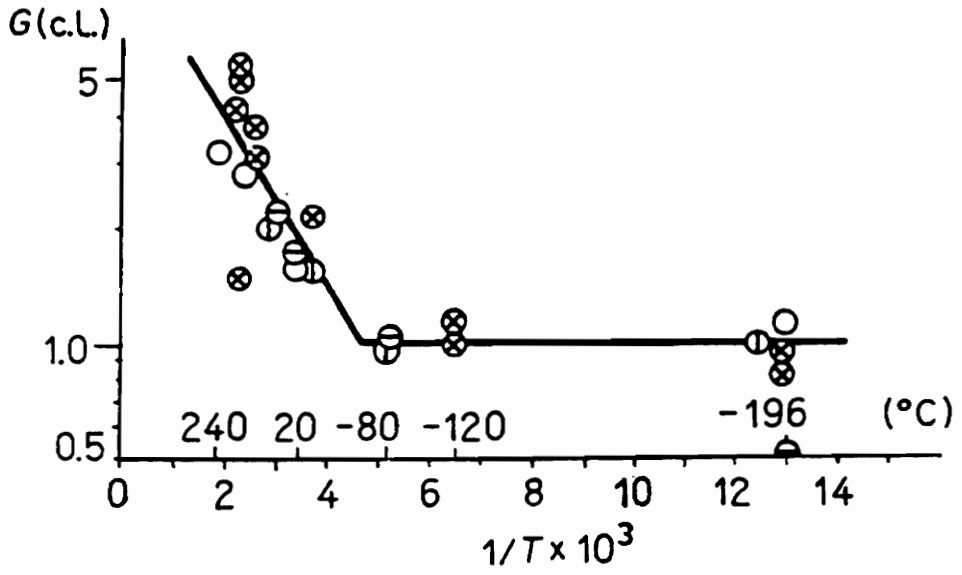

Figure 3-9. Plot of the radiation-chemical yields for crosslinking (G(c.l.) = G(X)) as a function of 1/T of polyethylene (in the plot above, the results are normalized with other data on the basis of G(c.l.) = 1 at -80°C and at -196°C). (ref.40)

kinetics increases as well. Figure 3-10 illustrates this kinetics effects showing that the gel fraction formed in irradiated polyethylene rises with increasing temperature.

(d)-The Presence of Oxygen

This factor often has a very influential effect on the final response of irradiated polymers. Thus, some polymers that normally crosslink under radiation in the absence of oxygen, undergo chain scission if irradiated in the presence of oxygen. In such conditions, additional reactions occur in the system, leading to degradation, due to the high reactivity of oxygen with free radicals. When irradiation is carried out in air, some radicals are assumed to react with oxygen to form peroxidic oxidative degradation of the carbon chain. A possible mechanism is outlined below

-Primary Reaction Step

$$-CH_2-CH_2- \rightarrow \bullet CH-CH_2- + \bullet H \qquad (36)$$

-Reaction with Oxygen

$$-\bullet CH-CH_2- + O_2 \rightarrow O_2\bullet-CH-CH_2- \qquad (37)$$

-Decomposition and Rearrangement

$$\bullet O_2-CH-CH_2- \rightarrow -HC=O + \bullet OCH_2- \qquad (38)$$

Similar reactions can occur with polymers that normally undergo degradation. It has been shown that polyethylene, which normally crosslinks when irradiated in the absence of oxygen, requires a higher radiation dose to crosslink in air. The earliest results in the influence of oxygen on the

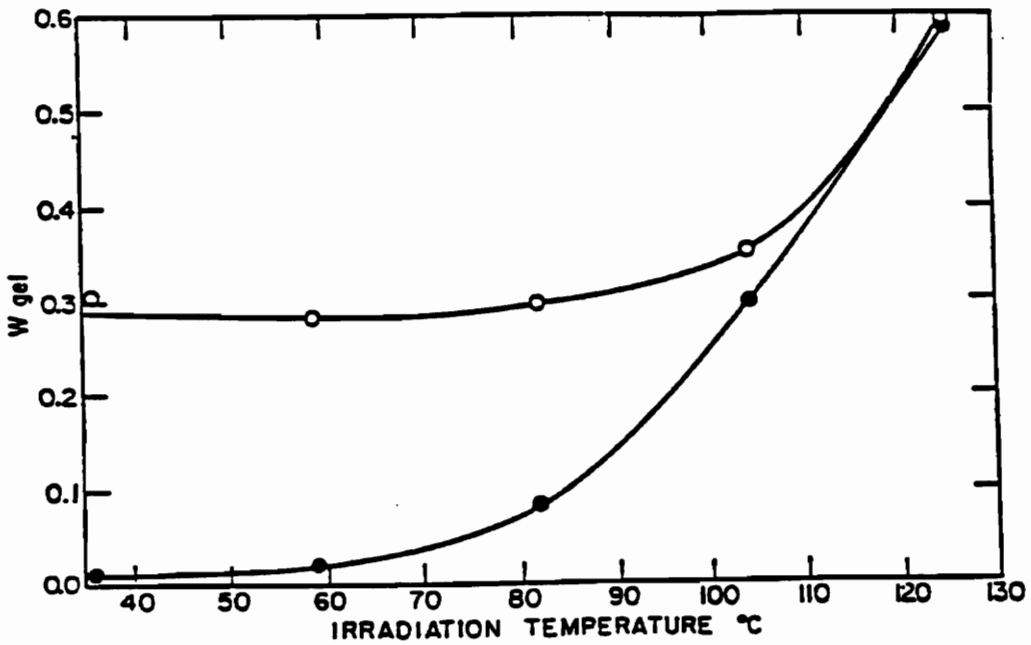

Figure 3-10. Gel fraction versus irradiation temperature for polyethylene post-treated by (O) storage at 140°C for two hours, and (●) stored in air for three days. (ref.41)

radiation response of polyethylene showed a marked oxidation of the polymer.

Charlesby (42) and Dole (43) reported that the weight of the sample increased after irradiation in air, whereas gas evolution resulted in a decrease in weight under vacuum. Also, it has been shown that under oxygen, the mechanical properties (i.e. elongation at break) of the irradiated polymer decreased, whereas in the absence of oxygen, they were improved. The efficiency of crosslinking is also affected by the presence of oxygen - it is much higher if irradiation is carried out in vacuum than in air.

Baskett (44), and Alexander and Toms (45), also reported that the gel content for a given dose was smaller for polyethylene irradiated in air than under vacuum. This change in the crosslinking efficiency after irradiation can be explained by two effects which may occur simultaneously (a)- the oxidative degradation of the crosslinked polymer and (b)- the inhibition of the crosslink mechanism by the presence of oxygen, this latter acting as a free radical scavenger. It is assumed that oxygen reacts with polymeric free radicals, thus preventing the reactions of the crosslinking process.

Alexander and Toms (45) also studied the effect of oxygen on the solubility of polyethylene. In thick samples such as rods, the difference in solubility is relatively unsignificant, even when the irradiation is carried out for

many hours. In thin specimens, the effect is much more important and could result either from an increase in the number of chain scissions, or a reduction in the number of crosslinks. These observations are illustrated in Fig.3-11.

This concludes the brief description of the influence of several factors on the radiation response of polymers. The following sections will review the previous studies conducted on (1)-the effects of γ- radiation on a deuterated polystyrene-poly(vinyl methyl ether) PSD/PVME blend by Briber et al.(46), and (2)-the effects of electron-beam radiation on PS/PVME blends by McHerron and Wilkes (3).

The effect of γ-radiation crosslinking on the phase diagram and scattering behavior for a compatible linear PSD/PVME blend has been investigated by Briber et al., using small angle neutron scattering (SANS). This technic has emerged as being an important tool for examining the concentration fluctuations present in polymer blends in the one phase region as the spinodal is approached. In their study, Briber et al. investigated the effects of crosslinking as a function of the crosslink density for a series of samples of constant composition close to the critical composition for the compatible polymer blend of PSD/PVME. It must be stressed that this system is not equivalent to the hydrogenated PS/PVME system in that the binodal curve for the former is ca. 40°C

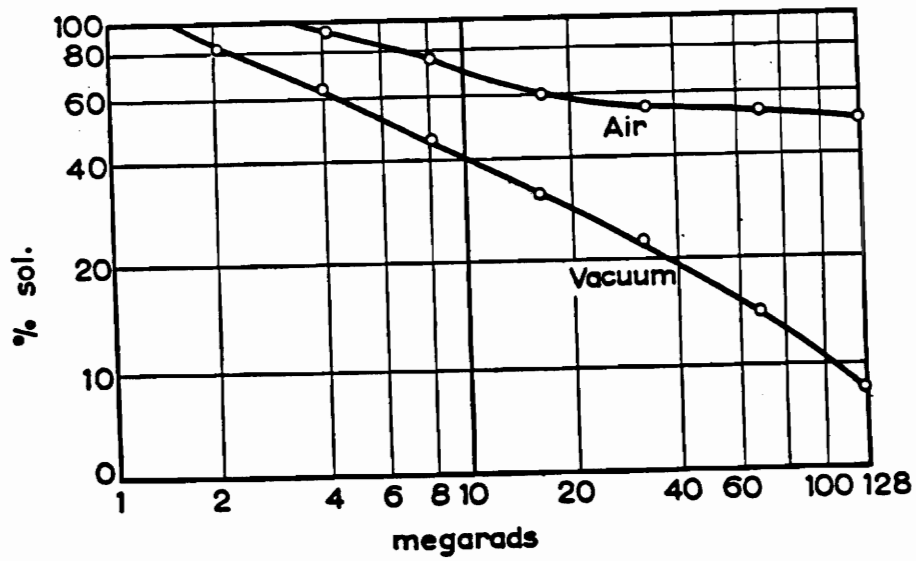

Figure 3-11. Decrease in the sol fraction with electron dose for 18 μ specimen irradiated in air or in vacuum. (ref.45)

above the latter system. They found that the inverse of the measured spinodal temperature varies linearly with the radiation dose and inversely with N_c, the number of units between crosslinks. This results in a shift of the single phase region of the phase diagram with increasing radiation dose, as shown in Fig 3-12. With a dose of 125 Mrads, the lower critical temperature (LCST) rises from 140°C for the unirradiated blend to an extrapolated value of 430°C.

In a previous study, Mcherron and Wilkes (3) investigated the effects of electron-beam irradiation on PS/PVME blends. In particular, they studied the effects of dose, blend composition, and state of miscibility on the radiation behavior of this system, more precisely, on the gel content and thermal behavior.

The gelation response of a series of irradiated PS/PVME blends, illustrated in Fig.3-13, was determined. It resulted that the change in the gel fraction with dose was composition dependent. This is not surprising with a blend composed of components with very different radiation sensitivity. Their results suggested that there is a significant amount of radiation grafting occurring between the two components at low PVME content, which was somewhat unexpected. Indeed, PS is often used to afford radiation protection in polymeric materials due to the stabilizing effect of the phenyl group. However, it was found that it is not the case in this blend

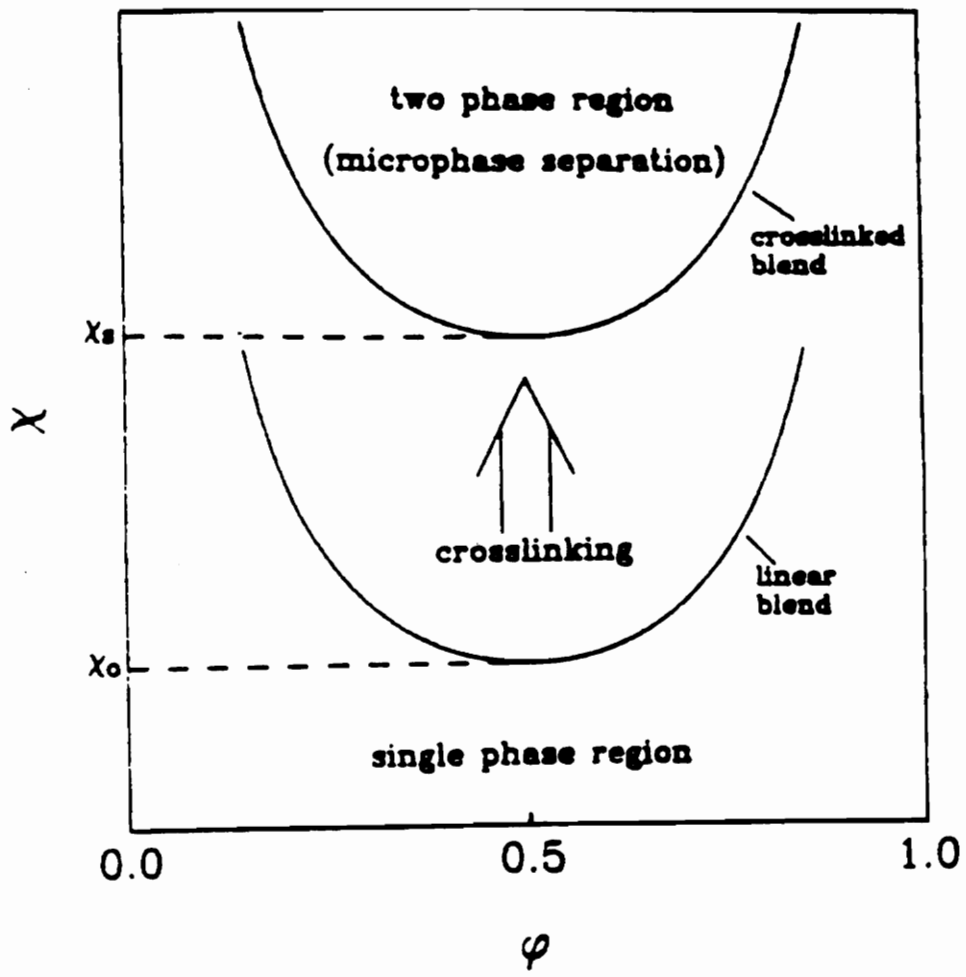

Figure 3-12. Schematic phase diagram showing the effect of crosslinking on the PS/PVME blend investigated. (ref.46)

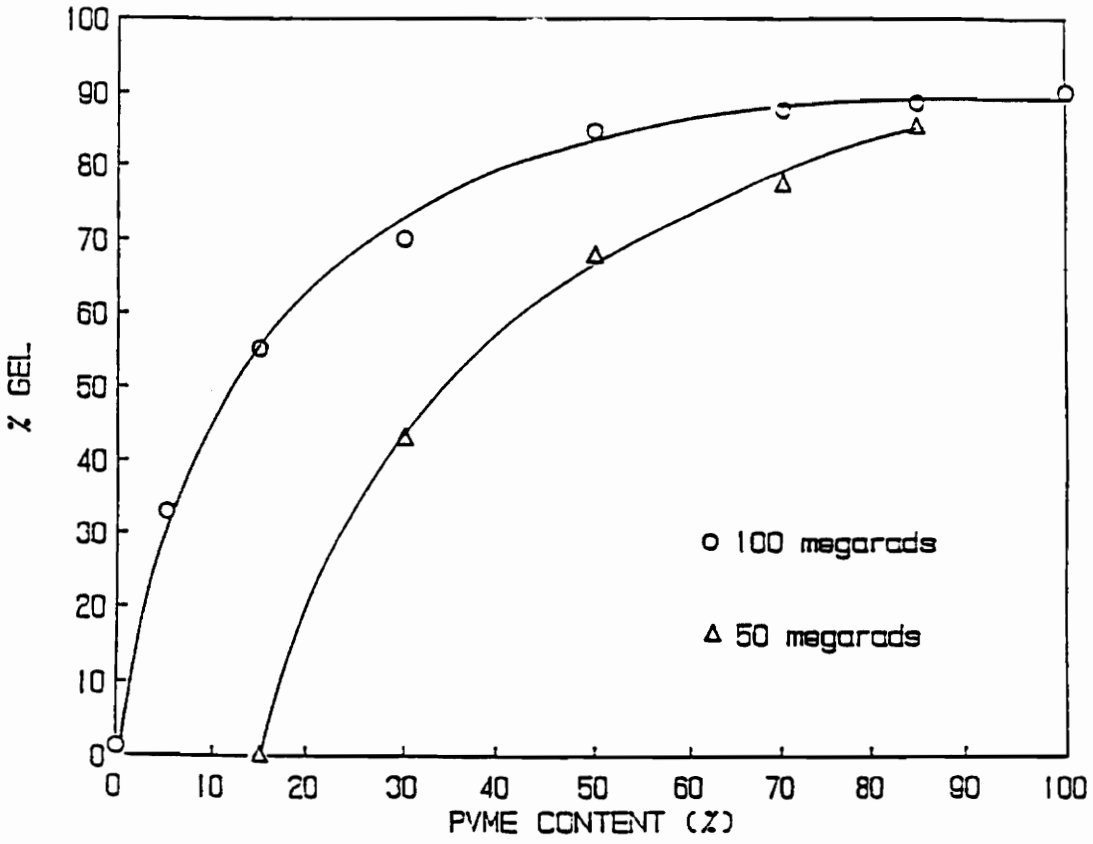

Figure 3-13. Plot of the gel fraction versus composition of miscible PS/PVME blends that have been irradiated to the indicated dose. (ref.3)

system.

The level of phase separation was also found to influence the response of this system to radiation as shown by the gel fraction measurements. Figure 3-14 illustrates the effects of phase separation time on the gel-composition curve for a dose of 50 Mrads. For the range of separation time studied, the curve is transformed from a non linear to a linear curve as the time of phase separation is raised. At all compositions, except 15 wt% PVME, the gel content decreases as the phase separation time increases. Phase separation may affect the composition and dose dependence of gel formation by inducing changes in localized compositions of the systems. Indeed, PVME preferentially crosslinks with radiation, while PS displays considerable resistance to crosslinking or chain-scission. Irradiation of the blends that were phase separated were found to slow the rate of phase dissolution at 100°C, but did not have a large effect on the glass transition behavior of the blends. Figure 3-15 displays the glass transition temperatures of unirradiated PS/PVME systems. These data have been collected earlier by McHerron and Wilkes (3), and show the behavior of the blend compositions under consideration in this present study. As shown, there is not a linear relationship between the composition (wt % PVME content) and the glass transition temperature (Tg) of the systems. The Tg decreases as the PVME

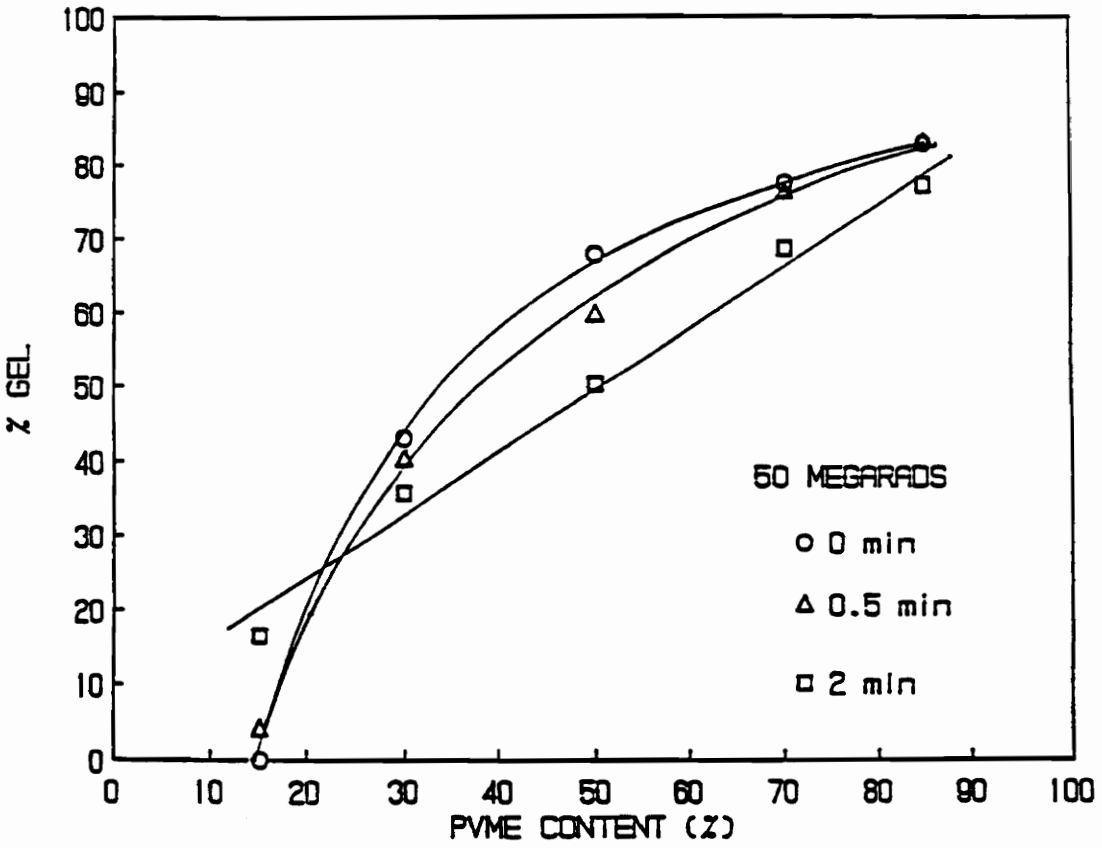

Figure 3-14. Plot of gel fraction versus composition of PS/PVME blends that have been irradiated to 50 Mrads after phase separation at 160°C for the indicated times. (ref.3)

content increases, this trend being sharper for the high PS content systems, and less pronounced for the PVME rich blends. Figures 3-16 and 3-17, taken from the same study (3), display, respectively, the DSC behavior obtained for the unirradiated blends and for the corresponding phase separated systems (2min at 160°C) that have been exposed to 100 Mrads. Comparison between these two figures indicates a very similar thermal behavior. The upper glass transitions of the irradiated blends, although not as distinct as the corresponding glass transitions of the unirradiated blends, may be the result of a different thermal history. The unirradiated blends were quenched from 160°C and immediately placed in the DSC furnace for analysis. The irradiated blends were quenched from 160°C, prepared for radiation exposure at room temperature, exposed to the electron beam, and then analyzed by DSC (3). Figure 3-18 illustrates the phase separation temperature versus the composition for the blend series investigated in this previous study. As shown, these blend systems display LCST behavior with a critical composition in the range of 70-80 wt % PVME at a critical temperature of around 115°C. The work presented in this thesis will deal with aspects that have not yet been investigated, in particular, studying the effects of dose levels and blend composition on the rheological properties of the PS/PVME blends. Indeed, the melt processing properties of commercial polymers can be adjusted by alterations in the

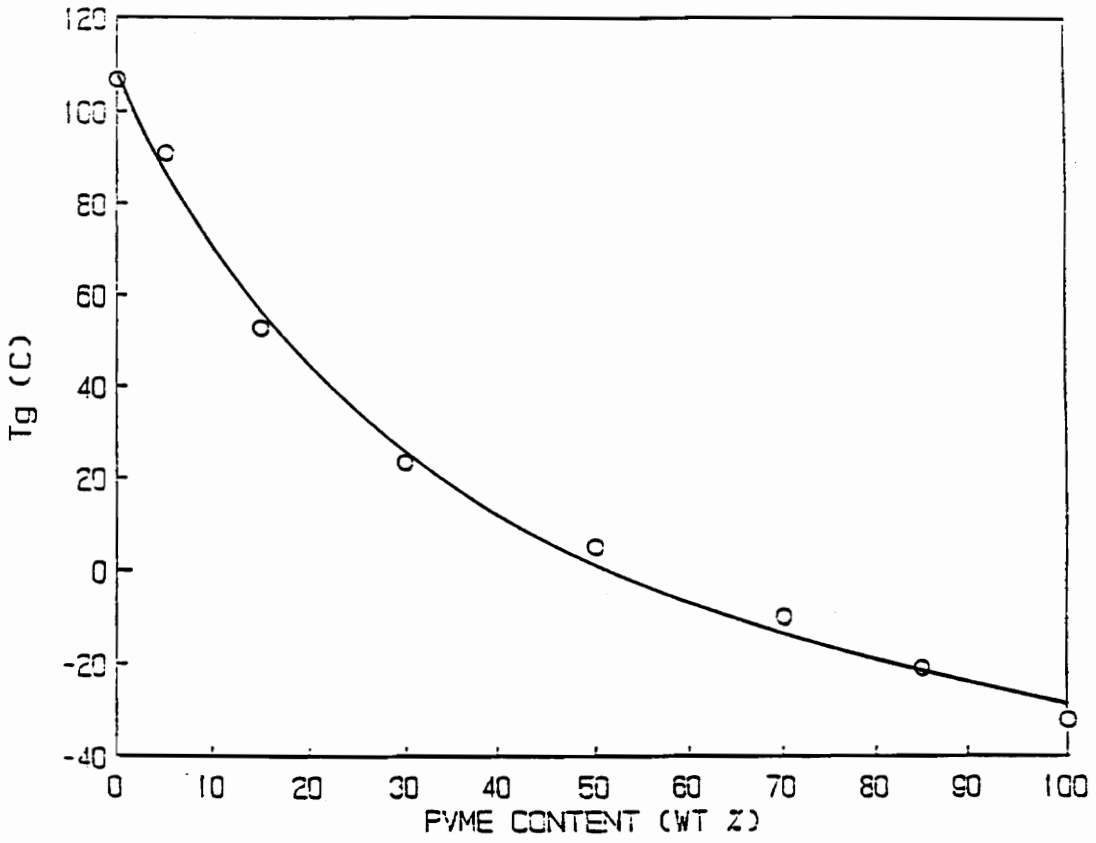

Figure 3-15. Plot of the glass transition temperatures Tg versus composition for PS/PVME blends. (ref.3)

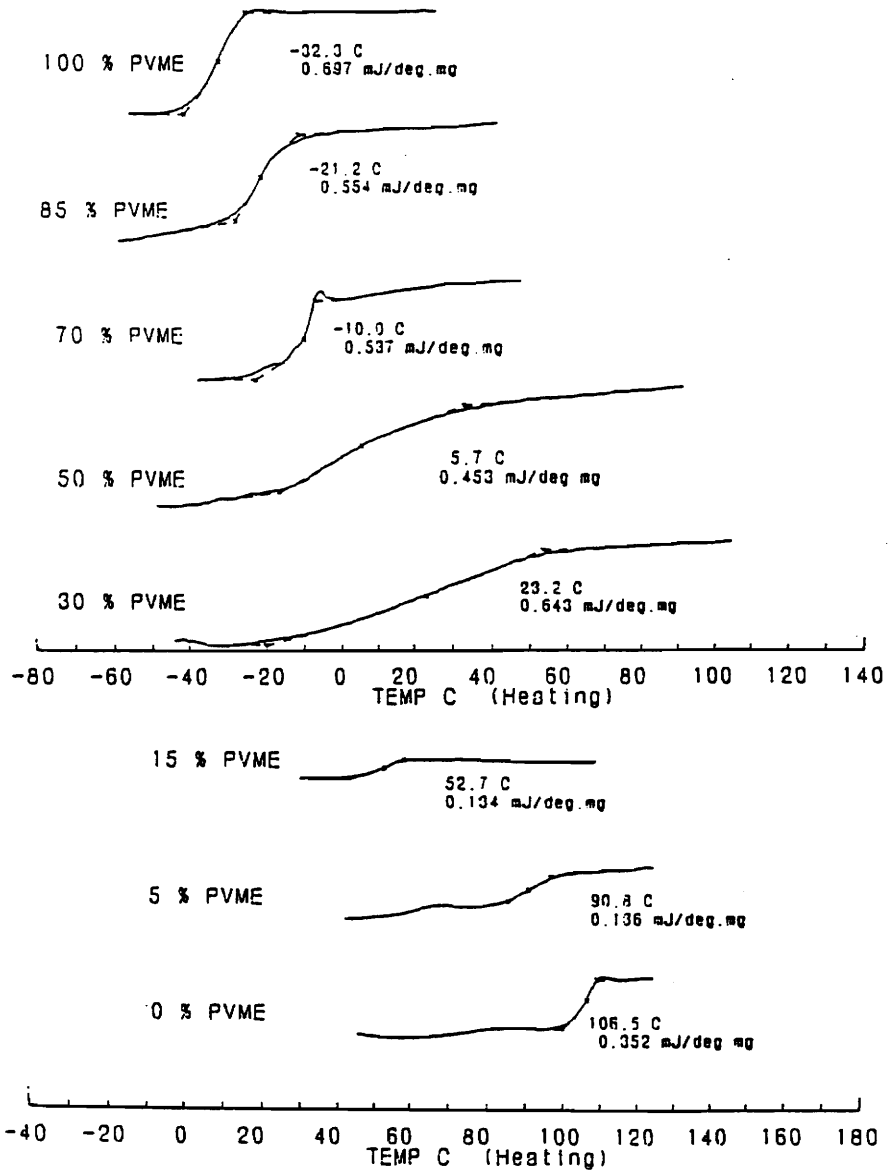

Figure 3-16. DSC scans of miscible PS/PVME blends. (ref.3)

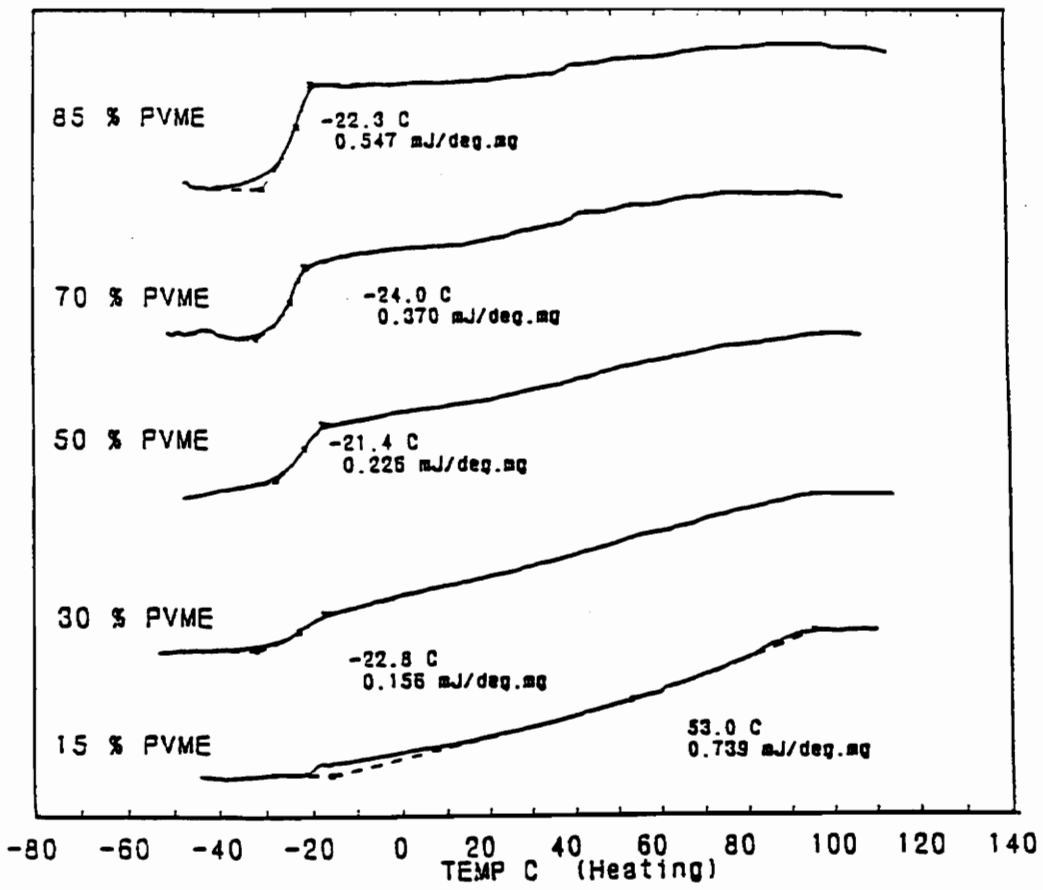

Figure 3-17. DSC scans of PS/PVME blends that have been phase separated at 160°C for two minutes followed by irradiation to 100 Mrads. (ref.3)

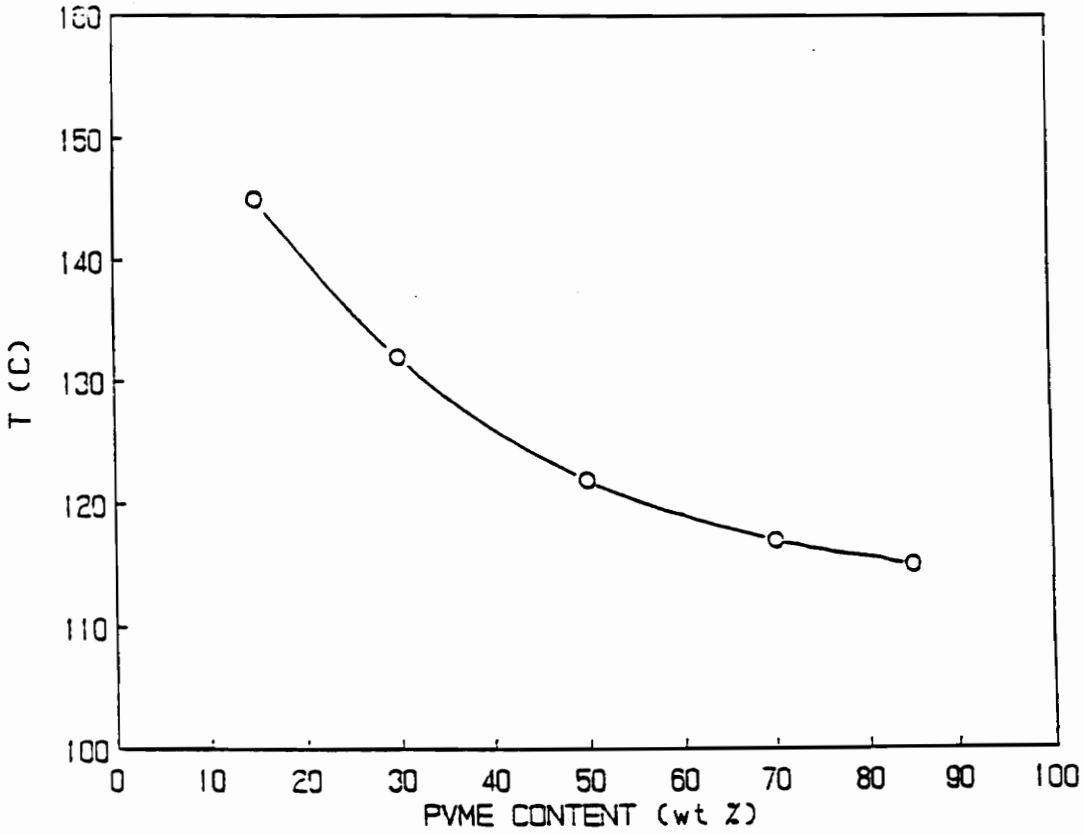

Figure 3-18. Plot of the cloud point temperature versus composition (wt % PVME) for a series of PS/PVME blends. (ref.3)

average molecular weight, molecular weight distribution and frequency of long branches in the molecules, the viscoelastic parameters associated with flow depending on molecular weight. Graessley et al.(47) investigated the effects of branching on the viscous state of polymeric materials. Comparing the viscosities for unbranched and branched molecules, he came to the following relationship

$$\mathrm{Ln}\eta_{br}/\eta_{unbr} = an_s + \text{const.} \qquad (39)$$

where η_{br} is the viscosity for the branched molecule

η_{unbr} is the viscosity for linear chains

n_s is the degree of polymerization of the side chain

a is a constant.

This result suggests that the effect of branching on the viscosity might be an exponential increase with the length of the side chain. However, this experimental result on the viscosity of branched polymers must be assessed with care. If two polymers of identical molecular weight are compared, one branched and the other unbranched, the branched one could possibly show a lower viscosity. Hiemenz (48) considers two factors that possibly could explain this behavior. First, since the side chains contribute to the molecular weight, the backbone chain is shorter for the branched polymer. Second, the branched molecule is more compact and the arms may actually be below the entanglement threshold in terms of chain length. Therefore, its behavior varies with the number,

location, and length of the branches. A branched molecule and a linear polymer having entanglements would then display different behavior. A possible explanation for the enhancement of the viscosity in some branched polymers is given by Graessley (49). Using the reptation model, when the molecule contains a long branch, this branched chain is pinned in its tunnel of obstacles at the branch point. Reptation, which allows free movement to a linear chain along its contour is largely diminished. Any branch point is supposed to reduce mobility if at least three strands starting from it are each long enough to participate in several entanglements.

In the work presented here, electron beam radiation is used to induce grafting between the two components composing the PS/PVME blends. The purpose of creating such modifications is to modify the shear rate responses, and to gain a control on the viscosity of the systems, in order to alter their processabilities.

This concludes the review given on the effects of radiation on polymer blends, specifically on the previous studies conducted on the PS/PVME blend system. The next section will describe the materials and the experimental procedures employed.

IV-EXPERIMENTAL

4.1 Materials

Measurements in this study were made with polystyrene obtained from Dow Chemical with a weight average molecular weight (M_w) of 300,000 and a polydispersity (M_w/M_n) of 2.5. Poly(vinyl methyl ether) was obtained from Dajac Labs with no specified molecular weight. By comparing the cloud point curve obtained for this blend system with curves reported on in the literature (5), the weight average molecular weight of PVME was estimated to be in the range of 50,000 -100,000.

4.2 Sample Preparation

Blending to different compositions was made using toluene as a solvent (polymer:solvent = 1:9) at room temperature. The polymeric compositions investigated were 90, 95, 98, and 100 wt % in PS. Ternary solutions were cast on teflon sheets and were left in an air current for 24 hours to remove the solvent. The resulting films were then placed under 25 in. Hg of vacuum at 80°C for 48 hours to eliminate residual toluene. Systems with high PS content (95 wt %, 98 wt %, and 100 wt %) were heated at 120°C under vacuum for 48 hours, since their glass transition temperature is above 80°C. The films obtained were transparent with a thickness of ca. 3-4 mils.

Before performing the rheological measurements, they were stored in a refrigerator for two to three days in average.

4.3 Radiation Exposure

Films were irradiated at electron-beam doses ranging from 2 Mrads to 10 Mrads/pass in a nitrogen atmosphere with a residual oxygen content of 200-300 ppm, using a Energy Sciences CB 150 electrocurtain, (see Fig.4-1). This system has a tungsten linear filament geometry as the electron source. Dose levels were investigated by changing the conveyor speed line and the electron beam current intensity according to the following equation

$$D = KI/S \tag{40}$$

where D is the total dose (Mrads)

K = 66.1 Mrads ft/mA/min

I is the current intensity (mA)

S is the speed of the conveyor (ft/min).

The samples were placed on an aluminum tray and run through the conveyor system of the EB machine. All samples were passed through the electrocurtain at ambient temperature, operating at an accelerating voltage of 175 kV.

4.4 Cloud Point Temperature

Cloud points of the blend systems were measured with a Zeiss optical microscope equipped with a Linkam PR 600 hot stage. Cloud points were taken at the temperature at which the first sign of cloudiness appears in the heating mode. For

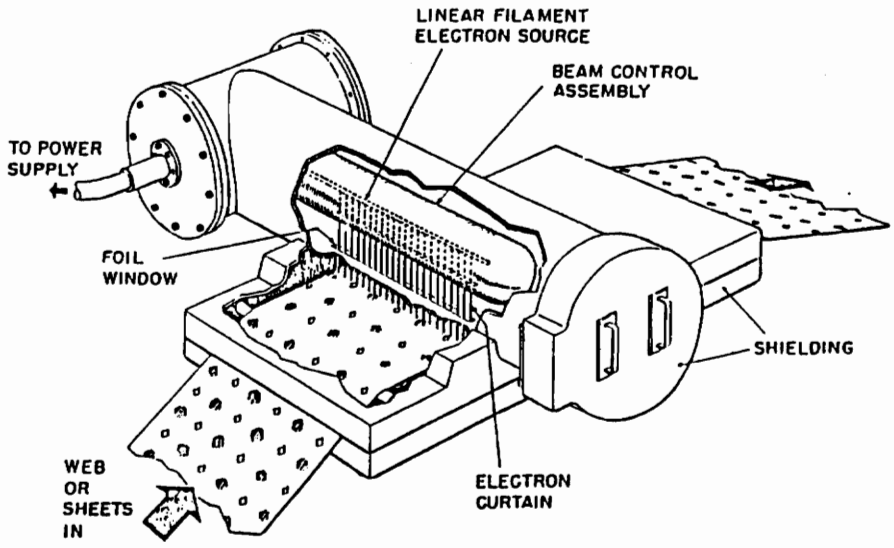

Figure 4-1. Schematic drawing of the ESI CB150 electrocurtain: electron beam chamber and conveyor system.

each blend composition, the following procedure was used : (a) a film was placed on a glass slide in the hot stage for two minutes at some predetermined temperature. (b) The slide was removed from the hot stage and the film was inspected for turbidity with the microscope. (c) The temperature of the hot stage was increased 5°C and the film was placed in the hot stage for two more minutes. This procedure was repeated until some signs of cloudiness appeared in the film. Then, a new sample was placed in the hot stage at the highest temperature where no turbidity was yet observed. The same procedure as above was used but with an increment in temperature of 2°C. The cloud point temperature, Ts, was estimated by the average of the temperatures just before and after turbidity appeared, with an associated experimental error of ± 1°C.

4.5 Gel Content Determination

Weighed films with various compositions were extracted in tetrahydrofuran (THF) for 48 hours using a Soxhlet extractor. After extraction, in the case of gel formation, the sample was placed under 25 in.Hg of vacuum at 80°C for the 90 wt % in PS blend, and at 120°C for systems with higher PS content, for 48 hours. No further weight reduction is expected after this drying time. The gel fraction is calculated by dividing the weight of the insoluble fraction (if any) by the initial weight of the film, and is the average of at least two extractions.

4.6 Rheological Measurements

Rheological experiments were carried out on a Rheometrics System RMS 800 rheometer with parallel plate geometry in the 170-230°C temperature range. The blend samples consisted of discs with a thickness of ca. 1.5 mm that were prepared by pressing several films together with a hot press for 10 min at a temperature of(Tg+40°C) and a pressure of 0.2 psi. The gap between the parallel plate was at least 1 mm with the 2.5 cm diameter plates.

Preliminary strain sweep experiments were performed in the 1-10 % range at a frequency of 0.1 rad/s, and indicated linear viscoelastic behavior up to 10 % strain. Therefore, frequency sweeps were performed under a constant strain of 3 % in the 0.1-100 rad/s range.

V-RESULTS AND DISCUSSION

5.1 Characterization of the Unirradiated PS/PVME Blends

Figure 5-1 depicts the cloud point temperatures for the unirradiated PS/PVME blends investigated in this work. This blend series displays LCST behavior with a critical point around 115°C and a critical composition in the range of 70 to 80 wt % PVME, based on comparison of this curve with that obtained with the same materials by McHerron (3)(see Fig.318).

The viscosity - frequency responses of the unirradiated PS/PVME systems [(100/0), 98/2, 95/5, 90/10, and 0/100] are displayed at different temperatures in Fig.5-2 - Fig.5-6 respectively. Based on the Tg of the blend systems shown in Fig.3-15, and in order to be in the temperature region near where the Arrhenius Law applies, the temperatures investigated in this work were 170°C, 185°C, 200°C, 215°C, and 230°C for the 100/0, 98/2, 95/5, and 90/10 systems. Since PVME is a low molecular weight compound with a value of Tg around -32°C, the temperatures carried out for this pure material were 90°C, 110°C, 130°C, and 150°C. Rheological experiments were indeed not possible to run at higher temperatures, the instrument being not sensitive enough to measure the low viscosity displayed by pure the PVME above 150°C. It is essential to

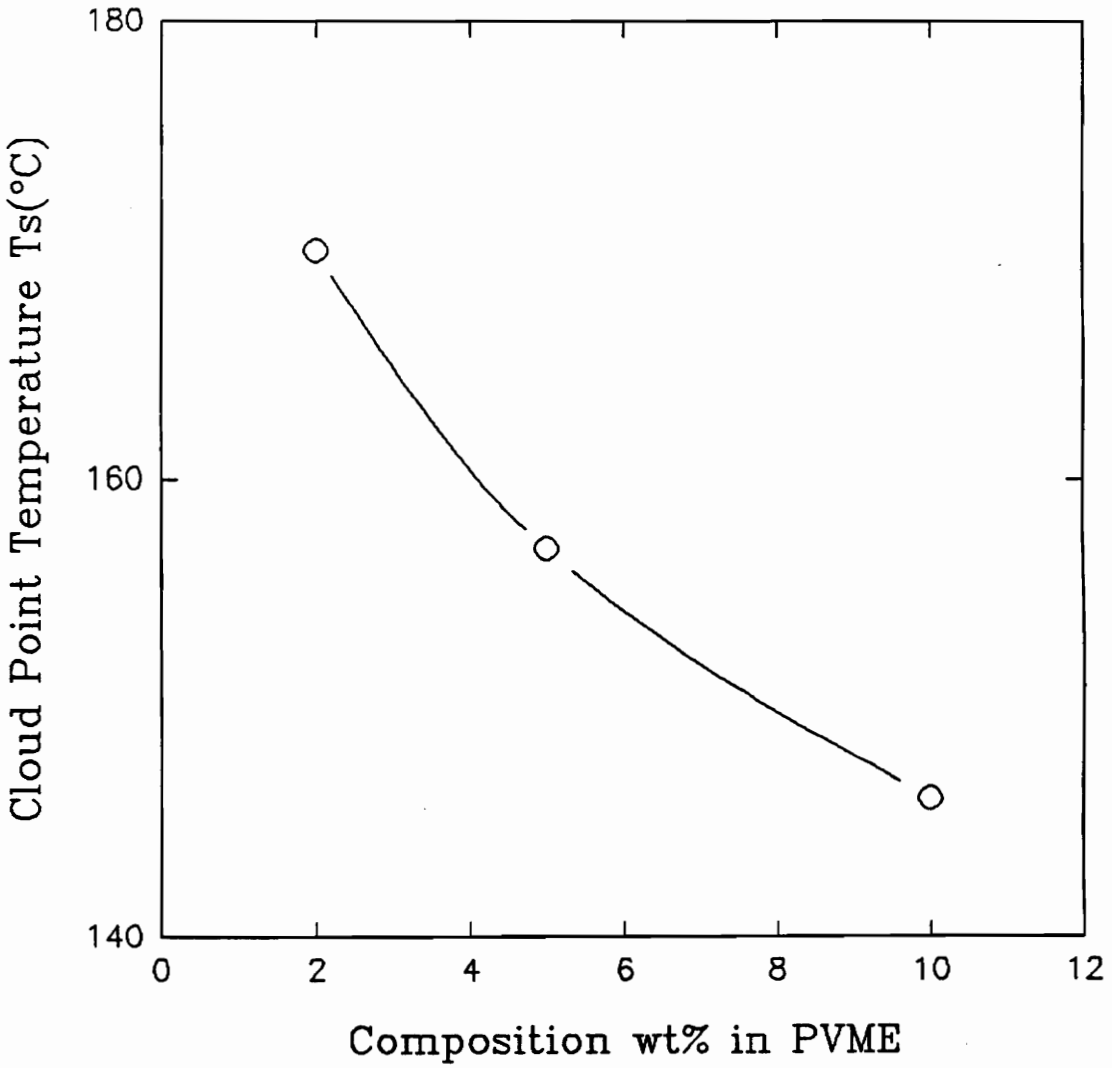

Figure 5-1. Plot of the cloud point temperature, Ts, versus composition (wt % PVME) for the unirradiated PS/PVME blends investigated in this study.

know the glass transition temperature of each system before performing the rheological measurements, because it may influence the temperature dependence of the viscosity (see section 2.2). In addition, it is important to know the state of each blend during irradiation, since it may have an affect on the extent of radiation induced changes in the systems.

As stated earlier, due to instrumental limitations, it is sometimes not possible to carry out the rheological measurements at a low enough shear rate to obtain the zero-shear viscosity. This was the case in this work, and therefore, this region where the behavior is shear rate independent, or Newtonian, does not appear in the viscosity - frequency responses of the systems investigated, except for pure PVME. Indeed, for this polymer which is of low molecular weight material, the minimum frequency investigated (0.1 rad/s) is low enough to obtain the zero-shear viscosity in the temperature range carried out. As shown, all the systems clearly display shear thinning behavior, characterized by the decrease of the viscosity as the shear stress increases, pure PVME displaying this behavior only a little at the lowest temperature investigated. As expected, the viscosity of the blends decreases with temperature, but it also decreases as the PVME content increases, based on comparison of the viscosity - frequency response of pure PS with that of each blend. This results from the effect on the blend viscosity of

the addition of a lower Tg component with low molecular weight, PVME, to the high molecular weight PS (see section 2.3). The erratic behavior displayed by pure PVME in the 0.1-0.2 rad/s frequency range is due to instrumental limitations, the rheometer being not sensitive enough to accurately measure the very low viscosity of this material at these torque values. It is interesting to notice an "abnormal" behavior of the viscosity occurring for the 95/5 and 90/10 systems. They both show an increase of the value at 200°C compared to that obtained at 185°C, as well as some unusual crossings of the viscosities at intermediate frequencies. Since the rheological measurements have been carried out above the phase separation temperature Ts for all the blends, this behavior is distinctly believed to be the result of phase separation on the viscosity, i.e the effects of kinetics occurring during the formation of the two distinct phases. However, it should be noted that these abnormalities do not appear with the 98/2 blend. Keeping in mind the explanation given above, the PVME content is so low in this 98/2 system that the viscosity - frequency response is less sensitive to the phase separation kinetics. This is purely speculation, however, and further experimentation is necessary to understand the phase separation process occurring in these systems.

The temperature dependence of the viscosity is displayed in Fig.5-7 and Fig.5-8 for each system. Table 5-1 gives the

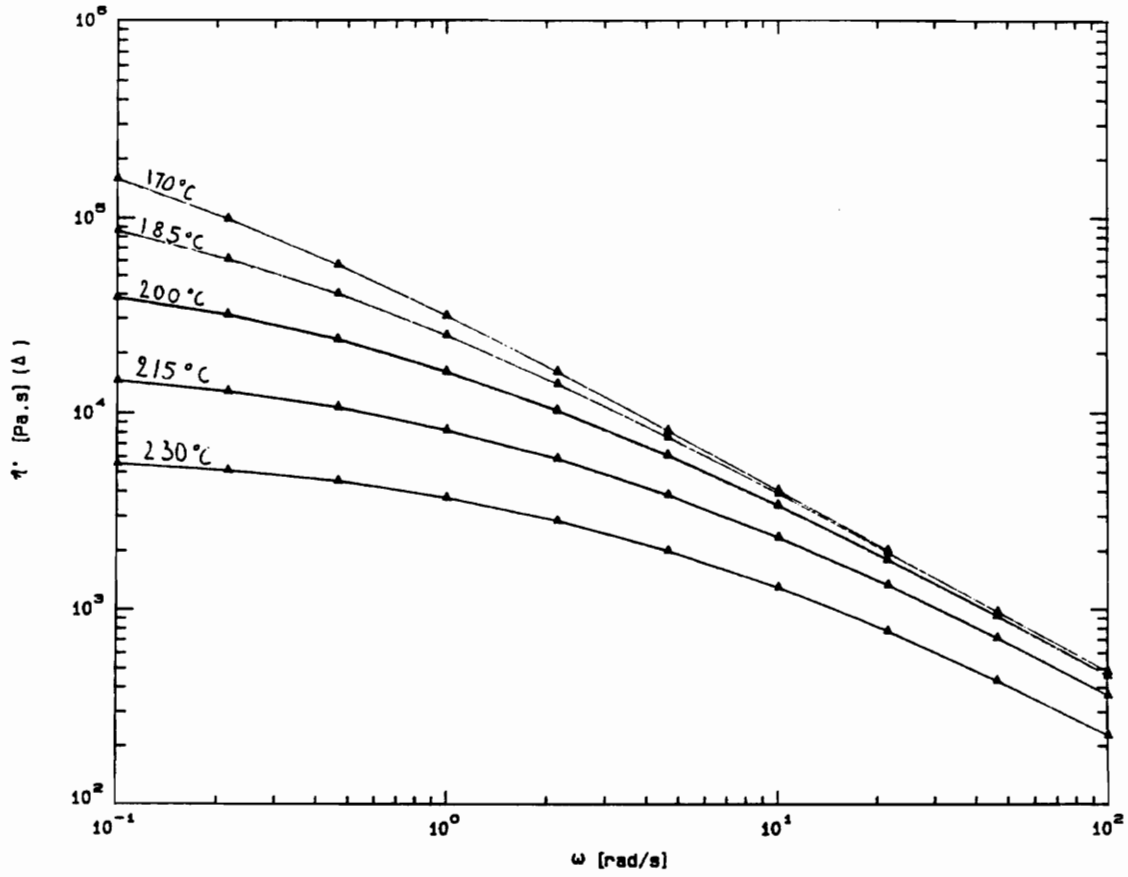

Figure 5-2. Plot of the dynamic viscosity, eta', versus frequency, w, at different temperatures for pure unirradiated PS.

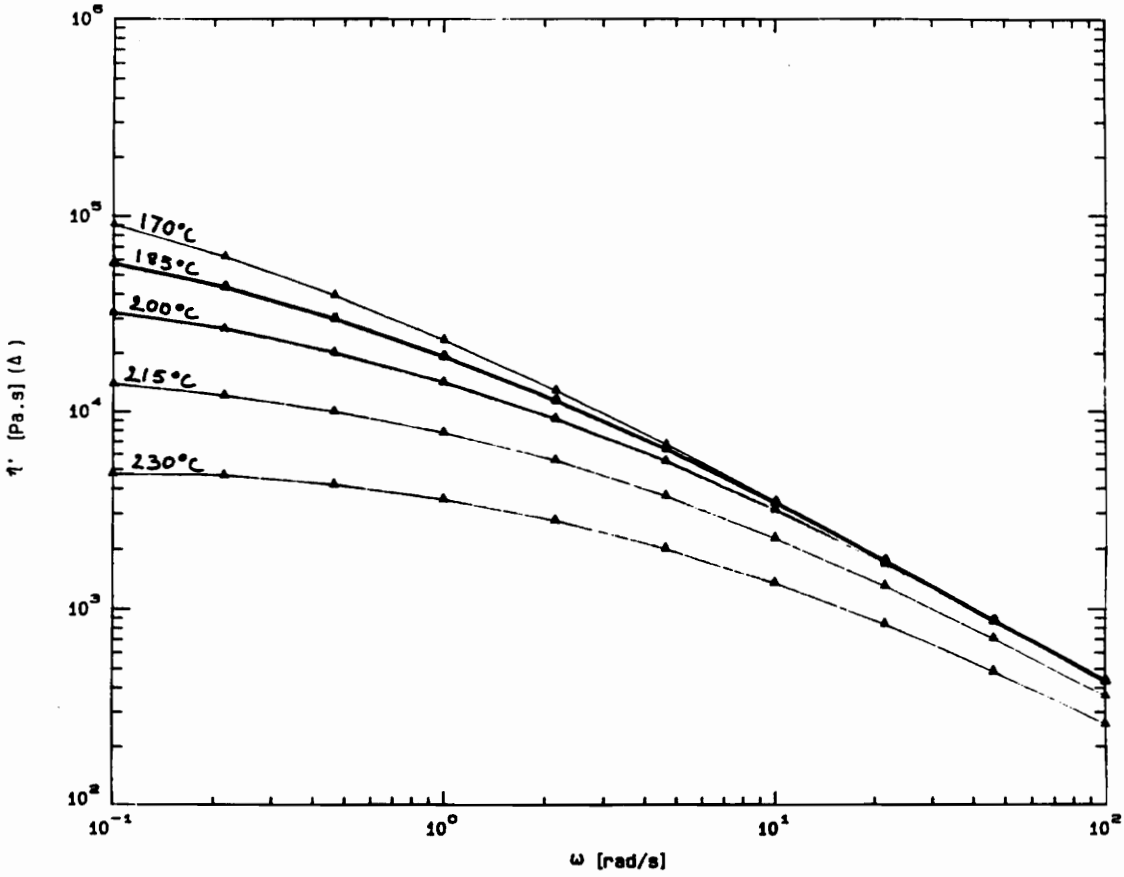

Figure 5-3. Plot of the dynamic viscosity, eta', versus frequency, w, at different temperatures for the unirradiated 98/2 PS/PVME blend.

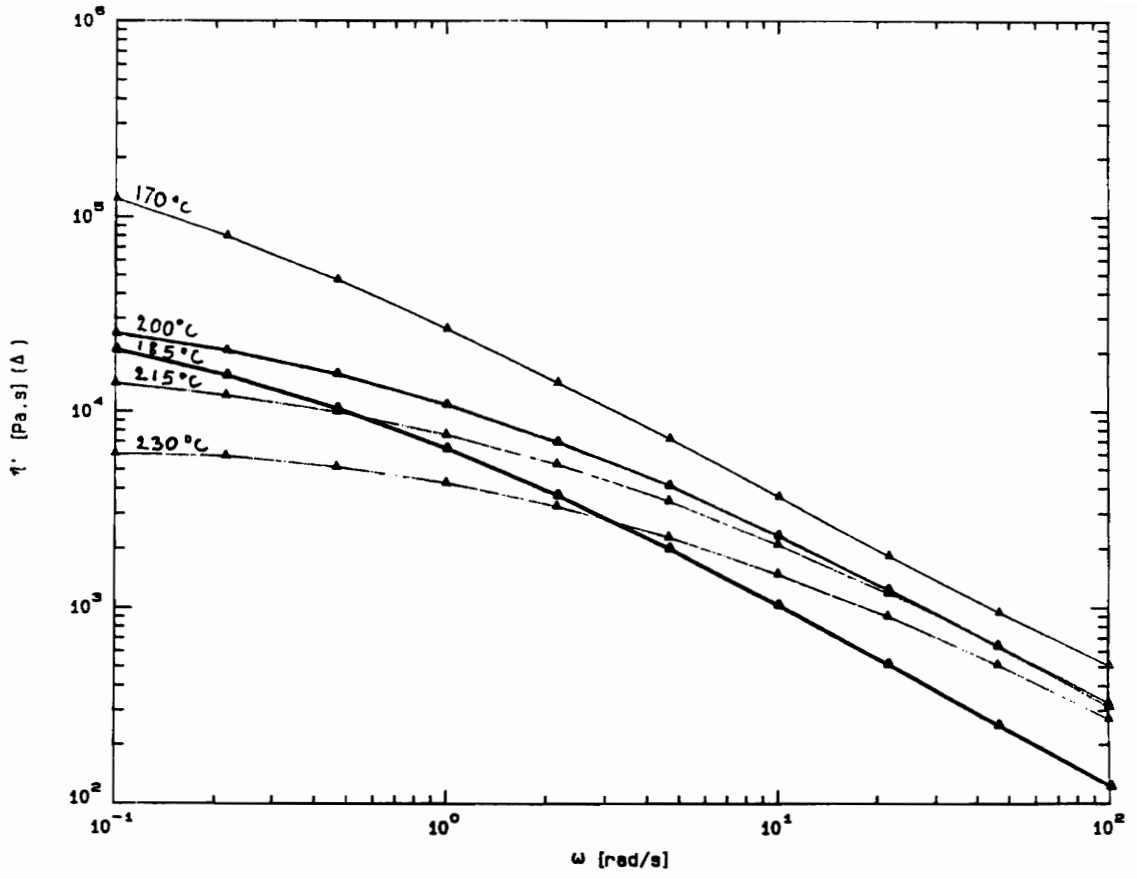

Figure 5-4. Plot of the dynamic viscosity, eta', versus frequency, w, at different temperatures for the unirradiated 95/5 PS/PVME blend.

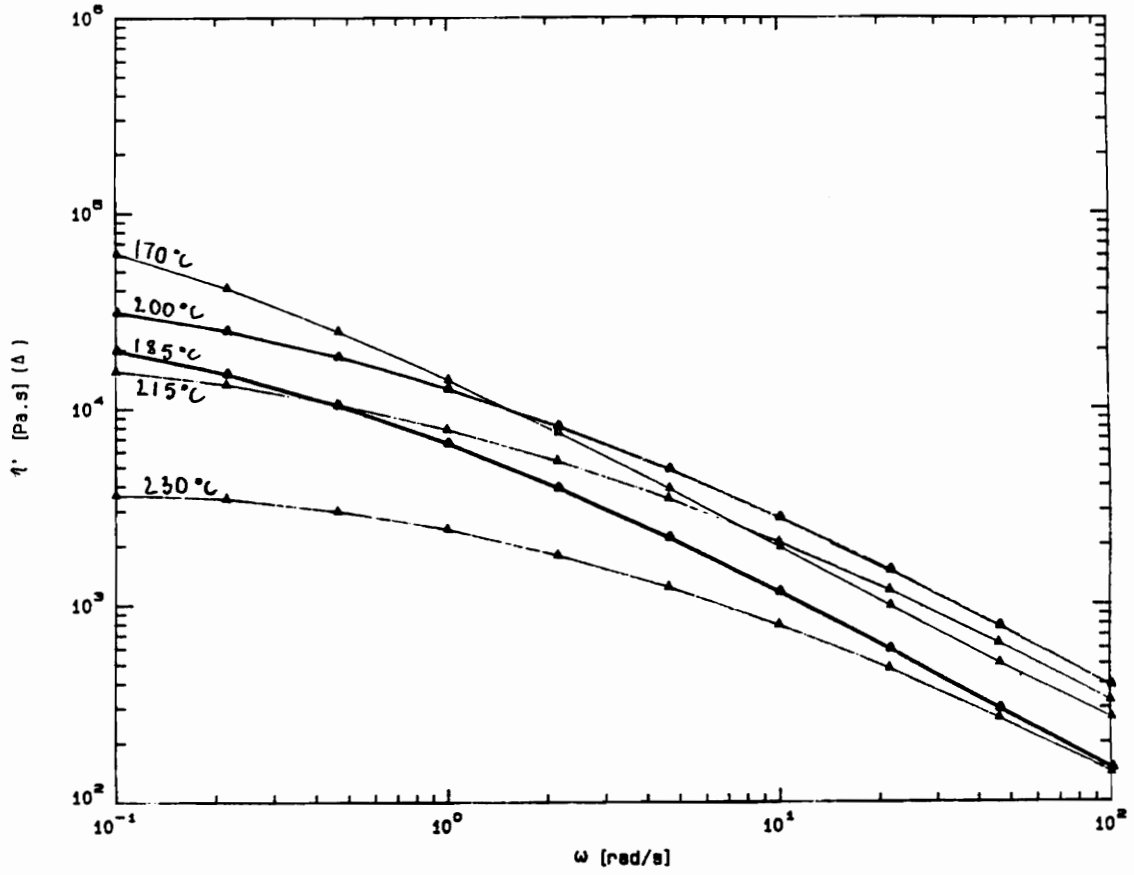

Figure 5-5. Plot of the dynamic viscosity, eta', versus frequency, w, at different temperatures for the unirradiated 90/10 PS/PVME blend.

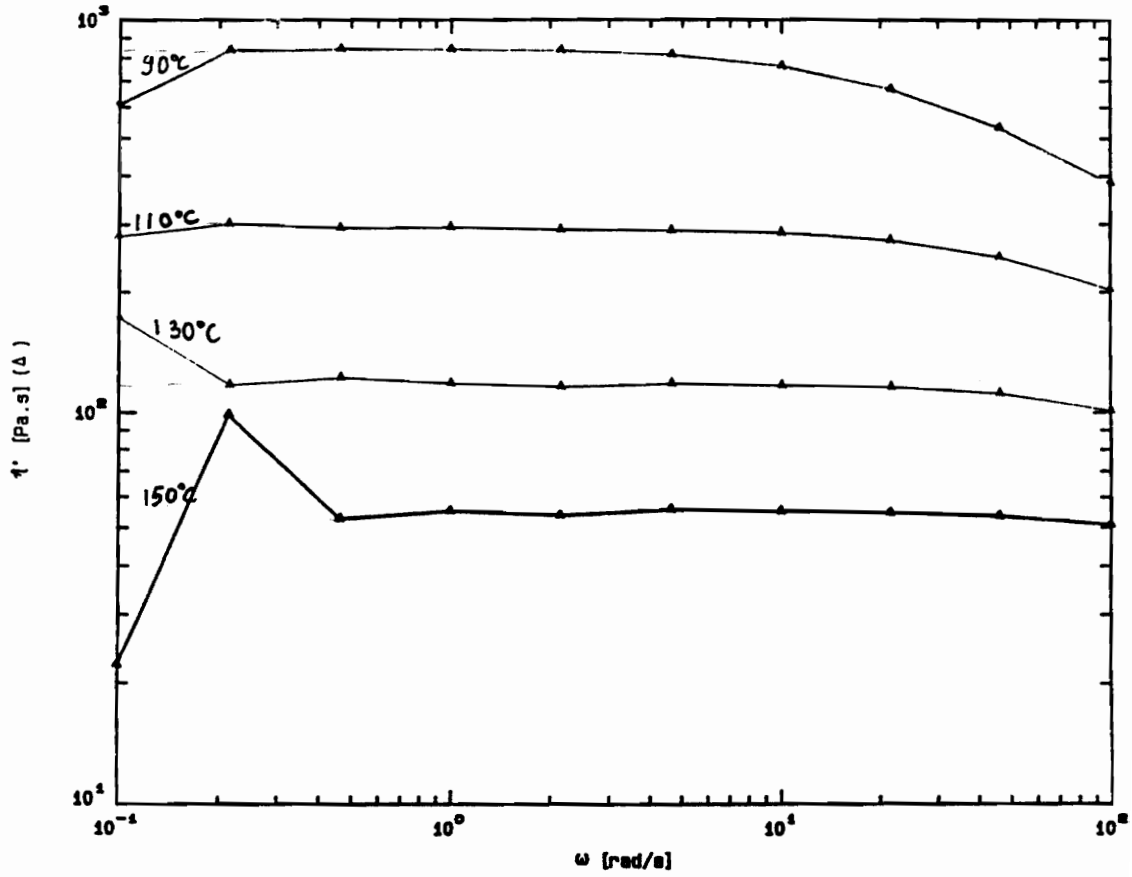

Figure 5-6. Plot of the dynamic viscosity, eta', versus frequency, w, at different temperatures for pure unirradiated PVME.

corresponding flow activation energy, Ea, calculated from the slope of each plot (assuming a linear fit). The error associated with the reported values does not exceed ± 2 Kcal/mol. It must be noted that the investigator had to consider the phase separation of the systems in the temperature range investigated. However, as shown, the general linear behavior of the Arrhenius plots was not affected. As explained in section 2.2, any chemistry or structure that makes the chain backbone stiffer or promotes branching generally leads to a higher Ea. Here, the phenyl group attached to the PS backbone chain produces a large impediment to steric rotation effect. By looking at the structure of PVME shown earlier in Fig.1-9, it indicates that the steric effect of the side group attached to the backbone chain is clearly not as large as that of PS, the methyl-ether group being smaller than the phenyl group. Notice that as the PVME content increases in the blend composition, the value of Ea decreases. This is believed to be due to the fact that PVME has a lower Ea (14 Kcal/mol) than PS (30 Kcal/mol), the system average segmental movement becoming easier as the PVME content increases within the PS-rich phase. Using an Arrhenius form of the temperature dependence of viscosity, Wissbrun (16) found a value of 31 Kcal/mol for PS at 200°C, which is good agreement with the value reported here.

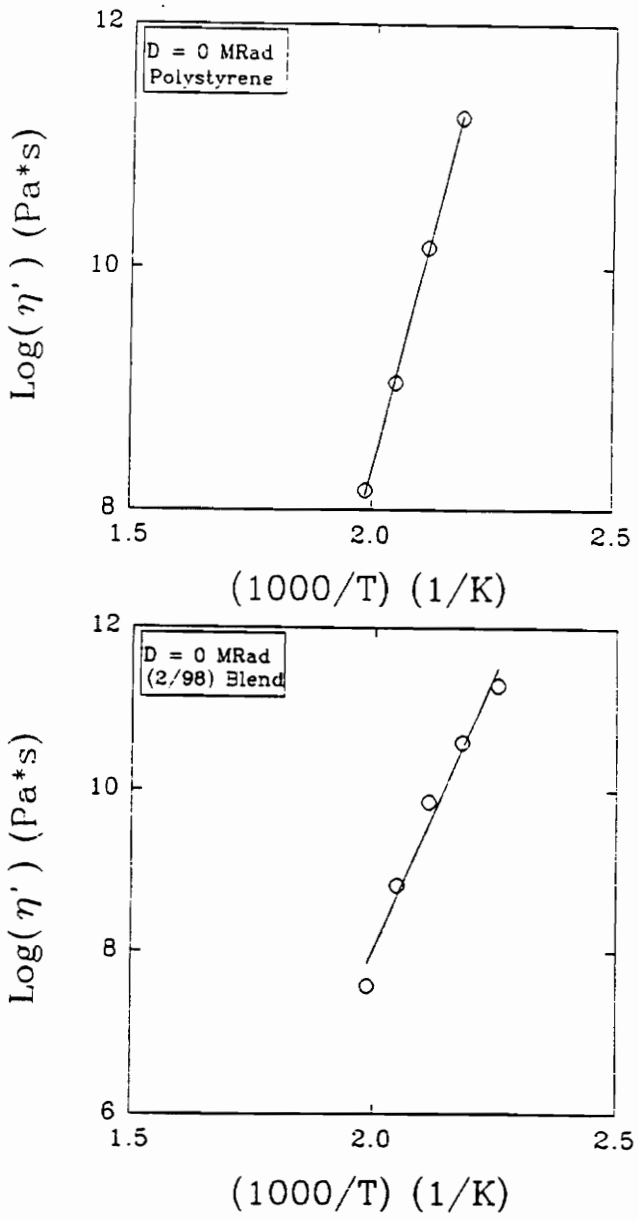

Figure 5-7. Arrhenius plots of the log of the dynamic viscosity obtained at a constant shear stress for (1) pure unirradiated PS, and (2) unirradiated 2/98 PVME/PS blend.

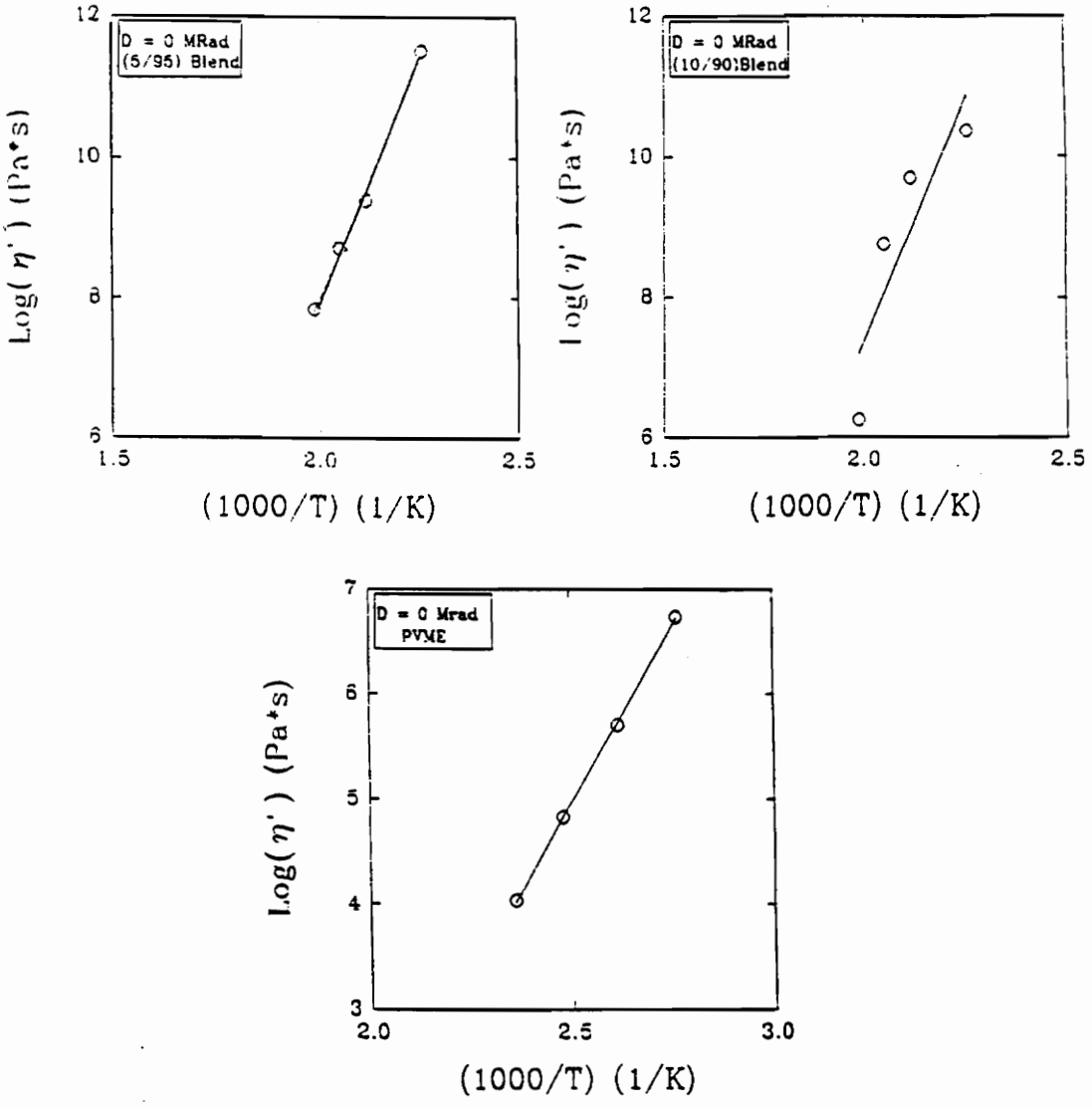

Figure 5-8. Arrhenius plots of the log of the dynamic viscosity obtained at a constant shear stress for (1) unirradiated 5/95 PVME/PS blend, (2) unirradiated 10/90 PVME/PS blend, and (3) pure unirradiated PVME.

Table 5-1. Values of the flow activation energy obtained with the unirradiated PS/PVME blend systems - associated shear stress range (in N/m^2) of the rheological measurements for each system.

System PS/PVME	Flow Activation Energy (± 2 Kcal/mol)	Shear stress range of the rheological measurements (N/m^2)
100/0	14	50-5100
98/2	21	70-2700
95/5	26	90-3800
90/10	21	10-1000
100/0	14	-

5.2 Characterization of the Irradiated PS/PVME Blends

As expected, no traces of gel were found after irradiation up to 10 Mrads for all the systems under consideration in this work. This is in accordance with the results obtained by McHerron (3) shown in Fig.3-13 where no gel was formed for a system containing 15 wt % of PVME irradiated to 50 Mrads. This is a consequence of low radiation doses investigated in this study, combined with a low PVME content in the blend systems.

The cloud point curves for the series of PS/PVME blends, unirradiated and irradiated to 10 Mrads, are displayed in Fig.5-9. As shown, irradiation to 10 Mrads distinctly results in a slight increase of the phase separation temperature Ts. Irradiation to the lowest doses, 2 and 5 Mrads, did not greatly change Ts. This increase observed at a level of 10 Mrads can be due to two different phenomena occuring under irradiation. It may imply that some radiation grafting has occurred between the two blend components. Notice that as the PVME content increases in the blend systems, the difference between the two curves becomes larger. As the PVME content increases in the composition system, more grafting events would be likely to occur, resulting in a higher difference between the two cloud point curves. Or the enhancement of the cloud point temperature could result from a drop of the components molecular weight under irradiation (see Fig.1-10

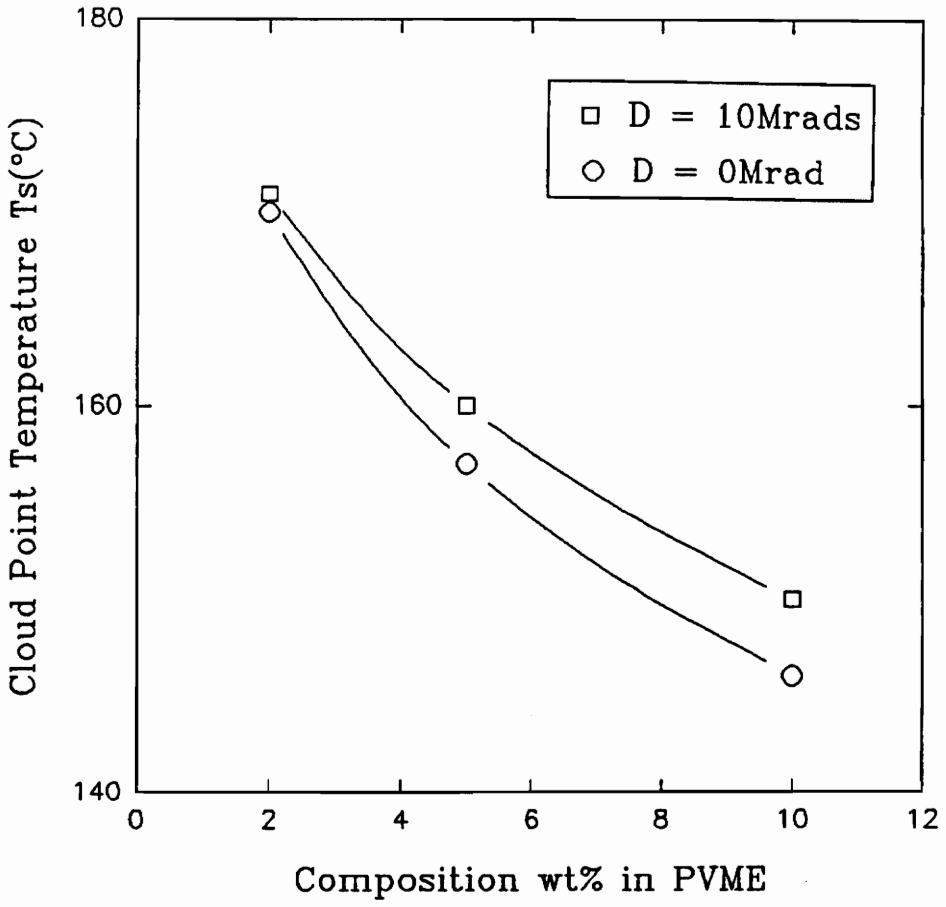

Figure 5-9. Plot of the cloud point temperatures, Ts, versus composition (wt % PVME) for PS/PVME blends irradiated to the indicated dose.

and 1-11). The resistance displayed by pure PS in the dose range investigated contradicts this hypothesis. Other data will show later in this study that this increase in the phase separation temperature under irradiation is not due to a degradation of PVME either. Hence, the effect of electron beam radiation on the phase separation process results in the single phase region extending to a higher temperature, with the cloud point temperature increasing from 146°C for the unirradiated 90/10 blend to 150°C for the same system irradiated to 10 Mrads. This result is in agreement with the study of Briber et al.(46) mentioned earlier in the literature review. Specifically, they investigated the effect of γ-radiation crosslinking on the phase diagram for a compatible linear deuterated polystyrene/poly(vinyl methyl ether) PSD/PVME blend, the component weight average molecular weight being 460,000 for PS and 120,000 for PVME. Their results showed that, with a dose of 125 Mrads, the cloud point temperature rises from 140°C for the unirradiated system to an extrapolated value of 430°C. This much larger increase in temperature observed is due essentially to the much higher radiation dose applied leading to extensive grafting.

The following section will now present the rheological results obtained for each system separately, and how the influence of irradiation alters the flow curves.

Polystyrene

Figures 5-10 - 5-12 show the viscosity - frequency responses of PS after irradiation to 2, 5, and 10 Mrads respectively. Comparison of these responses with that obtained for the unirradiated PS (see Fig.5-2) indicates that no major changes occurred due to radiation. Figures 5-13 and 5-14 show superpositions made between the viscosity - frequency responses of the unirradiated material with that of the 2 Mrads and 10 Mrads irradiated material. As shown, only small increases in the viscosity occur after irradiation. This behavior was expected, since PS is known to be quite stable with respect to radiation. Very large doses are generally required to produce any noticeable change. Hence, polystyrene can be used to promote radiation protection in polymeric materials due to the stabilizing nature of the phenyl group. This protective effect of the aromatic group is thought to arise through a number of possible mechanisms such as energy transfer or radical-radical reactions (40).

98/2 Blend System

Figures 5-15 - 5-17 show the viscosity versus frequency responses obtained after irradiation to 2, 5, and 10 Mrads respectively for the 98/2 blend system. As shown in Fig. 5-18 and 5-19, comparison of the responses between the unirradiated and the irradiated systems to 2 Mrads and 10 Mrads indicates that no major changes in the viscosity occurred over the entire frequency range. Using this viscosity - frequency

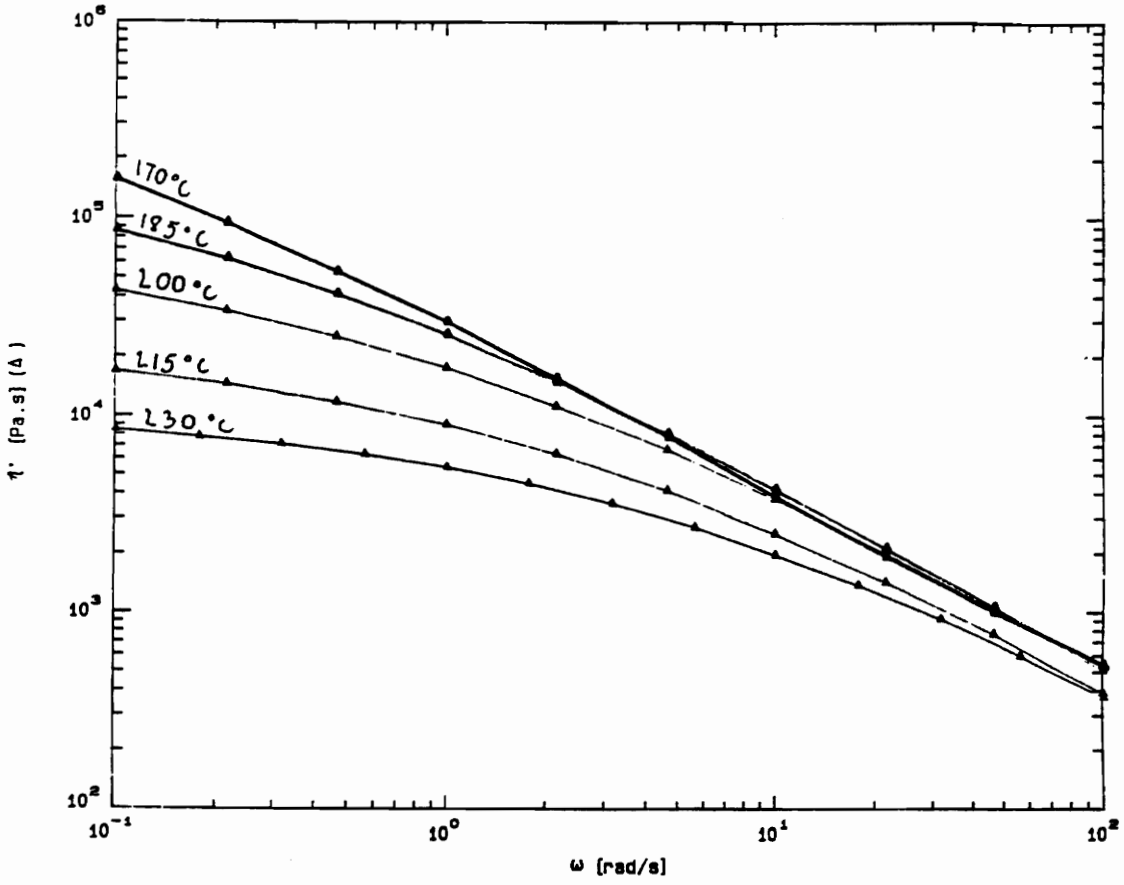

Figure 5-10. Plot of the dynamic viscosity, eta', versus frequency, w, at different temperatures for pure PS irradiated to 2 Mrads.

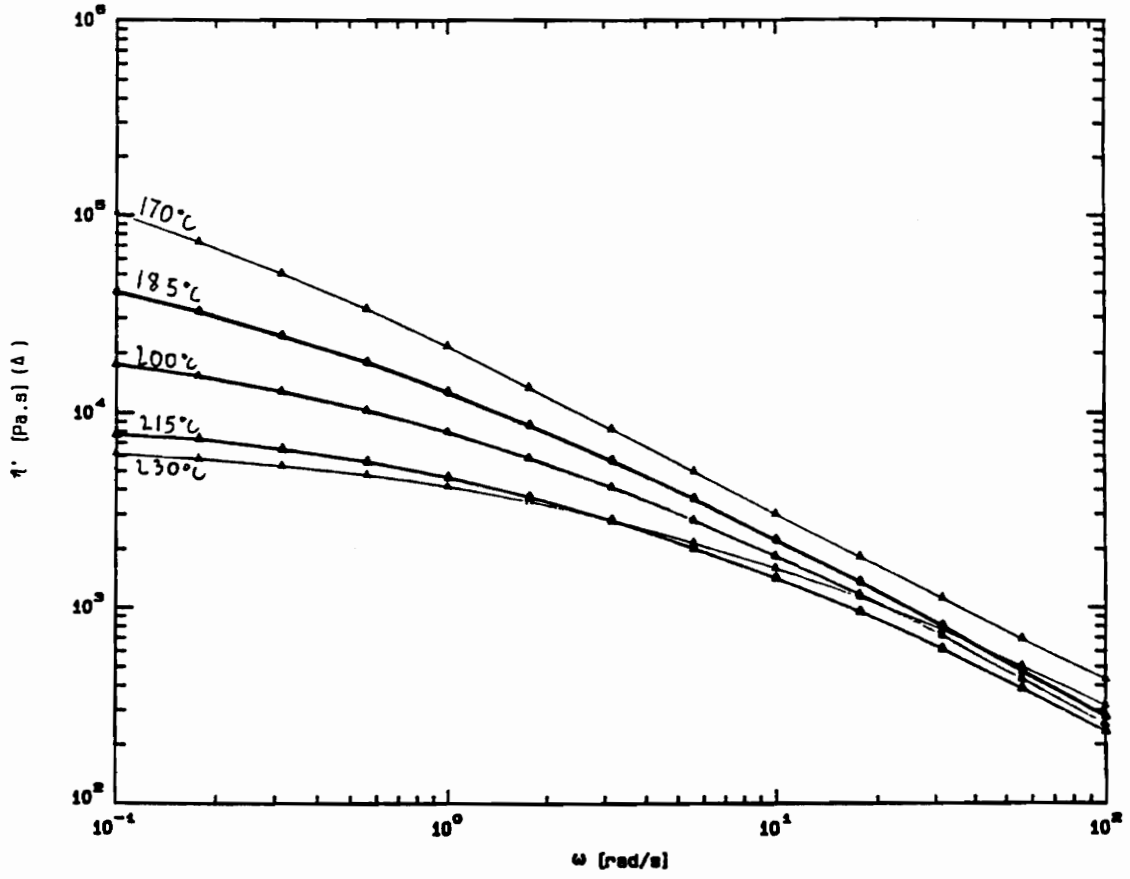

Figure 5-11. Plot of the dynamic viscosity, eta', versus frequency, w, at different temperatures for pure PS irradiated to 5 Mrads.

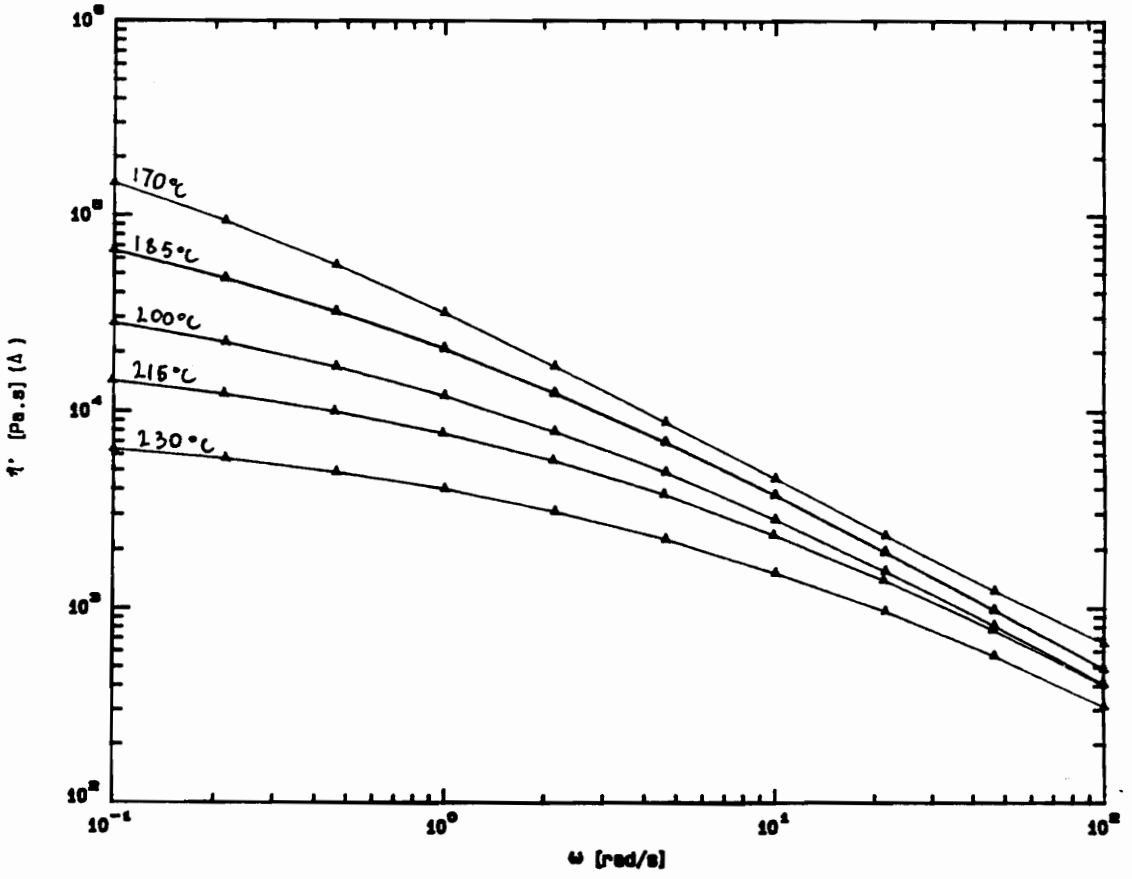

Figure 5-12. Plot of the dynamic viscosity, eta', versus frequency, w, at different temperatures for pure PS irradiated to 10 Mrads.

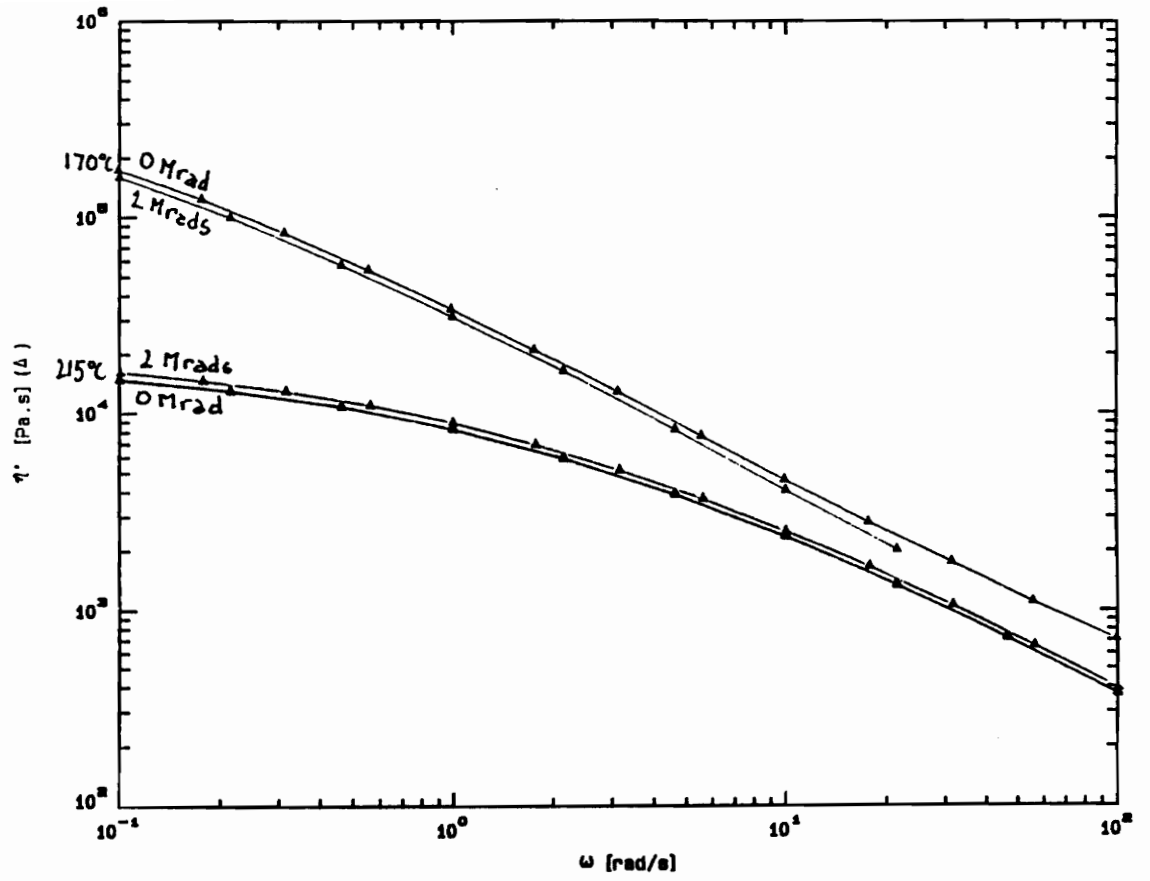

Figure 5-13. Superposition of the dynamic viscosity-frequency responses of pure PS (1) unirradiated (0Mrad), and (2) irradiated to 2 Mrads, at 2 different temperatures.

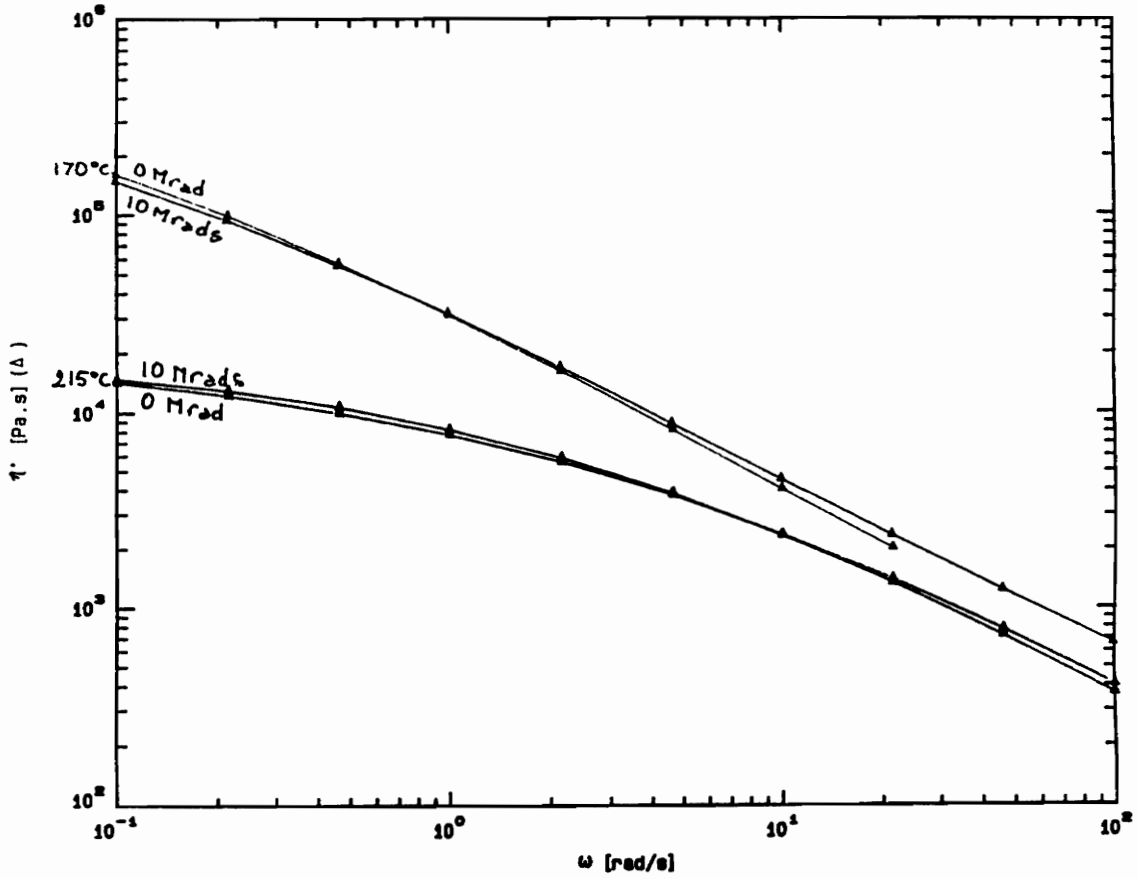

Figure 5-14. Superposition of the dynamic viscosity-frequency responses of pure PS (1) unirradiated (0Mrad), and (2) irradiated to 10 Mrads, at 2 different temperatures.

response as a guide, the 98/2 blend thereby displays similar radiation resistance in this dose range to that of pure PS. The weight percentage of PVME in this system is very low, and apparently this small amount of PVME does not induce any more significant changes in the viscosity, at least on this scale of sensitivity, than what was observed with pure PS.

95/5 Blend System

The viscosity - frequency responses of the 95/5 system irradiated to 2, 5, and 10 Mrads are illustrated respectively in Fig.5-20 - 5-22. It must be mentioned that comparison of these curves with that obtained for the unirradiated blend (see Fig.5-4) is difficult because of the rise of the viscosity observed at 200°C for the unirradiated material. As stated earlier, this apparent abnormal behavior is believed to be due to the appearance of two phases in the blend systems, i.e. to the influence of the resulting kinetics on the viscosity. Indeed, the phase separation temperature has been crossed for all the systems at the temperature range investigated. Also, notice that this behavior does not appear with the irradiated systems. This would mean that a decreasing rate of the phase separation kinetics has occurred due to radiation. This may imply that irradiation of the system has induced grafting between the two components, resulting in a higher compatibility of the two polymers. Or, as said before, it may imply that the PVME molecular weight

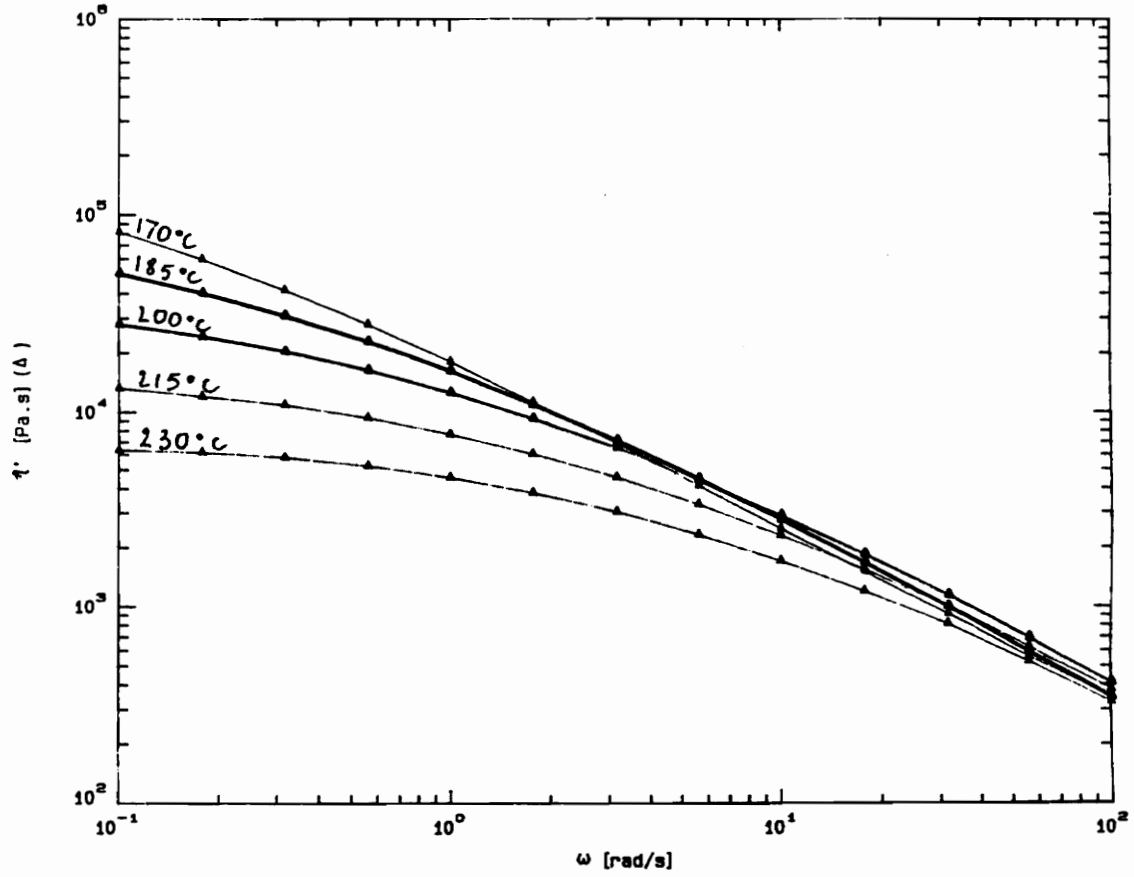

Figure 5-15. Plot of the dynamic viscosity, eta', versus frequency, w, at different temperatures for the 98/2 PS/PVME blend irradiated to 2 Mrads.

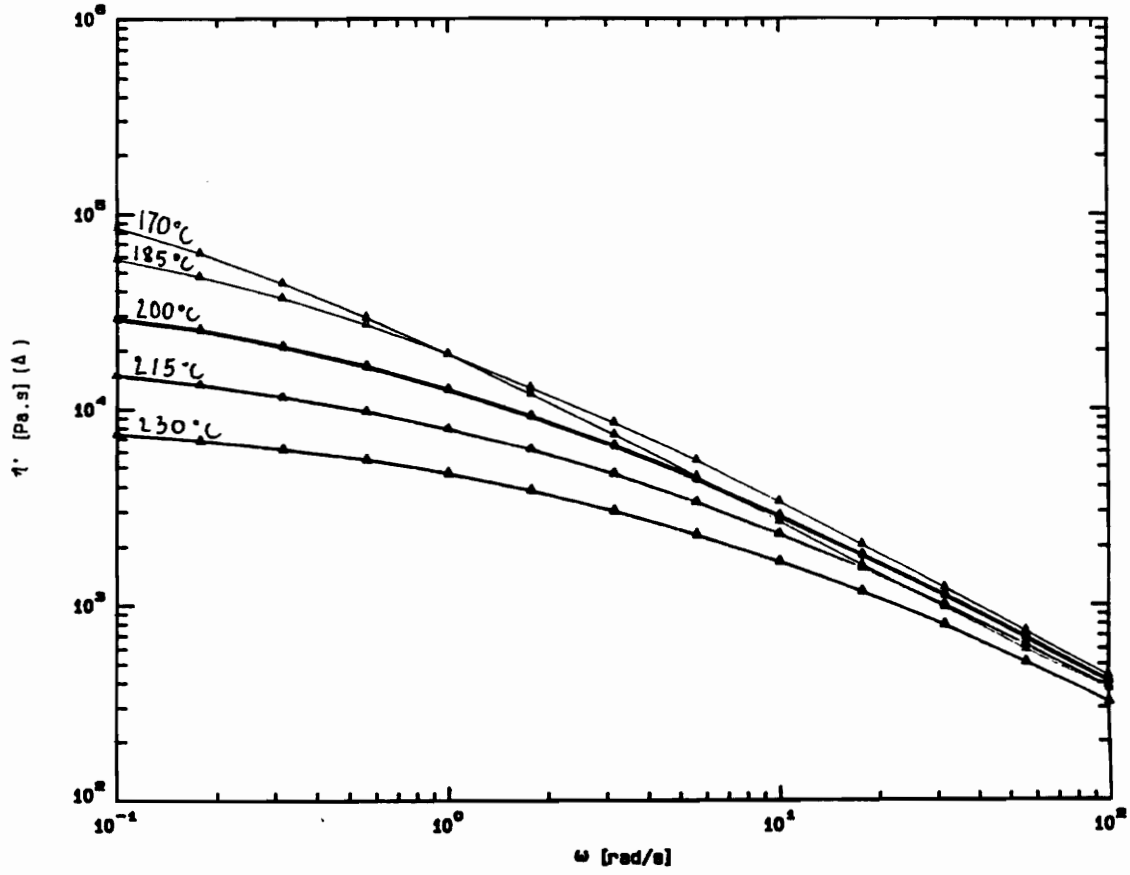

Figure 5-16. Plot of the dynamic viscosity, eta', versus frequency, w, at different temperatures for the 98/2 PS/PVME blend irradiated to 5 Mrads.

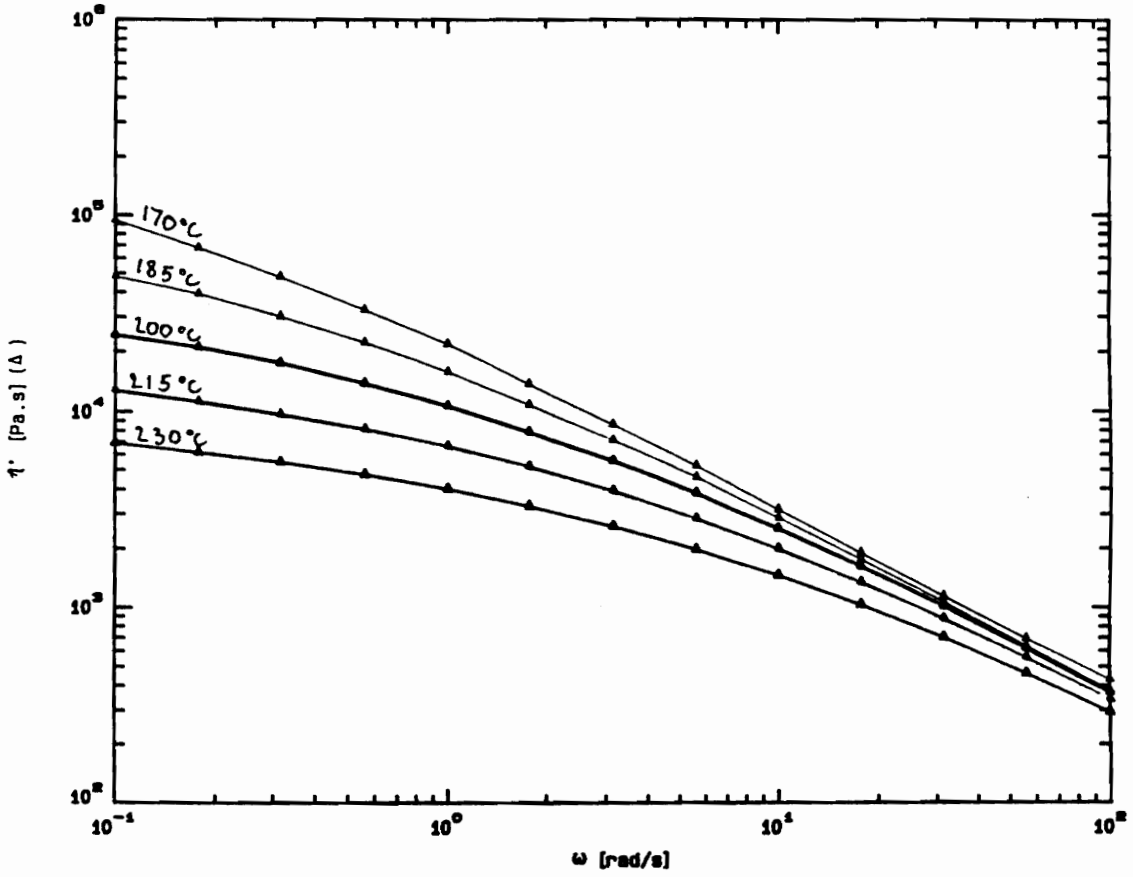

Figure 5-17. Plot of the dynamic viscosity, eta', versus frequency, w, at different temperatures for the 98/2 PS/PVME blend irradiated to 10 Mrads.

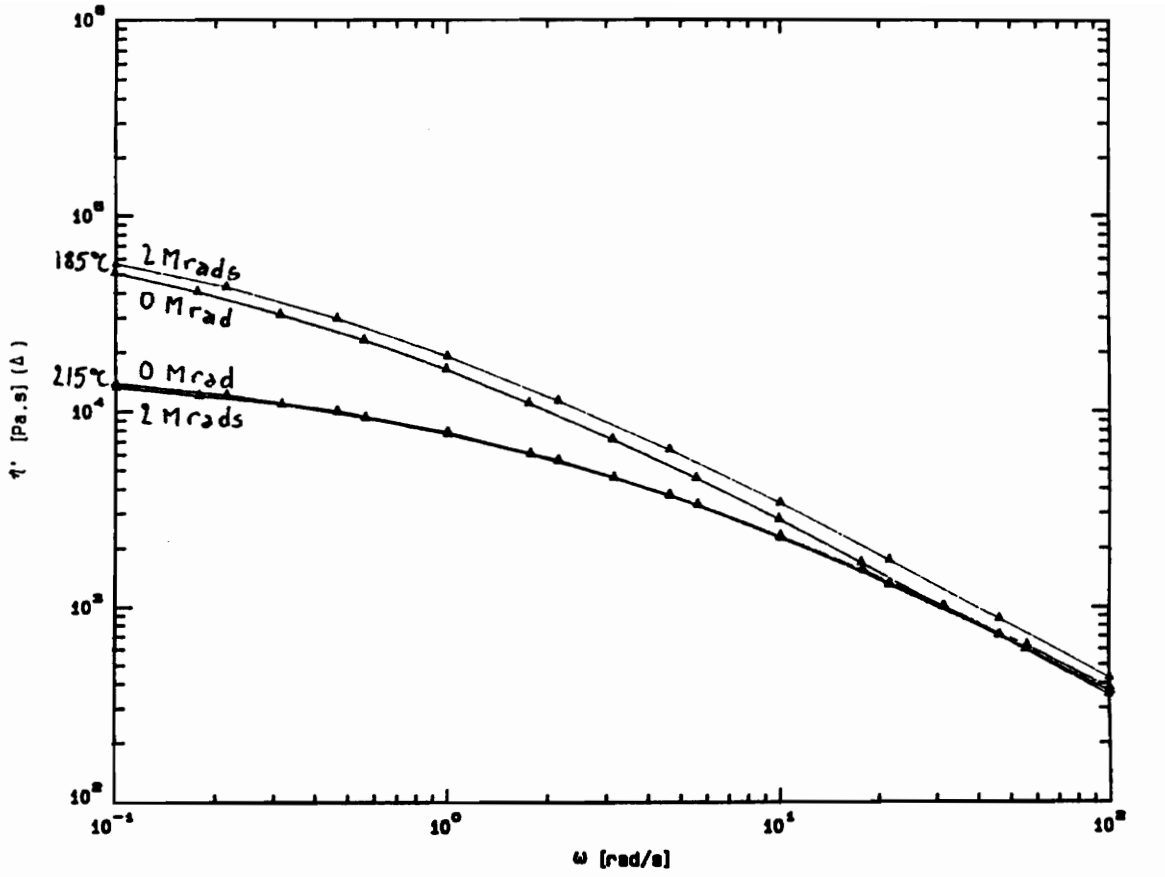

Figure 5-18. Superposition of the dynamic viscosity-frequency responses of the 98/2 PS/PVME blend (1) unirradiated (0Mrad), and (2) irradiated to 2 Mrads, at 2 different temperatures.

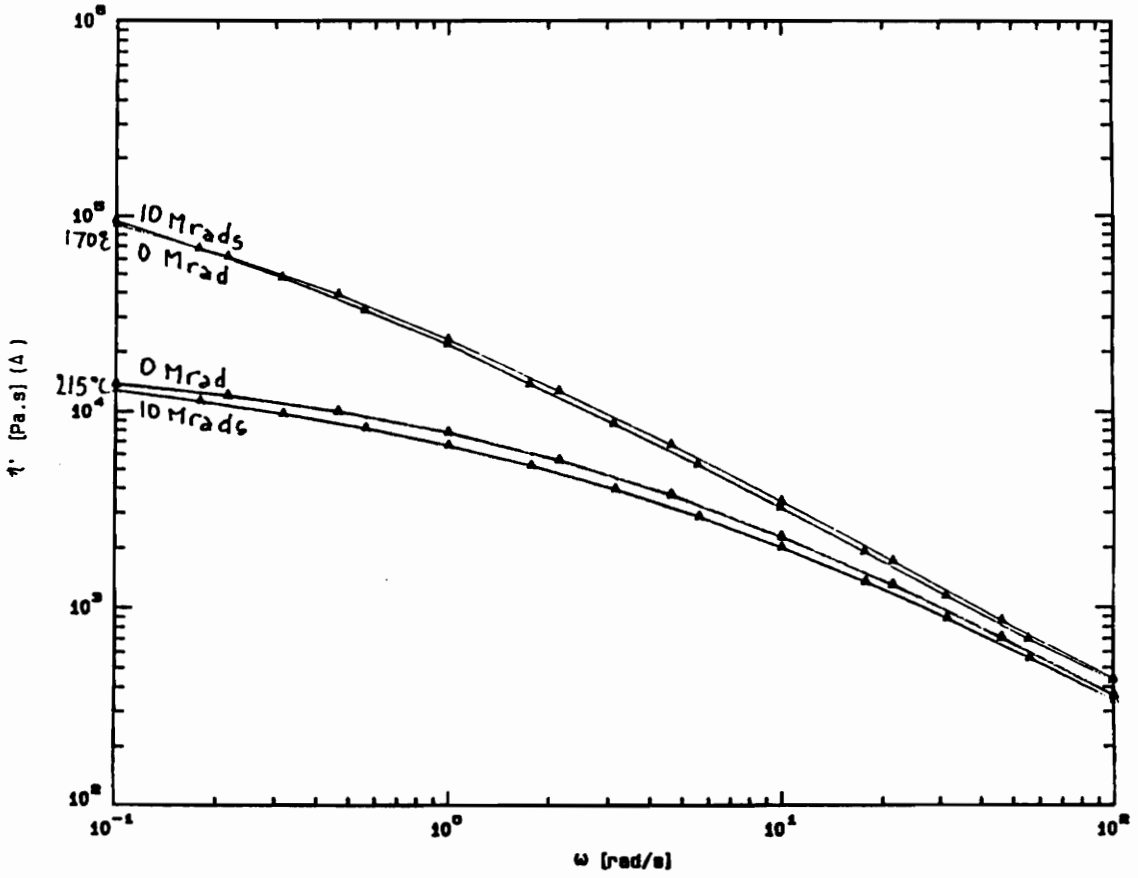

Figure 5-19. Superposition of the dynamic viscosity-frequency responses of the 98/2 PS/PVME blend (1) unirradiated (0Mrad), and (2) irradiated to 10 Mrads, at 2 different temperatures.

has decreased due to irradiation, resulting in a higher phase separation temperature, and therefore less effect of the phase separation on the rheological behavior. However, superposition of the rheological responses between the unirradiated and the irradiated systems are displayed in Fig. 5-23 and 5-24. As shown, irradiation of this system to the different dose levels investigated does not result in a clear and general behavior. Figures 5-23 shows good superposition, indicating radiation resistance of the system, while Fig.5-24 shows signs of possible degradation by a decrease of the viscosity. Any degradation would be surprising, since both of the components generally undergo crosslinking under radiation. These results may be due to the increase of the viscosity observed at 200°C for the unirradiated material, invalidating the comparison with the irradiated material.

90/10 Blend System

Figures 5-25 - 5-27 depict the rheological response of the 90/10 blend system after undergoing irradiation to 2, 5, and 10 Mrads respectively. Comparison of these curves with that obtained for the unirradiated material is illustrated in Fig.5-28 and 5-29. It is interesting to note that like the 95/5 system, the unirradiated 90/10 blend shows an increase of its viscosity at 200°C (see Fig.5-5). However, this latter system is obviously more sensitive to radiation, displaying a significant increase in its viscosity after irradiation.

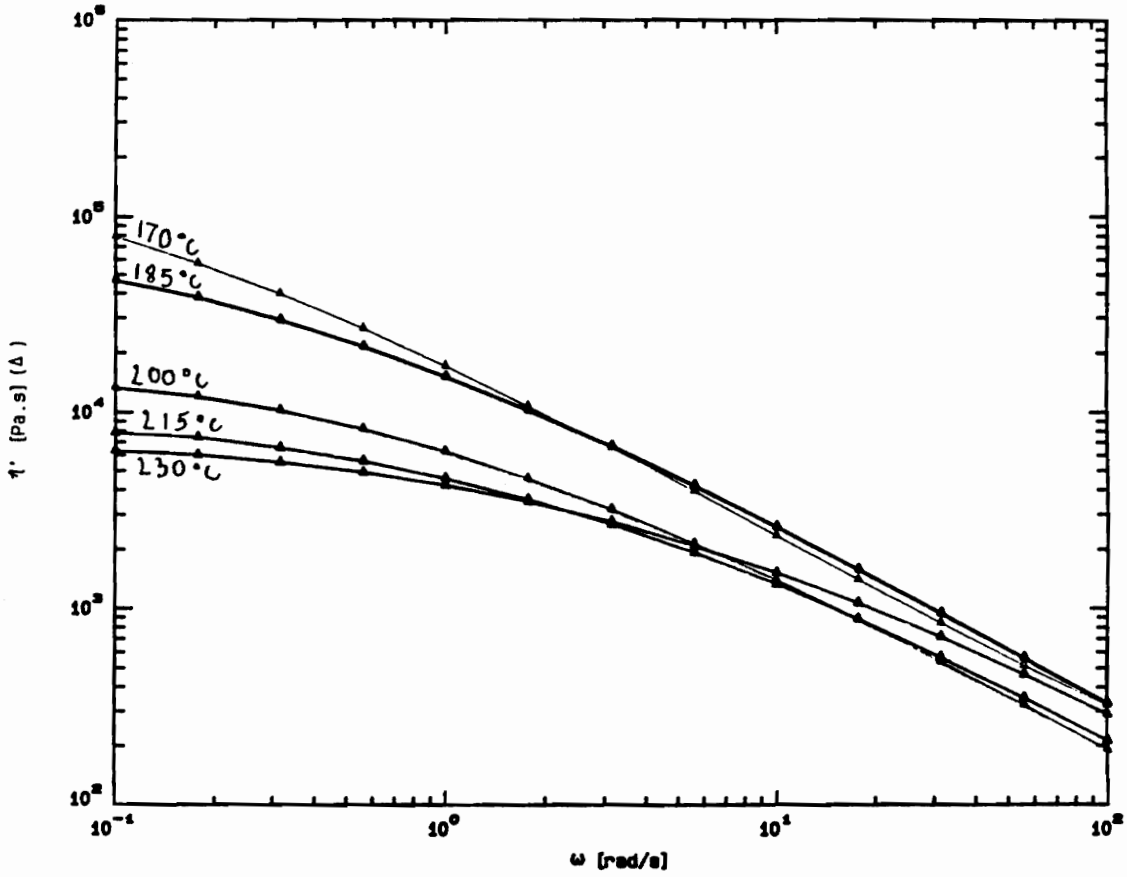

Figure 5-20. Plot of the dynamic viscosity, eta', versus frequency, w, at different temperatures for the 95/5 PS/PVME blend irradiated to 2 Mrads.

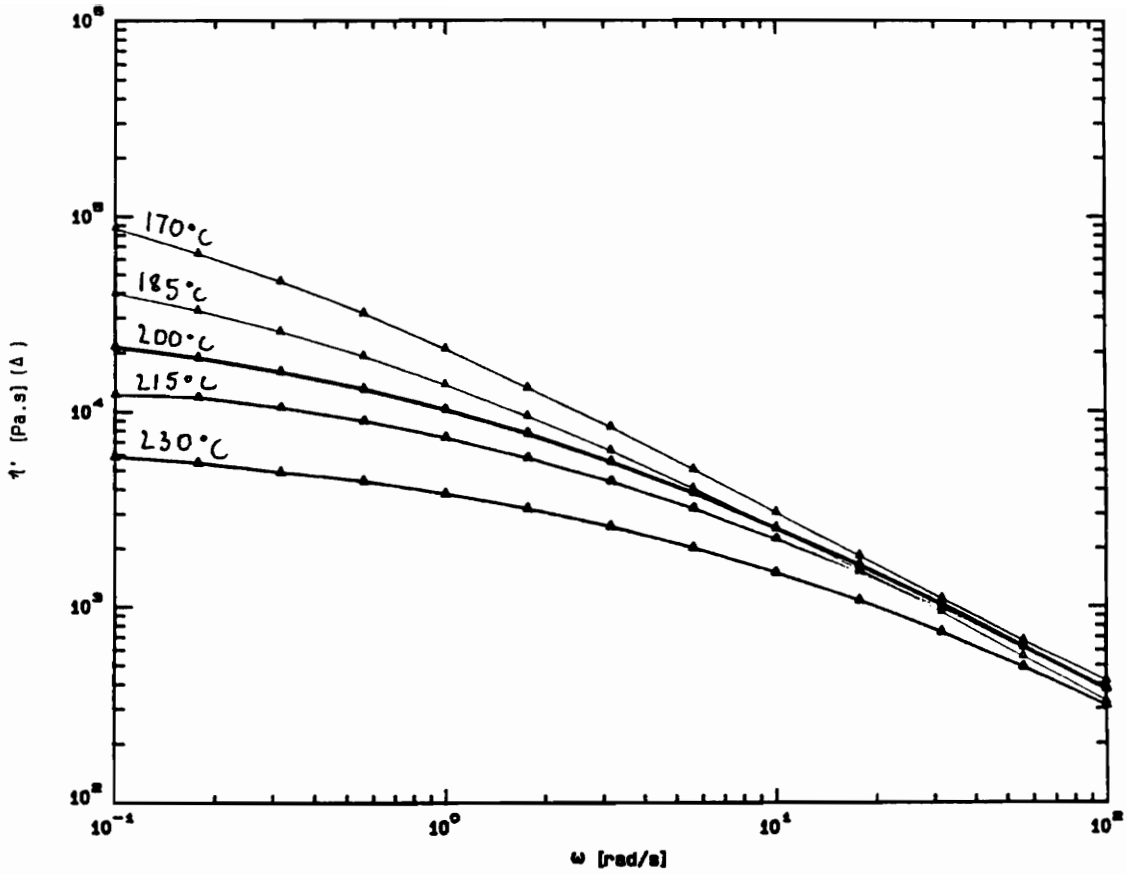

Figure 5-21. Plot of the dynamic viscosity, eta', versus frequency, w, at different temperatures for the 95/5 PS/PVME blend irradiated to 5 Mrads.

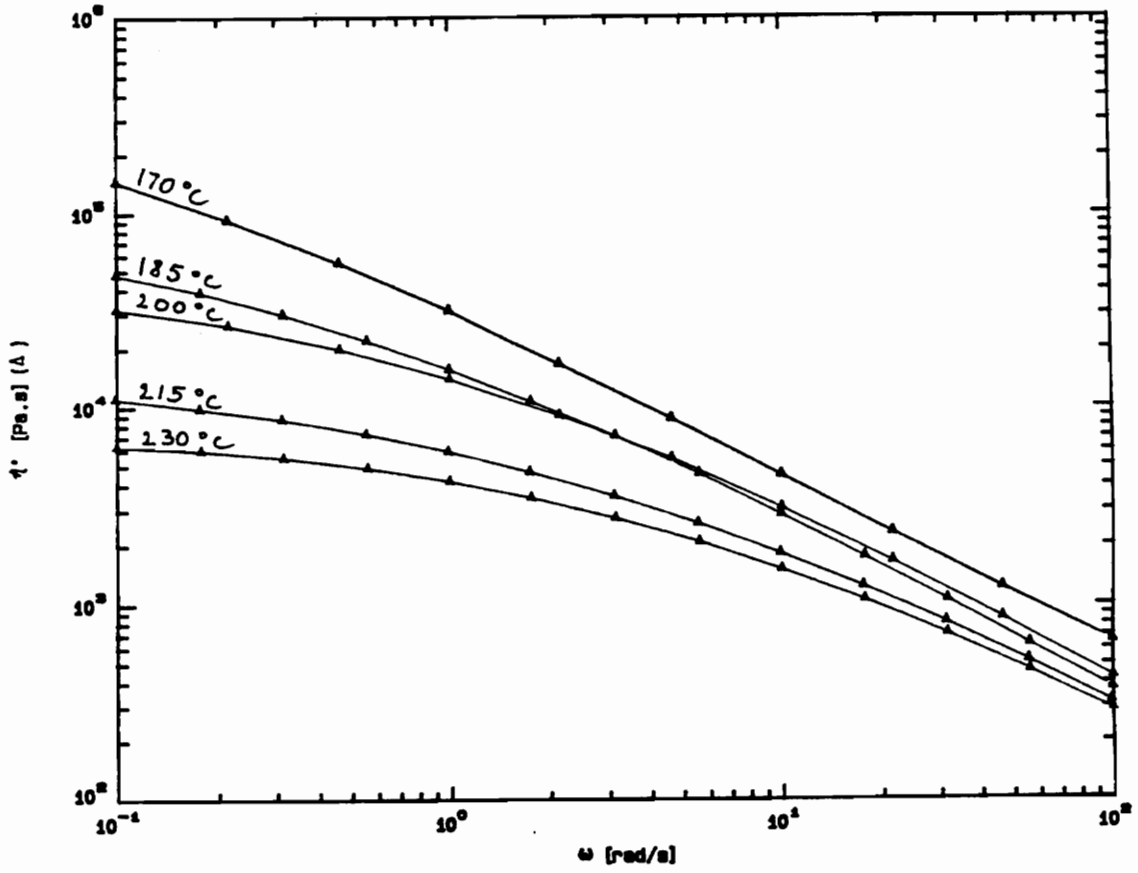

Figure 5-22. Plot of the dynamic viscosity, eta', versus frequency, w, at different temperatures for the 95/5 PS/PVME blend irradiated to 10 Mrads.

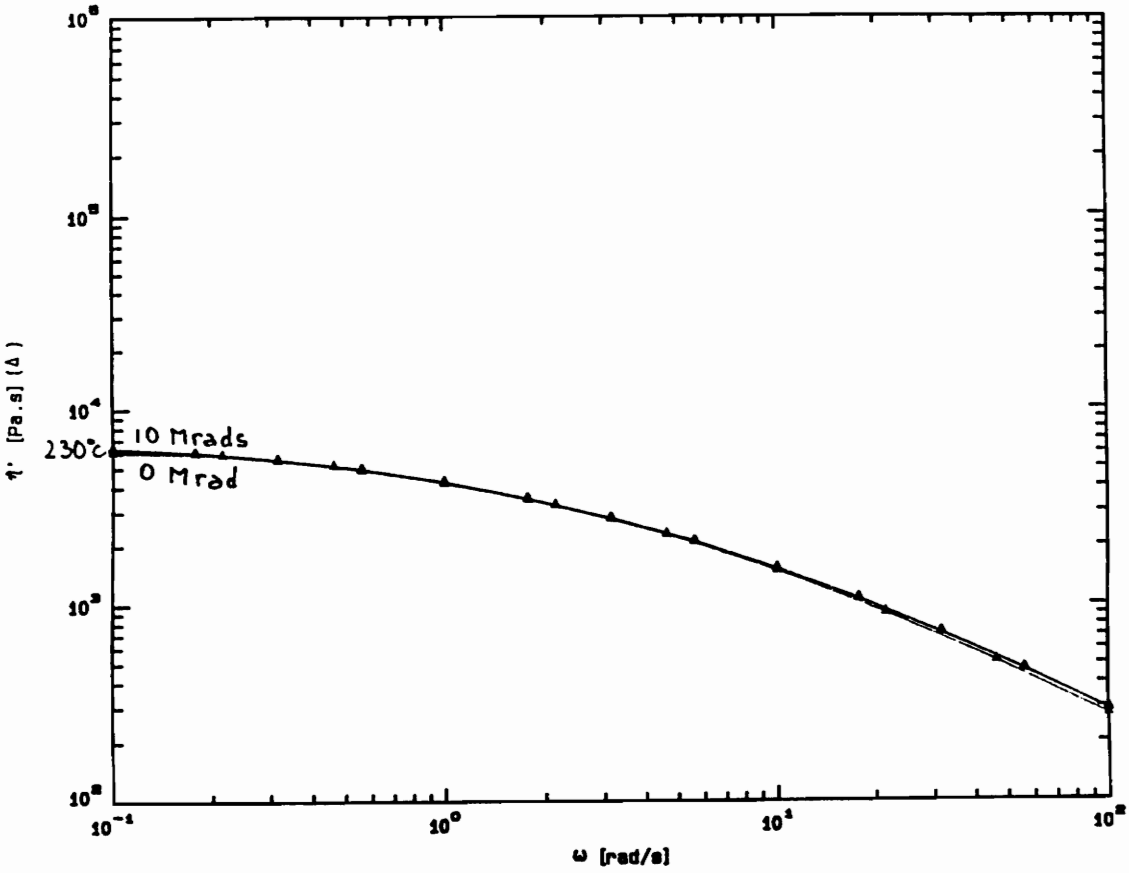

Figure 5-23. Superposition of the dynamic viscosity-frequency responses of the 95/5 PS/PVME blend (1) unirradiated (0 Mrad), and (2) irradiated to 10 Mrads, at 230°C.

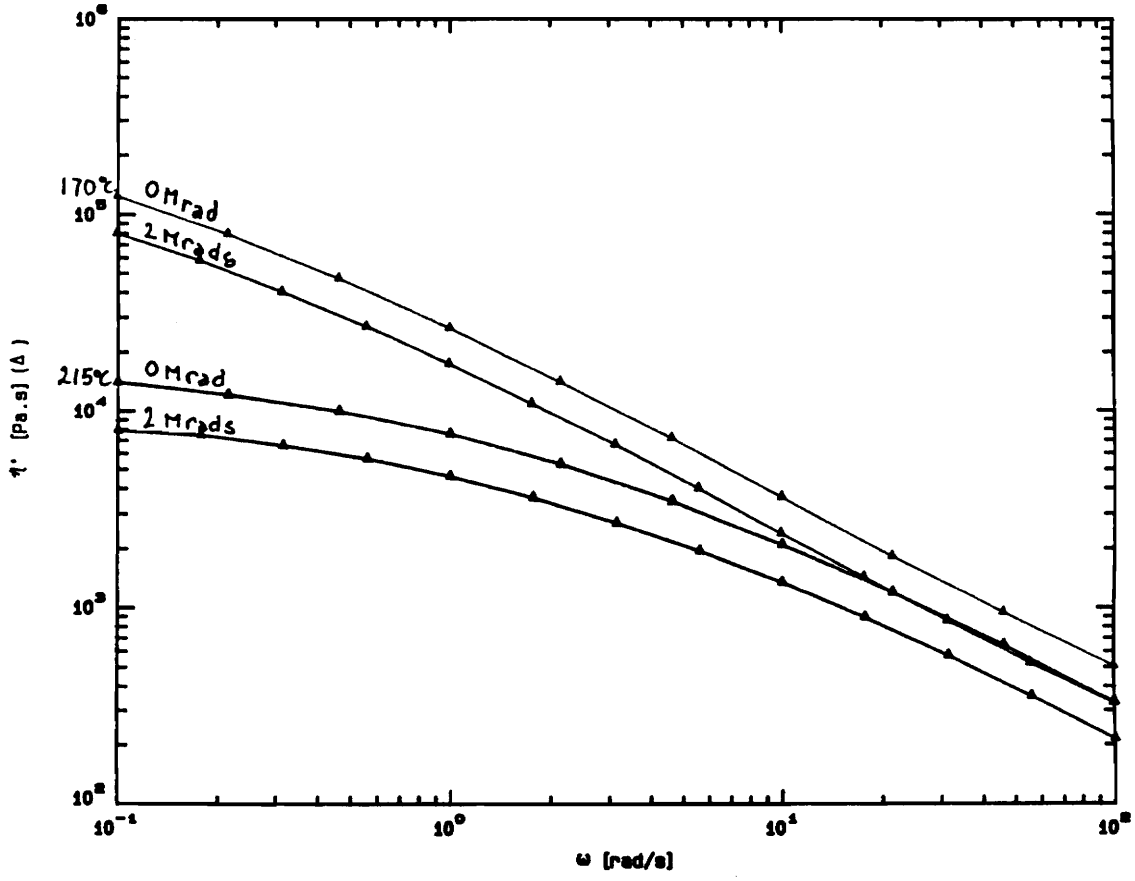

Figure 5-24. Superposition of the dynamic viscosity-frequency responses of the 95/5 PS/PVME blend (1) unirradiated (0 Mrad), and (2) irradiated to 2 Mrads, at 2 different temperatures.

After a radiation dose of 10 Mrads, the system viscosity rises from 6.10^4 to 8.10^4 Pa*s at 170°C, and from about 4.10^3 to 9.10^3 Pa*s at 230°C. At the lowest radiation dose, 2 Mrads, nearly the same enhancement of the viscosity is observed on a log scale. This implies that the weight average molecular weight of the system has increased under irradiation. It was shown earlier that the 90/10 system displayed the largest increase in the cloud point temperature after irradiation to 10 Mrads. As shown earlier in Fig.5-9, it rises from 146°C for the unirradiated material to 150°C for the same blend irradiated to this dose level. The investigator mentioned then that this enhancement of the phase separation temperature under irradiation could be due to a drop of the PVME molecular weight. Two results contradict this hypothesis. First, a drop of the PVME molecular weight would not result in an increase of the 90/10 system weight average molecular weight under irradiation, shown by the enhancement of its viscosity. Second, FTIR analysis of gel fractions of PS/PVME blends irradiated to electron beam radiation, performed by McHerron (3), indicated that interactions between the two components occurred under irradiation, since both components were found to be present in the gel after irradiation. FTIR analysis of the insoluble fractions from his study, obtained after extraction, is displayed in Fig.5-30, in terms of PVME wt % present in the gel after irradiation versus the initial blend

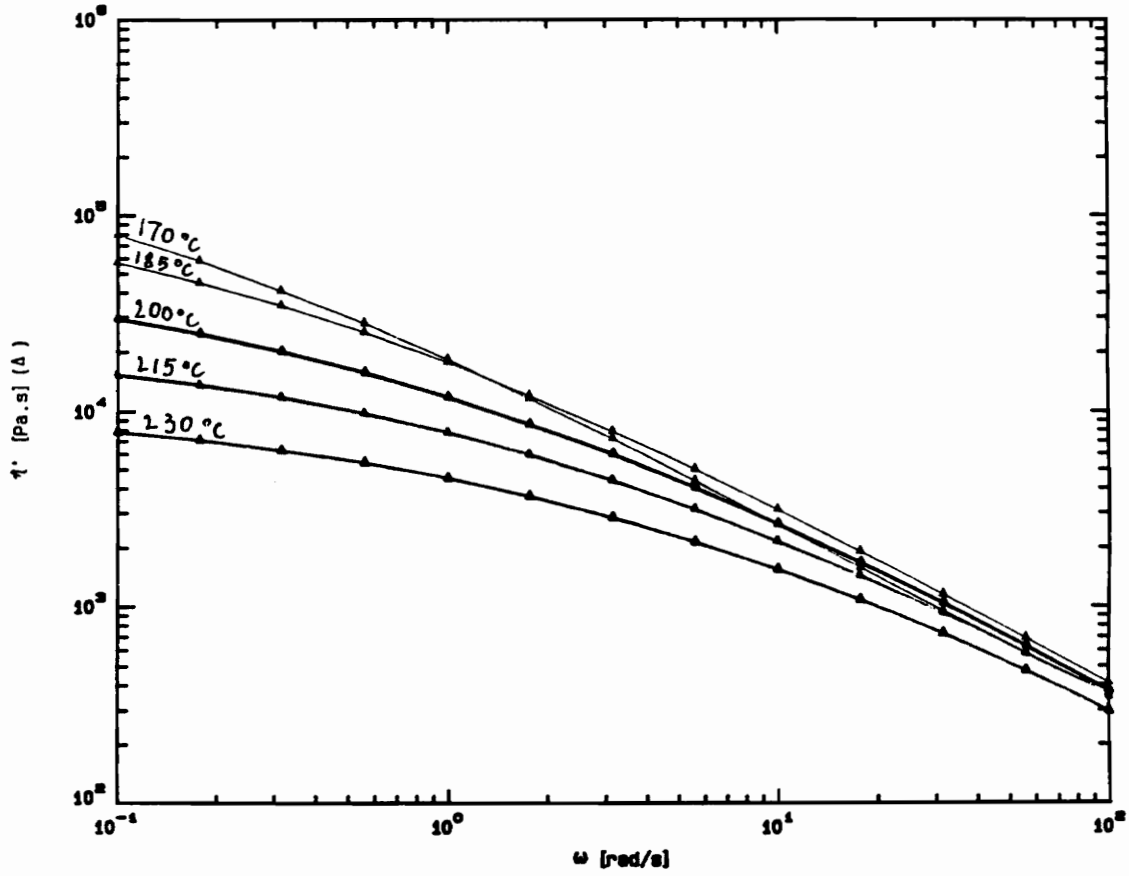

Figure 5-25. Plot of the dynamic viscosity, eta', versus frequency, w, at different temperatures for the 90/10 PS/PVME blend irradiated to 2 Mrads.

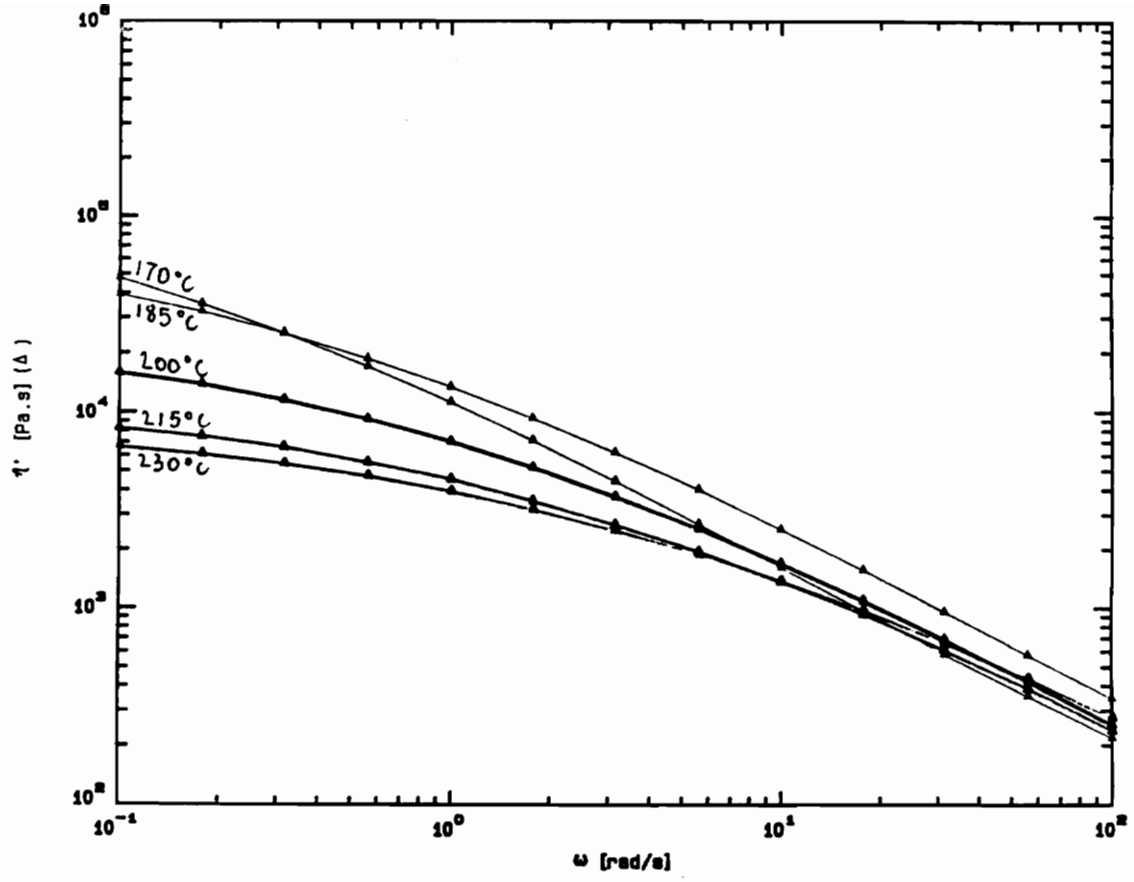

Figure 5-26. Plot of the dynamic viscosity, eta', versus frequency, w, at different temperatures for the 90/10 PS/PVME irradiated to 5 Mrads.

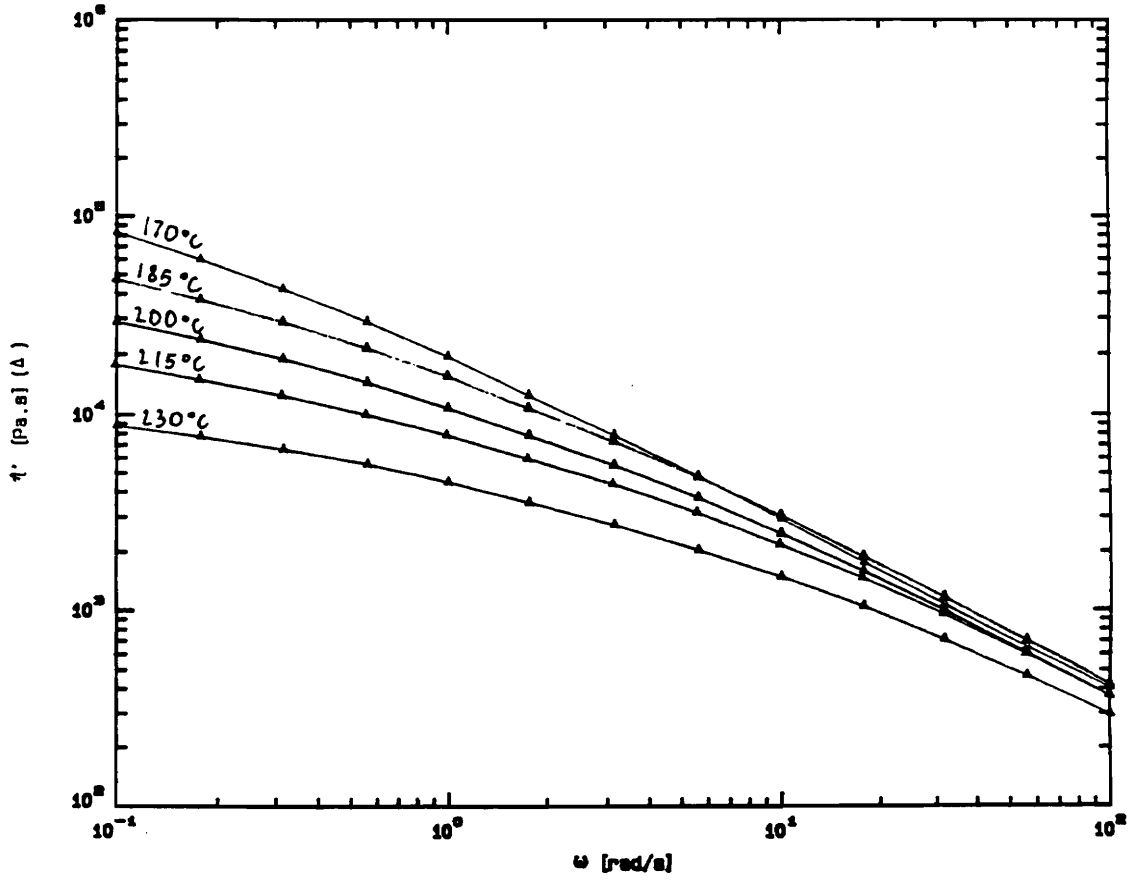

Figure 5-27. Plot of the dynamic viscosity, eta', versus frequency, w, at different temperatures for the 90/10 PS/PVME blend irradiated to 10 Mrads.

composition. Since PS displays radiation resistance behavior by itself, its presence in the gel fraction compositions indicates that radiation grafting has occurred between the two polymers. As shown in Fig.5-30, the compositions under consideration in this present study were not investigated. However, an extrapolation to the composition range of interest can easily be done. Hence, these data give strong indirect evidence that no drop of the PVME molecular weight occurred, since both components appear in the gel. Thereby, the significant enhancement of the 90/10 system viscosity observed under irradiation is believed to result from a significant amount of radiation grafting occurring between PS and PVME at this composition. This is in accordance with the increase of the cloud point temperature after irradiation to 10 Mrads, and the presence of both components in the gel after irradiation. This results in a higher compatibility of the two polymers. As mentioned in the literature review, a log-log plot of the storage modulus G′ versus the loss modulus G′′, at different temperatures, has been used to give an indication of the miscibility of the components of the blend. If they are miscible, the plots obtained at different temperature superpose at all frequencies. On the other hand, if the components are not miscible at the temperatures investigated, the plots do not superpose anymore outside the 5-100 rad/s range. As shown in Fig.5-31 - 5-33, this general behavior is

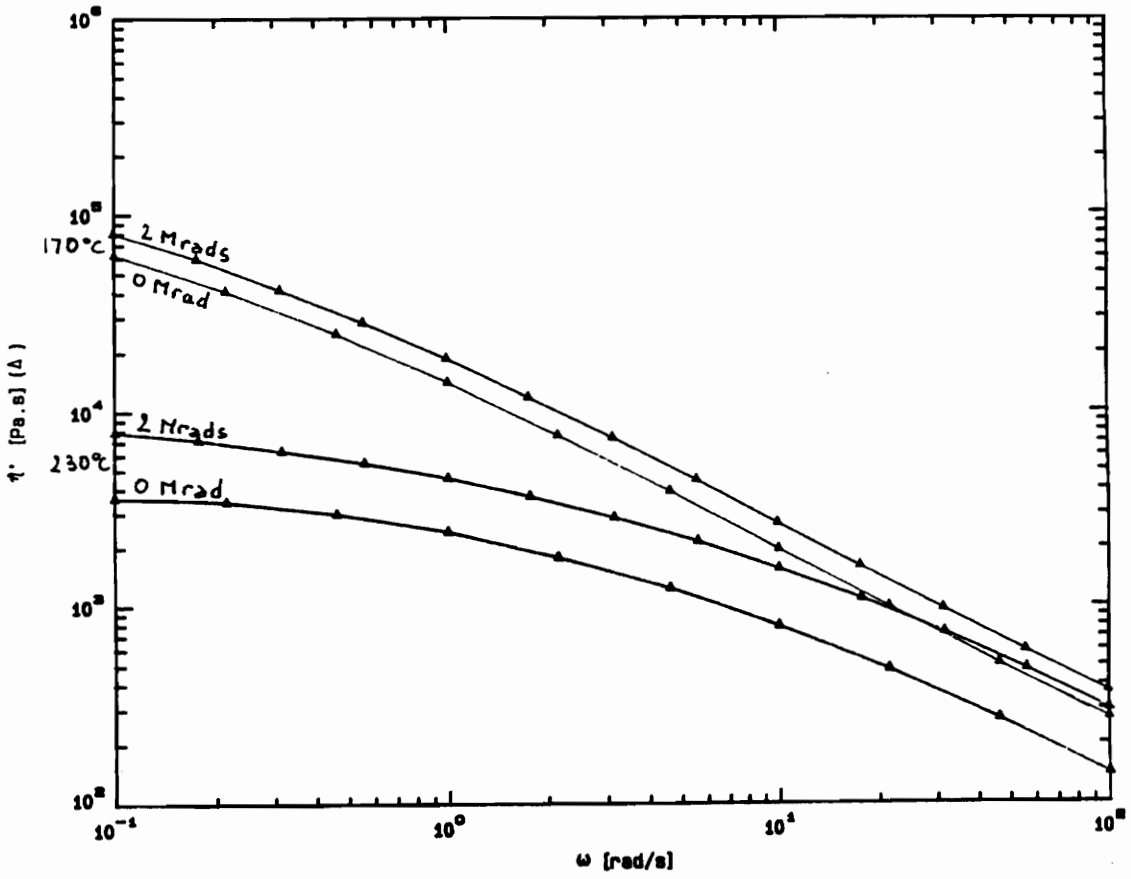

Figure 5-28. Superposition of the dynamic viscosity-frequency responses of the 90/10 PS/PVME blend (1) unirradiated (0 Mrad), and (2) irradiated to 2 Mrads, at 2 different temperatures.

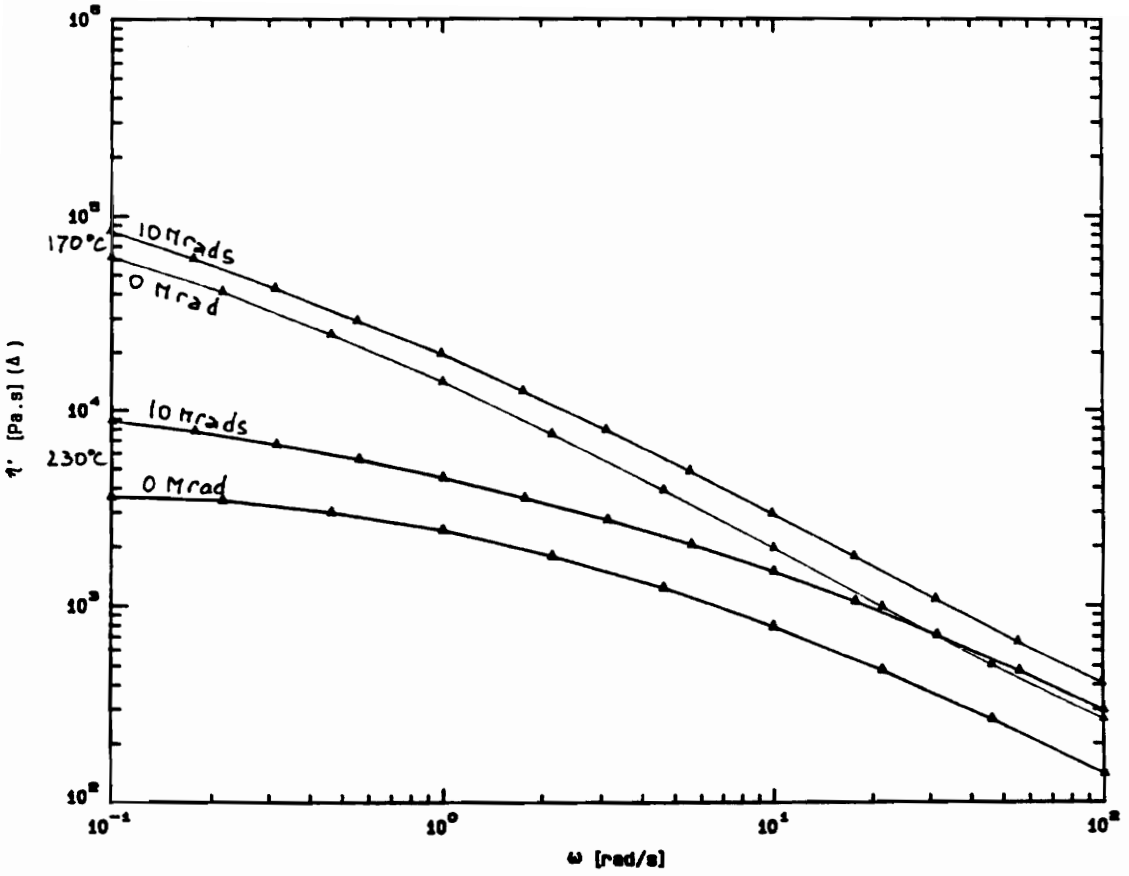

Figure 5-29. Superposition of the dynamic viscosity-frequency responses of the 90/10 PS/PVME blend (1) unirradiated (0 Mrad), and (2) irradiated to 10 Mrads, at 2 different temperatures.

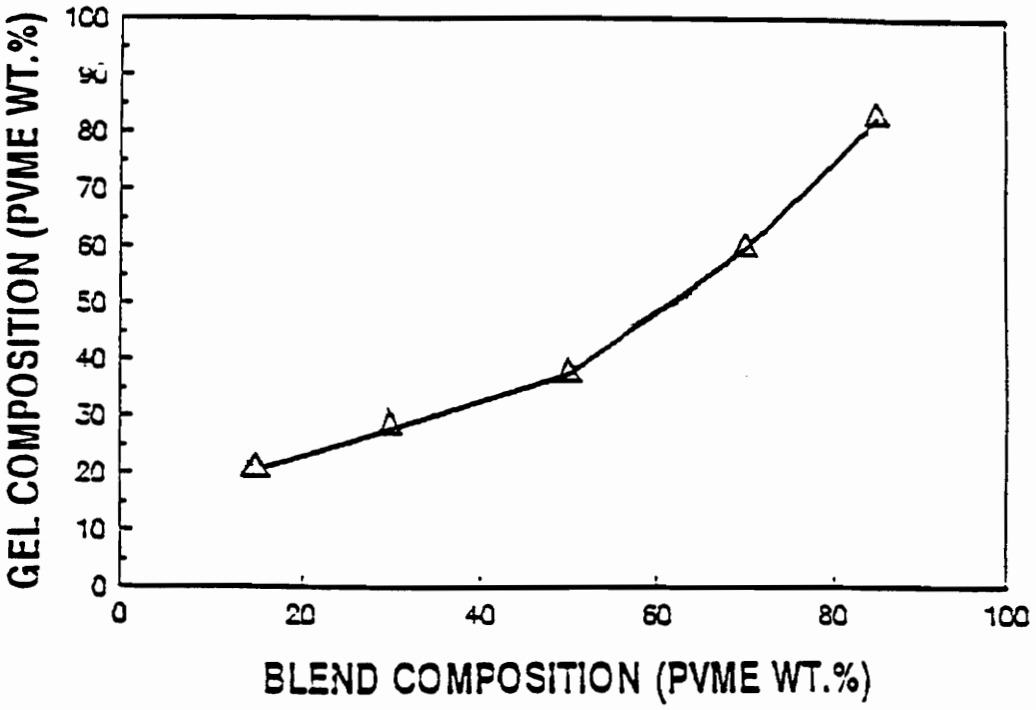

Figure 5-30. Plot of the gel composition (PVME wt %) versus composition (PVME wt %) of miscible PS/PVME blends. (data taken from (3))

not displayed by the unirradiated systems. The plots do not all superpose in the 5-100 rad/s range. This is speculated to result from different blend compositions investigated in this study, i.e. lower PVME content in the systems. Further tests are necessary to explain the behavior observed. However, irradiation to 10 Mrads, obviously, results in a better superposition of the plots for each system. This is favorable to the hypothesis that the grafting occurring induces a higher compatibility between PS and PVME. This effect is more pronounced for the 10/90 wt % system, which is in agreement with what was said before, i.e. this system is more prone to radiation grafting than the lower PVME content blends investigated. Below this PVME content, little effect of radiation is observed on the rheological behavior of the blend systems. This implies that PS has a protective effect for this low PVME content systems, but does not display radiation protection as the composition reaches ca. 10 wt % PVME. As the PVME content increases, more grafting events are likely to occur under radiation, resulting in some noticeable and significant changes in the behavior as the 90/10 composition is reached. However, the exact radiation chemistry occurring in these systems need to be further investigated. Figure 5-34 displays the viscosity, obtained at 0.2 rad/s and 170°C, versus the compositions and doses investigated. This figure summarizes the effects of dose and composition on the

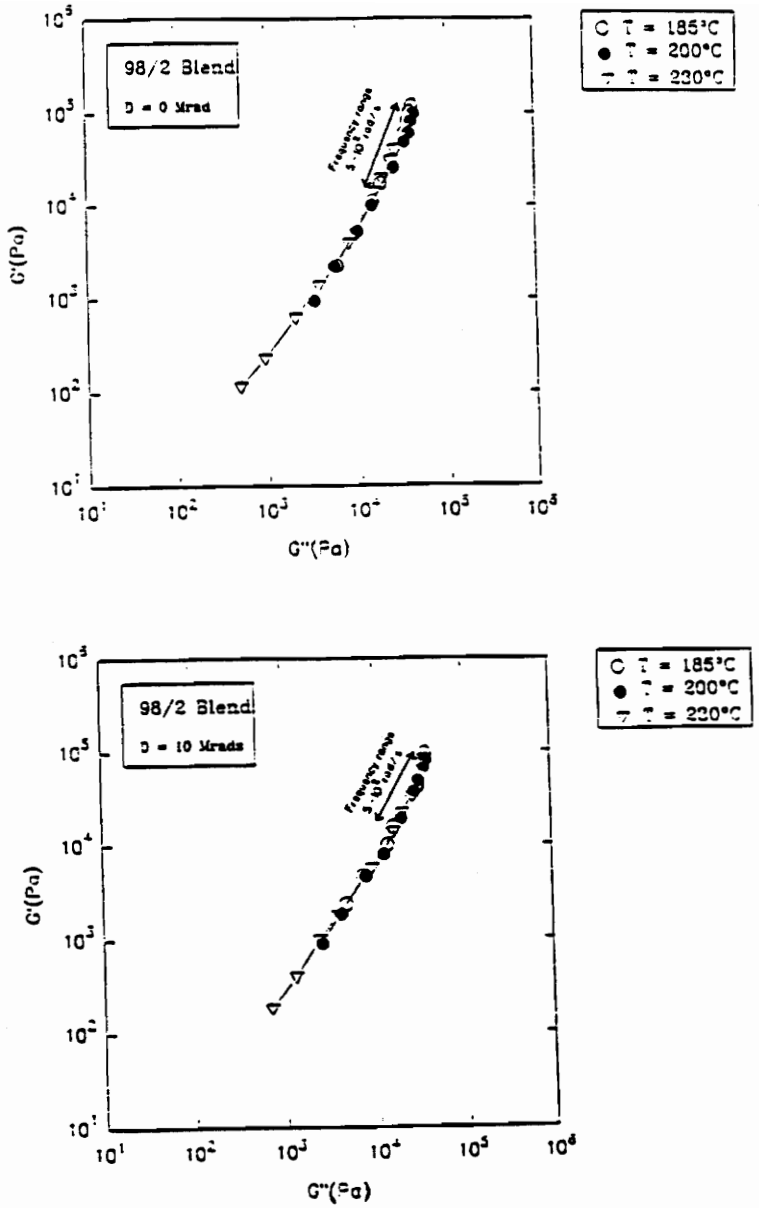

Figure 5-31. Plots, at the indicated temperatures, of the storage modulus (G′) versus the loss modulus (G′′) of the 98/2 PS/PVME blend (1) unirradiated (0Mrad), and irradiated to 10 Mrads.

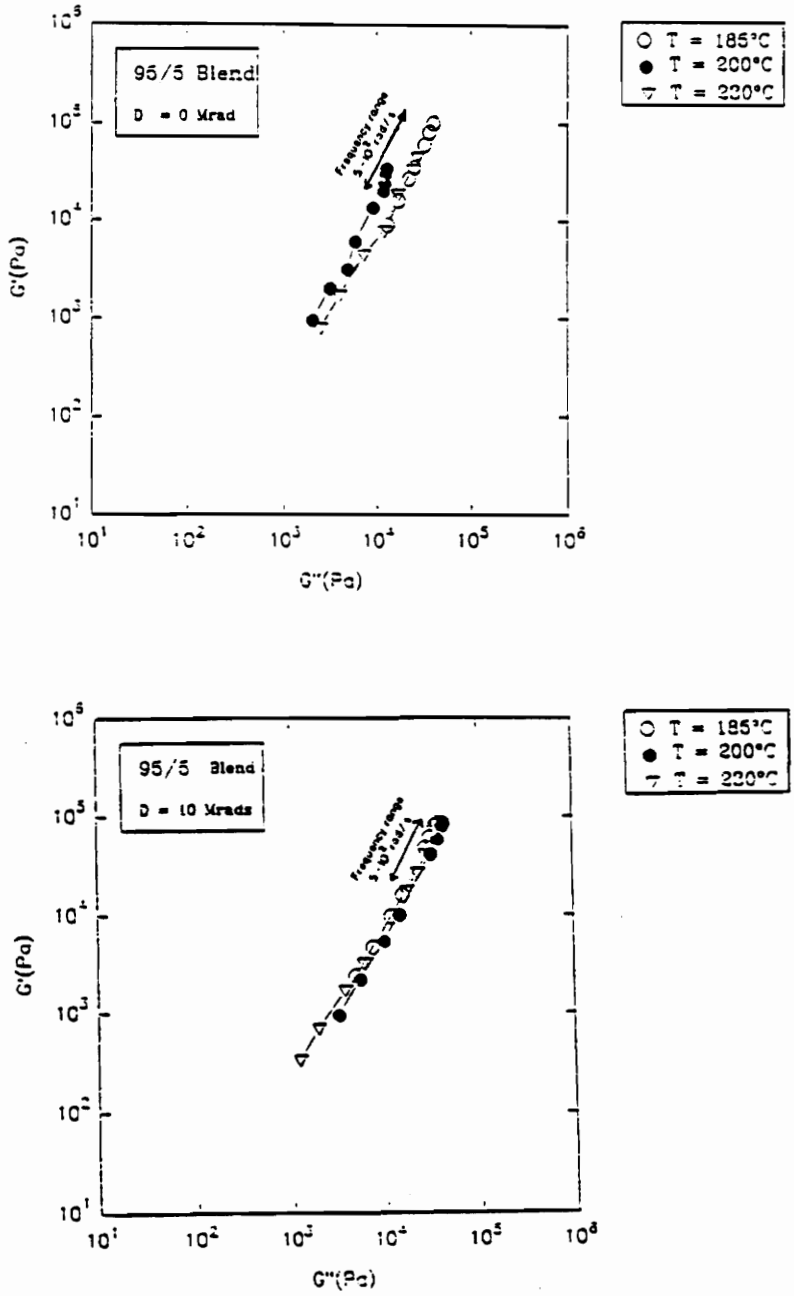

Figure 5-32. Plots, at the indicated temperatures, of the storage modulus (G') versus loss modulus (G'') of the 95/5 PS/PVME blend (1) unirradiated (0Mrad), and (2) irradiated to 10 Mrads.

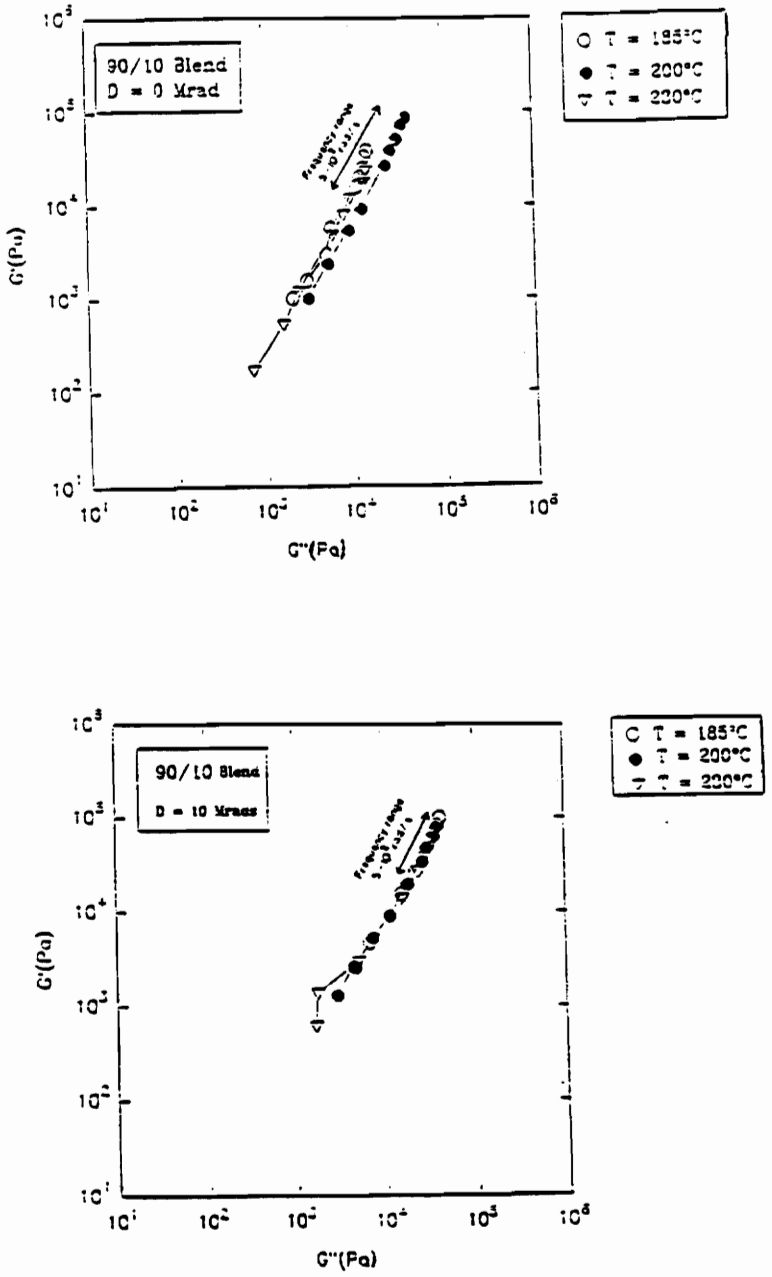

Figure 5-33. Plots, at the indicated temperatures, of the storage modulus (G′) versus loss modulus (G′′) of the 90/10 PS/PVME blend (1) unirradiated (0Mrad), and (2) irradiated to 10 Mrads.

viscosity at a frequency of 0.2 rad/s. It illustrates the radiation resistance of PS and the decrease of the viscosity as the PVME content increases in the systems. Also, no significant changes due to irradiation are observed, except for the 90/10 blend.

The temperature dependence of viscosity at all dose levels are displayed in Fig.5-35 - 5-42 for the PS, 98/2, 95/5, and 90/10 systems respectively. As shown by the linearity of these plots, the Arrhenius Law appears to apply in the temperature range investigated. However, it is interesting to notice the behavior of the 90/10 system. As the dose increases, the linearity of the plots is improved. This is speculated to be also the consequence of the grafting occurring between the two components and resulting in a higher compatibility of the two polymers. This implies that the viscosity displayed at this dose level is less affected by the phase separation process believed to occur at the temperature range investigated. This may be the reason for the better linearity of the Arrhenius plots. This tendency can be generalized to all the systems, the linearity being in general higher after irradiation to 10 Mrads. It is, however, more apparent for the 90/10 blend due to the dispersity of the points observed for the unirradiated material. Table 5-2 gives the resulting flow activation energies calculated from the slopes of these Arrhenius plots. As shown, the activation

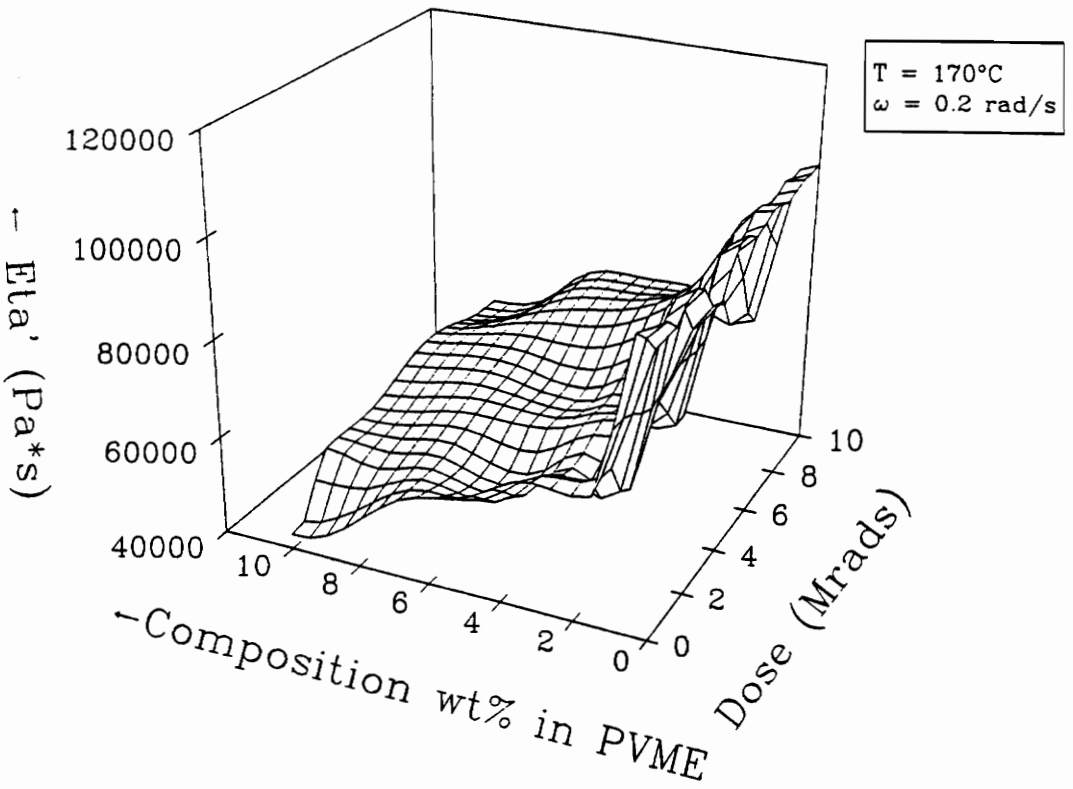

Figure 5-34. Plot of the dynamic viscosity, eta', versus dose and composition (wt % PVME) obtained at 170°C and 0.2 rad/s.

energy decreases as the PVME content increases in the blends, whatever dose level is applied. As explained before (see section 5.1), this trend is expected, based on the fact that PVME has a lower value of Ea, thus resulting in a more facilitated segmental motion of the chain as the PVME content increases in the systems.

For all system, no significant change in Ea occurred due to radiation. This result is somewhat surprising and a bit disappointing for the 90/10 system that clearly shows strong indirect evidence of radiation grafting occurring between the two components. This implies that the level of grafting, between PS and PVME, is not sufficient to significantly alter the segmental movement of the chains. Therefore, it does not raise the value of Ea from that displayed by the corresponding unirradiated blend.

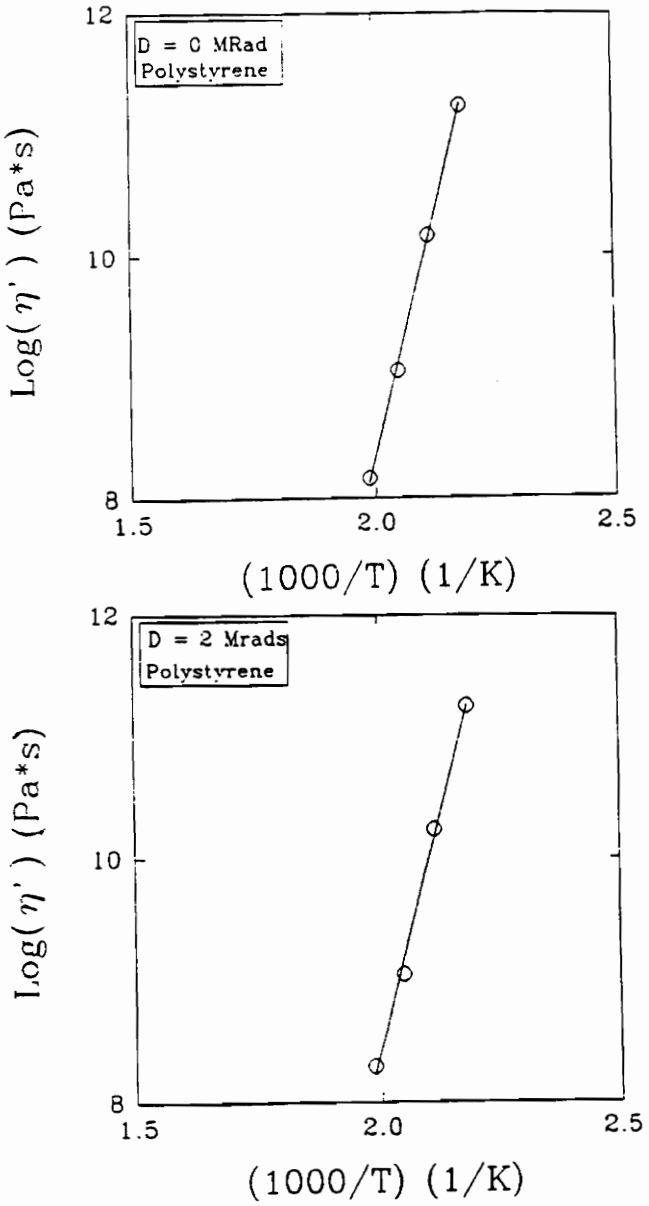

Figure 5-35. Arrhenius plot of the log of the dynamic viscosity obtained at a constant shear stress for pure PS (1) unirradiated (0Mrad), and (2) irradiated to 2 Mrads.

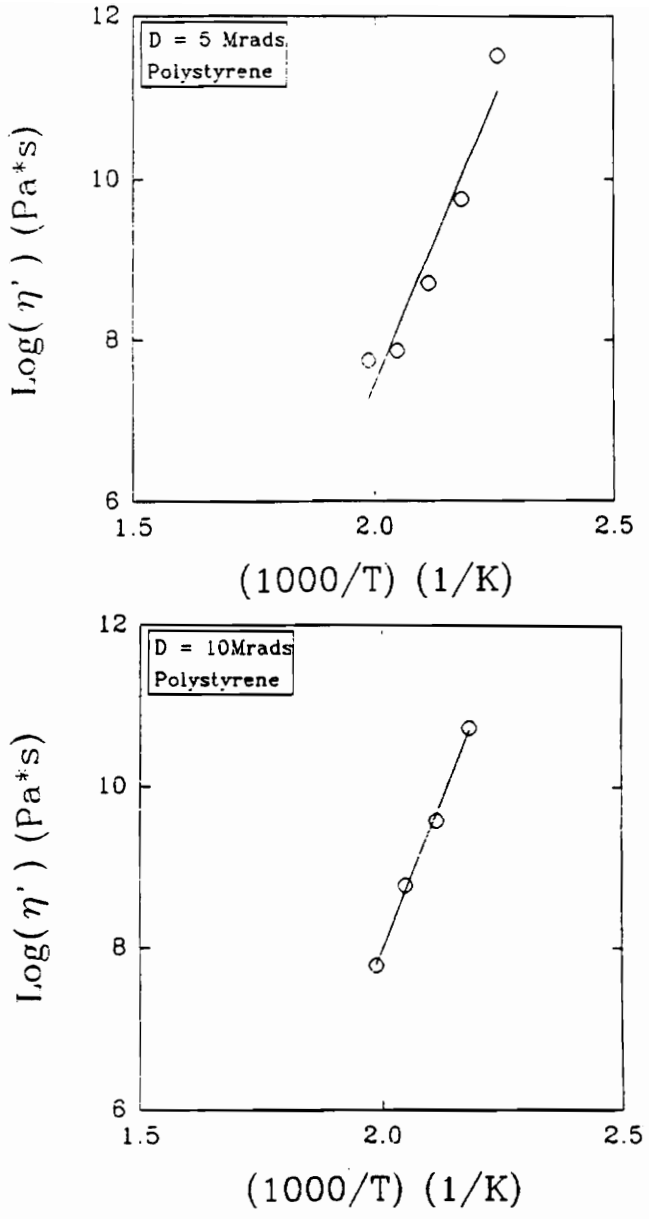

Figure 5-36. Arrhenius plot of the log of the dynamic viscosity obtained at a constant shear stress for pure PS (1) irradiated to 5 Mrads, and (2) irradiated to 10 Mrads.

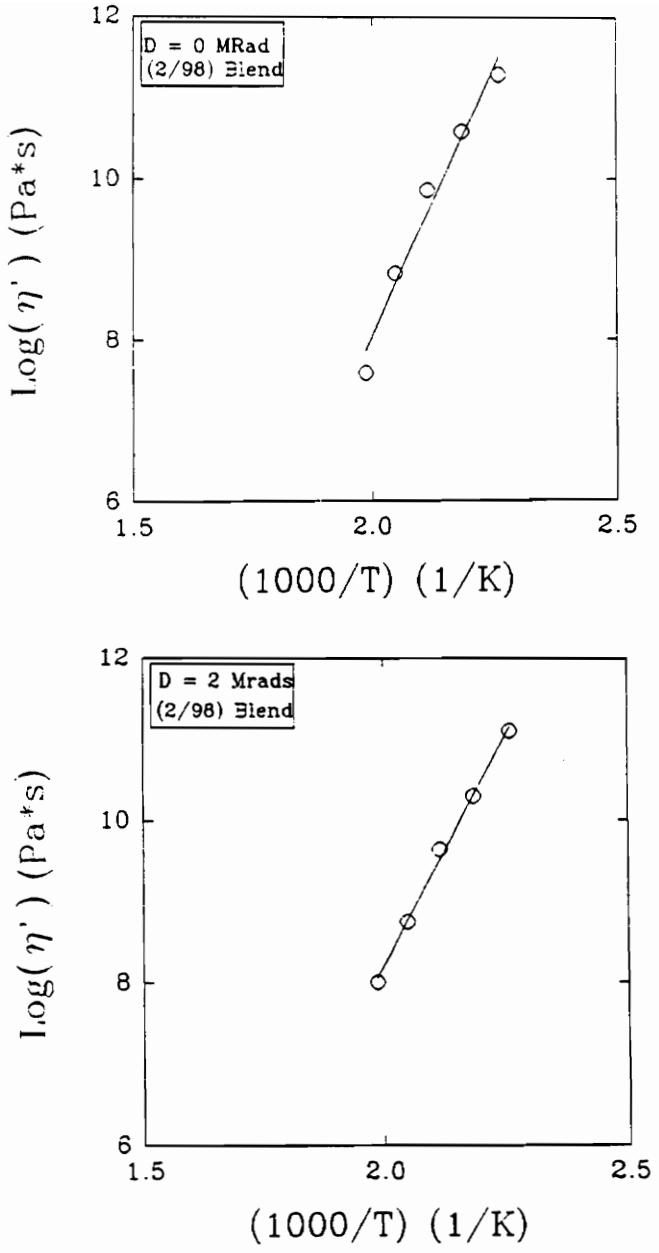

Figure 5-37. Arrhenius plot of the log of the dynamic viscosity obtained at a constant shear stress for the 2/98 PVME/PS blend (1) unirradiated (0Mrad), and (2) irradiated to 2 Mrads.

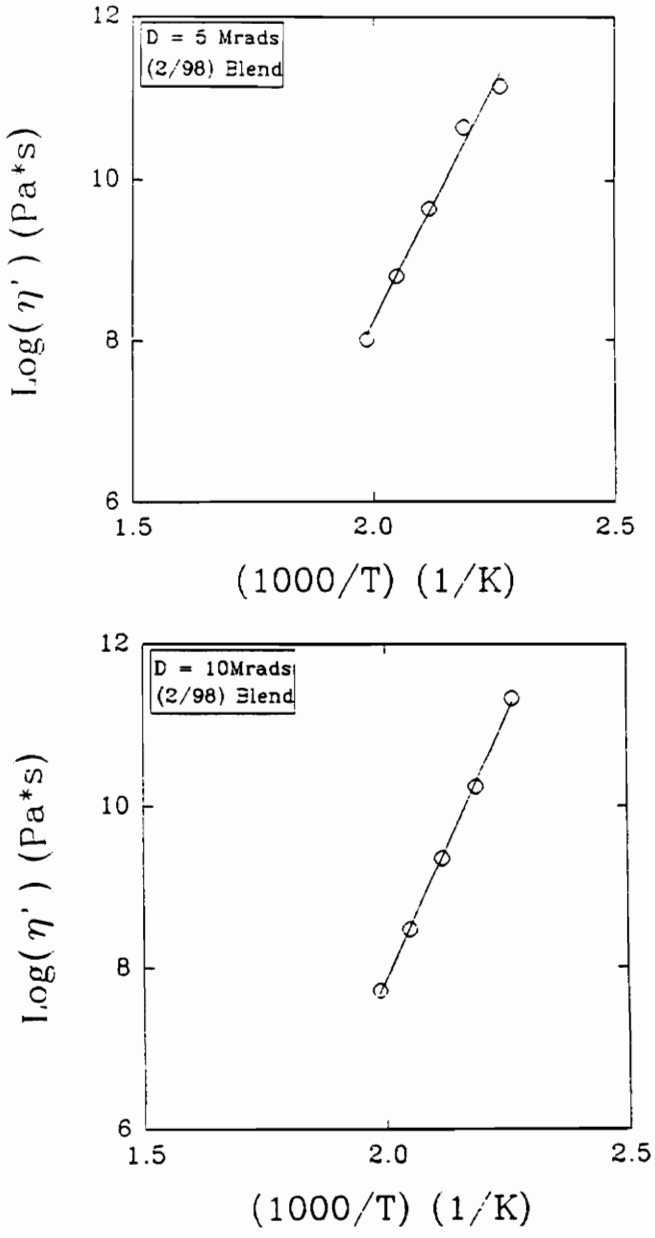

Figure 5-38. Arrhenius plot of the log of the dynamic viscosity obtained at a constant shear stress for the 2/98 PVME/PS blend (1) irradiated to 5 Mrads, and (2) irradiated to 10 Mrads.

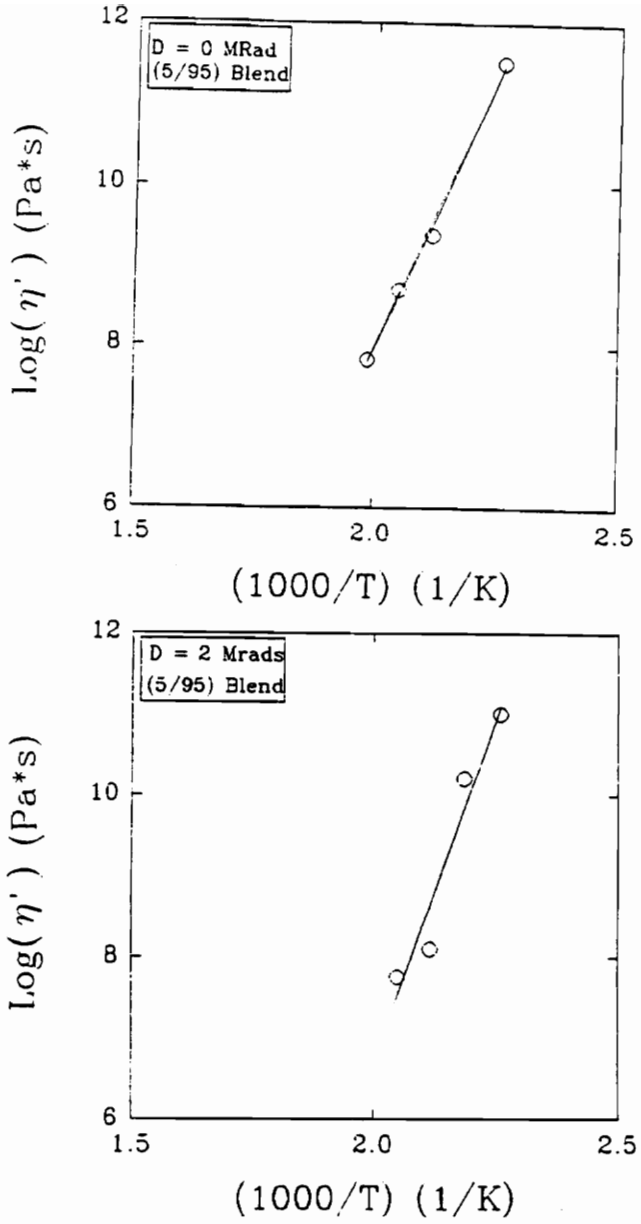

Figure 5/39. Arrhenius plot of the log of the dynamic viscosity obtained at a constant shear stress for the 5/95 PVME/PS blend (1) unirradiated (0Mrad), and (2) irradiated to 2 Mrads.

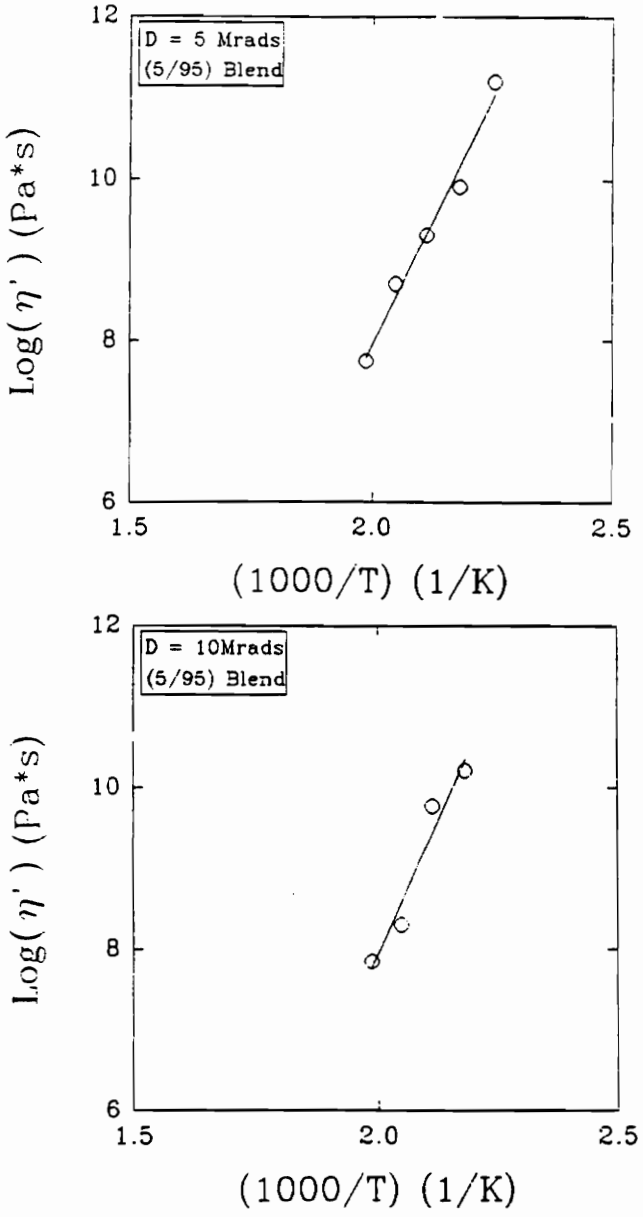

Figure 5-40. Arrhenius plot of the log of the dynamic viscosity obtained at a constant shear stress for the 5/95 PVME/PS blend (1) irradiated to 5 Mrads, and (2) irradiated to 10 Mrads.

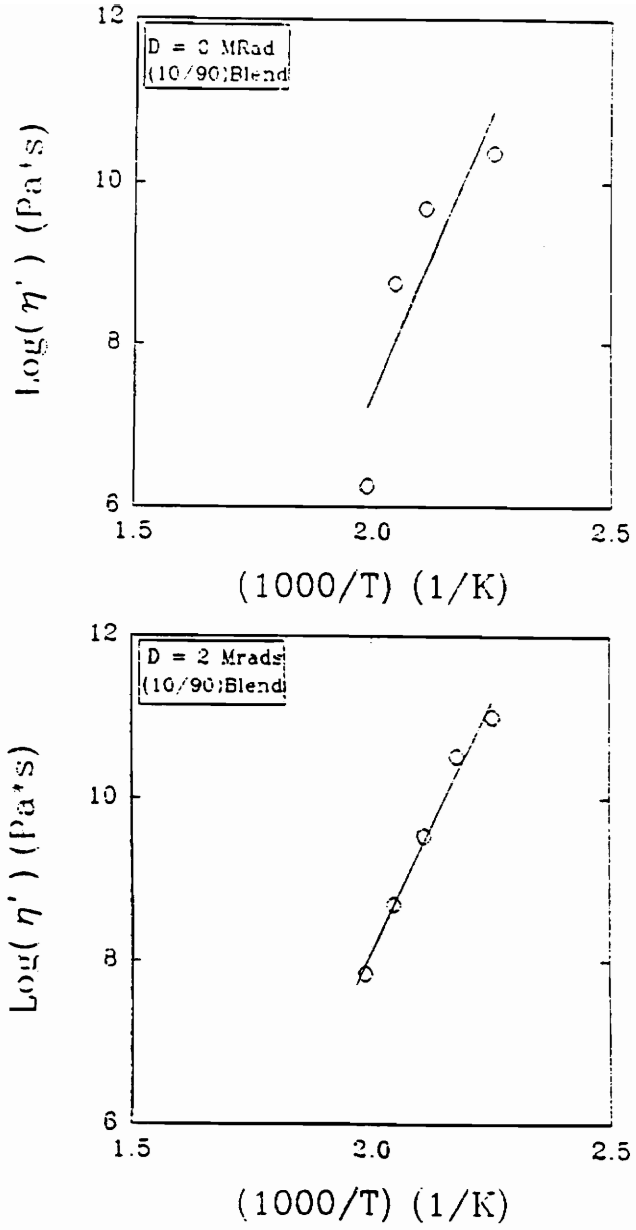

Figure 5-41. Arrhenius plot of the log of the dynamic viscosity obtained at a constant shear stress for the 10/90 PVME/PS blend (1) unirradiated (0Mrad), and (2) irradiated to 2 Mrads.

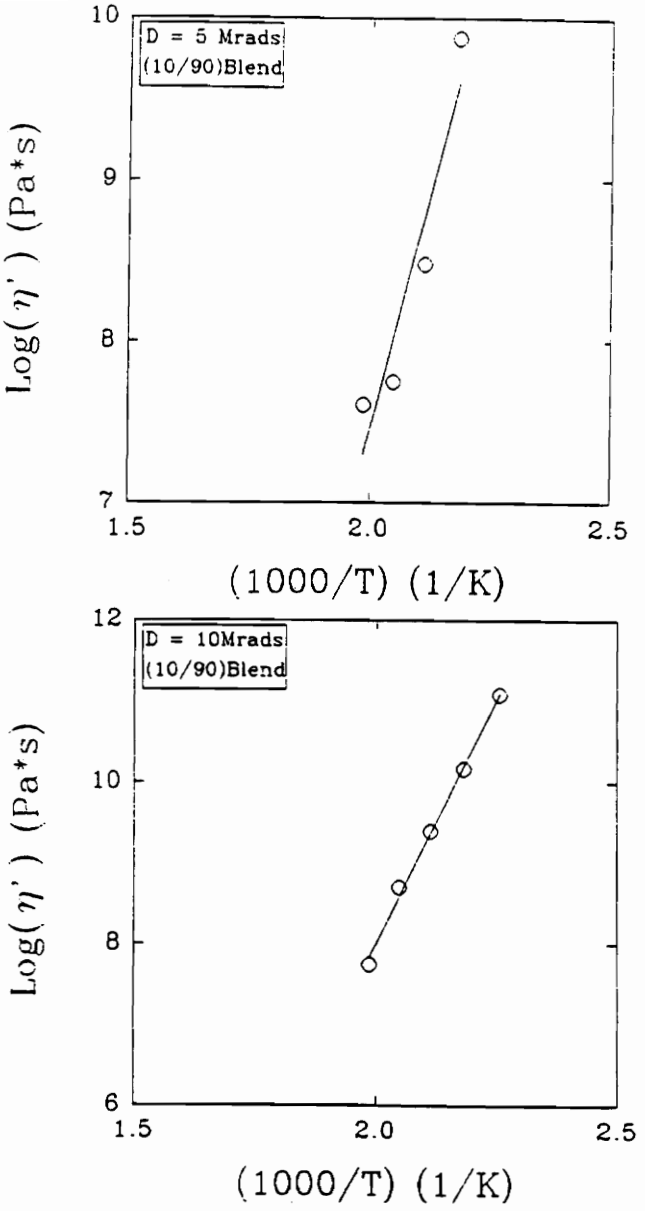

Figure 5-42. Arrhenius plot of the log of the dynamic viscosity obtained at a constant shear stress for the 10/90 PVME/PS blend (1) irradiated to 5 Mrads, and (2) irradiated to 10 Mrads.

Table 5-2. Values of the flow activation energy, in Kcal/mol, obtained with the PS/PVME systems irradiated to the indicated dose. (error associated: ± 2 Kcal/mol). Associated shear stress range (in N/m^2) of the rheological measurements for each system.

System	0 Mrad	2 Mrads	5 Mrads	10 Mrads
100/0	30	29	28	29
98/2	27	23	24	26
95/5	26	26	24	26
90/10	21	24	19	24
0/100	14	-	-	-

System PS/PVME	0 Mrad	2 Mrads	5 Mrads	10 Mrads
100/0	50-5100	100-5000	80-3200	70-5000
98/2	70-2700	100-1600	100-2300	70-2800
95/5	90-3800	80-2000	80-2300	80-3200
90/10	10-1000	90-1900	60-600	70-2200

CONCLUSION

This study has investigated the effects of dose, blend composition, and temperature on the rheological behavior of a series of PS/PVME blends exposed to electron beam irradiation. The irradiation was shown to significantly affect only the viscosity-frequency response of the system containing the highest PVME percentage , i.e. the 90/10 system. It was suggested that, for this system, radiation grafting occurred between the two polymers, as illustrated in a significant increase in the blend viscosity, as well as in the phase separation temperature after exposure to 10 Mrads. FTIR analysis of the gel fractions obtained after irradiation, taken from McHerron previous study on PS/PVME blends, indirectly strongly supports this hypothesis, by showing that both components are present in the gel after irradiation. This radiation grafting is believed to enhance the compatibility between the two polymers, illustrated by the higher superposition observed, after irradiation to 10 Mrads, in the log-log plots of the storage versus loss moduli. The other levels of blend composition investigated did not display any significant changes in their rheological response after irradiation. Since PS is the major component matrix phase in

these systems, these results are in accordance with the radiation resistance and radiation protection characteristic of this polymer. This would also suggest that a minimum of 10 wt % PVME is required to significantly alter the shear rate response of the blends after irradiation.

The temperature dependence of viscosity of the systems, illustrated by the flow activation energy, Ea, did not reflect any alteration due to radiation. For a given blend composition, no real change in the values of Ea were shown to occur with increasing dose. On the other hand, as the PVME content increased in the blend systems, the flow activation was shown to decrease. It was suggested that the addition of PVME to the PS-rich phase results in a more facilitated segmental movement of the chain of the systems. The level of grafting that is thought to occur between the two components of the irradiated 90/10 system obviously does not affect this general tendency.

RECOMMENDATIONS FOR FUTURE STUDIES

This study found that the range of low radiation doses and PVME contents investigated did not induce major modifications of the flow properties of the PS/PVME blends. Indeed, no real changes in the flow activation energy were noticed due to radiation. However, the shift of the phase separation temperature observed after exposure to 10 Mrads, combined with a corresponding increase in the viscosity, and the presence of both blend components in the gel after irradiation, indicated that some grafting occurred between the two polymers. This behavior was found to be more pronounced as the PVME content was increased. In order to obtain systems more sensitive to radiation (i.e., showing larger alterations of their rheological properties), the PVME content in the system composition could be increased further. However, this would result in a decrease in the phase separation temperature. Thus, investigations of the flow properties would become even more difficult if PVME content is increased further. It would therefore be preferable to study a pair of compatible polymers more sensitive to electron beam radiation that would display only UCST behavior, or that would display

LCST behavior above the temperatures carried out for the rheological experiments. Like in this study, a low molecular weight component could be added to a high molecular weight material in order to induce interactions and chemical reactions between the two polymers under irradiation.

It would also be interesting to investigate and develop a better understanding of the radiation chemistry occurring between the PS and PVME polymers during the irradiation. Pulse radiolysis of the system would indicate what free radicals, excited states, and chemical interactions are produced under irradiation, and how these evolve with dose and composition.

In this study, the determination of the phase separation temperatures of the systems (Ts) was done through cloud point measurements. Ts was taken as the temperature at which the first sign of cloudiness appeared. Another method suggested by Han (21) consists of plotting the storage modulus (G′) versus the loss modulus (G′′) at temperatures below and above the phase separation temperature of the blend. In the miscible region, he found that the results obtained at different temperatures lie on the same curve over the entire frequency range. In contrast, in the immiscible region, he observed that the experimental points obtained at different temperatures lie on the same curve in the 5 - 100 rad/s, but they did not superpose outside this range. This method was

tried in this present study, but it did not result in the behavior expected, in comparison with what Han observed. Therefore, it would be interesting to investigate this method further in order to understand why it did not work. Further investigation of this method would indeed be useful to find which parameters induce this difference in behavior (molecular weight, blend composition...).

REFERENCES

1. P.J. Flory, *Principles of Polymer Chemistry*, Cornell University, Press Ithaca, New york, 1953.

2. F.S. Bates, *Science*, 1991, 251, 898.

3. D.C. McHerron, *Creation and Modification of Polymeric Materials Using Electron Beam Radiation*, Nov.1991.

4. T. Nishi, T.T. Wang, and T.K. Kwei, *Macromolecules*, 1975, 8, 227.

5. J.M. Ubrich, F.B.C. Larby, J.L. Halary, and L. Monnerie, *Macromolecules*, 1986, 19, 810-815.

6. W.W. Graessley, *Viscoelasticity and Flow in Polymer Melts and concentrated Solutions*, in *Physical Principles of Polymers*, Edited by J.E. Mark, Amer. Chem. Soc., Wash. D.C., 1984, 97-151.

7. G.L. Wilkes, *J. of Chem. Educ.*, vol.58, No.11, Nov.1981, 880-92.

8. N. Alle and J. Lyngaae-Joergensen, *J. Rheol. Acta*, 19 : 94-103, 1980a.

9. C.D. Han and T.C. Yu, *J. Appl. Polym. Sci.*, 15 : 1163-80, 1971.

10. K. Iwakura and T. Fujimura, *J. Appl. Polym. Sci.*, 19 : 1427-37, 1975.

11. T.I. Ablazova, M.B. Tsebrenko, A.B.V. Yudin, G.V. Vinogradov, and B.V. Yarlikov, *J. Appl. Polym. Sci.*, 19:1781-98, 1975.

12. C.D. Han and Y.W. Kim, *Trans. Soc. Rheol.*, 19 : 2,245-269, 1975.

13. K. Hayashida, J. Takahashi, and M. Matsui, *Proc. 5th Int. Rheol. Congress*, vol.4, University of Tokyo Press, Tokyo,

523-35, 1970.

14. C.D. Han, Y.W. Kim, J. Parker, N. Siskovic, and C.R. Huang, *Appl. Polym. Symp.*, 20 : 191-98, 1973.

15. C.D. Han, Y.W. Kim, and S.J. Chen, *J. Appl. Polym. Sci.*, 19 : 2,831-843, 1975.

16. J. M. Dealy and K.F. Wissbrun, *Melt Rheology and its Role in Plastics Processing*, Van Nostrand Reinhold, New York, 401-406, 1989.

17. H. Schuch, *Rheol. Acta*, 27 : 384-96, 1988.

18. J.P. Montfort, G. Marin, J. Armand, and P. Monge, *Polymer*, 19 : 277, 1978.

19. J.P. Montfort, G. Marin, J. Armand, and P. Monge, *Rheol. Acta*, 18 : 623, 1979.

20. A. Ajji, L. Choplin, and R.E. Prud'Homme, *J. Polym. Sci.*: Part B, vol.29, 1573-78, 1991.

21. C.D. Han, *J. Appl. Polym. Sci.*, 33, 1199, 1987.

22. H.A. Schneider and J. Wirbser, *New Polymeric Mater.*, vol.2, No.2, 149-66, 1990.

23. H.A. Schneider, M.J. Breckner, and H.J. Cantow, *Polym. Bull.*, vol.14, 7, 1985.

24. J.G.M. Van Gisbergen, H.E.H. Meijer, and P.J. Lemstra, *Polymer*, vol.30, Dec.1989.

25. W.D. Coolidge, *Science*, 62, 441, 1925.

26. F.A. Bovey, *The Effects of Ionizing Radiation on Natural and Synthetic High Polymers* , Interscience, New York, N.Y., 1958.

27. A.J. Swallow, *Radiation Chemistry*, Longman Press, Great Britain, 1973.

28. H.A. Bethe, *Handb. Phys.*, 24, 273, 1933.

29. A. Charlesby, *Atomic Radiation and Polymers*, Pergamon Press, 1960.

30. T.E. Everhart and P.H. Hoff, *J. Appl. Phys.*, vol.42,

1971.

31. A. Charlesby, *Proc. Roy. Soc.*, London, 1954, A222, 60.

32. E.J. Lawton, P.D. Zemany, and J.S Balwit, *Amer. Chem. Soc.*, 76, 3437, 1954.

33. K.H. Sun, *Mod. Plast.*, vol.32, 141, Ser.1, Sept. 1954.

34. M. Dole, C.D. Keeling, and D.G. Rose, *J. Amer. Chem. Soc.*, 76, 4304, 1954.

35. A.B. Taubman and L.P. Yanova, *Academy of Sciences of the U.S.S.R.*, Moscow, 307-14, 1958.

36. A.M. El-Naggar, L.C. Lopez, and G.L. Wilkes, *J. Appl. Polym. Sci.*, vol.39, 427-46, 1990.

37. A. Charlesby, E. Von Arnim, and L. Callaghan, *Intern. J. Appl. Radiation and Isotopes*, vol.3, 226, 1958.

38. E.J. Lawton, J.S. Balwit, and R.S. Powell, *J. Polym. Sci.*, vol.32, 257, 1958.

39. W.H. Stockmayer, *J. Chem. Phys.*, vol.12, 125, 1944.

40. A. Chapiro, *Radiation Chemistry of Polymeric Materials*, Interscience Publishers, 1962.

41. A.M. Rijke and L. Mandelhern, *Macromolecules*, vol.4, 594, 1971.

42. A. Charlesby, *Proc. Roy. Soc.*, London, A215, 187, 1952.

43. M. Dole, *Report of Symposium IX, Army Chemical Center*, Maryland, 1950.

44. A.C. Baskett, *Intern. Symp. Macromol. Chem.*, Milan - Torino, 1954, *Ricerca Sci. Suppl.*, A379, 1955.

45. P. Alexander and D. Toms, *J. Polym. Sci.*, vol.22, 343, 1956.

46. R.M. Briber and B.J. Bauer, *Macromolecules*, 21, 3296-3303, 1988.

47. W.W. Graessley, T. Masuda, J.E.I. Roovers, and Hadjichristidis, *Macromolecules*, 9 : 127, 1976.

48. P.C. Hiemenz, *Polymer Chemistry - The Basic Concepts*, Marcel Dekker, Inc., New York, 1984.
49. W.W. Graessley, *Accounts of Chemical Research*, 10, 332, 1977.

VITA

Valérie PIETRI was born on March 7, 1969 in Saint-Denis (La Réunion). After finishing her high school studies at Félix Esclangon's High School in Manosque (France), she attended the University of Technology of Compiègne (France) to obtain the degree of Engineer in Chemical Engineering. In the Fall of 1991, she began a Master Program in Chemical Engineering at Virginia Polytechnic Institute & State University. She worked under the guidance of Dr. Wilkes and obtained her M.S. degree in May 1993.

Valérie PIETRI